

Late Quaternary Evolution of Reedy Glacier, Antarctica

Claire E. Todd

A dissertation submitted in partial fulfillment of
the requirements for the degree of

Doctor of Philosophy

University of Washington

2007

Program Authorized to Offer Degree: Earth and Space Sciences

UMI Number: 3289774

INFORMATION TO USERS

The quality of this reproduction is dependent upon the quality of the copy submitted. Broken or indistinct print, colored or poor quality illustrations and photographs, print bleed-through, substandard margins, and improper alignment can adversely affect reproduction.

In the unlikely event that the author did not send a complete manuscript and there are missing pages, these will be noted. Also, if unauthorized copyright material had to be removed, a note will indicate the deletion.

UMI[®]

UMI Microform 3289774

Copyright 2008 by ProQuest Information and Learning Company.

All rights reserved. This microform edition is protected against unauthorized copying under Title 17, United States Code.

ProQuest Information and Learning Company
300 North Zeeb Road
P.O. Box 1346
Ann Arbor, MI 48106-1346

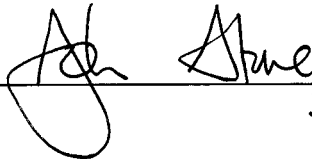
University of Washington
Graduate School

This is to certify that I have examined this copy of a doctoral dissertation by

Claire E. Todd


and have found that it is complete and satisfactory in all respects, and that any and all revisions required by the final examining committee have been made.

Chair of the Supervisory Committee:

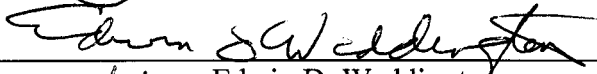


John Stone


Reading Committee:



John Stone



Edwin D. Waddington



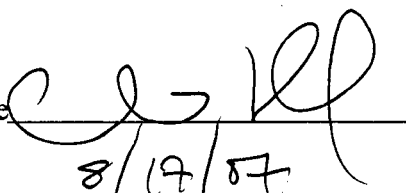
Howard B. Conway

Date: 17 - Aug - 2007

In presenting this thesis in partial fulfillment of the requirements for the doctoral degree at the University of Washington, I agree that the Library shall make its copies freely available for inspection. I further agree that extensive copying of the dissertation is allowable only for scholarly purposes, consistent with "fair use" as prescribed in the U.S. Copyright Law. Requests for copying or reproduction of this dissertation may be referred to ProQuest Information and Learning, 300 North Zeeb Road, Ann Arbor, MI 48106-1346, 1-800-521-0600, to whom the author has granted "the right to reproduce and sell (a) copies of the manuscript in microform and/or (b) printed copies of the manuscript made from microform."

Signature

Date


8/19/07

University of Washington

Abstract

Late Quaternary Evolution of Reedy Glacier, Antarctica

Claire E. Todd

Chair of the Supervisory Committee:
Professor John Stone
Earth and Space Sciences

Surface-exposure ages calculated from ^{10}Be concentrations in glacial erratics provide a history of ice-surface elevations along Reedy Glacier from approximately 17 kyr before present (B.P.) through the Holocene. These surface-exposure ages show that the most recent maximum ice thickness at Reedy Glacier occurred at different times at different locations along the glacier. For example, deposits at the Quartz Hills, located 70 m from the head of the glacier, have ages of 17.3 ± 1.1 kyr – 14.3 ± 0.9 kyr B.P., and indicate that the glacier surface was 250 m higher than present during this time. In contrast, deposits at the margin of McCarthy Glacier, a tributary of Reedy Glacier, show that ice thicknesses exceeded modern ice thicknesses by ~200 m from 9.4 ± 0.7 kyr to 8.0 ± 0.5 kyr B.P. Surface-exposure ages from nunataks near the mouth of Reedy Glacier provide a history of ice-surface elevations that begins approximately 7 kyr B.P., but these deposits do not capture the most recent maximum ice-surface elevation as these peaks were overrun by ice during the most recent maximum ice thickness in this area.

The history of ice-surface elevation at the mouth of Reedy Glacier provides a useful constraint on past ice-surface elevations in the southern Ross Sea Sector of the West Antarctic Ice Sheet (WAIS). Improved constraints on ice-surface elevations in

this region are needed to improve ice-sheet reconstructions of the WAIS during the last glacial maximum (LGM). Thus, I develop an inverse procedure to solve for the history of ice-surface elevations at the mouth of Reedy Glacier from surface-exposure-age data. I use an ice-flow model for our forward algorithm. This inverse procedure finds the history of ice-surface elevations that (1) yields glacier surfaces that best match our surface-exposure-age data at a defined tolerance, and (2) is within a range of ice-surface elevations that is physically reasonable. Results suggest that LGM ice thickness at the mouth of Reedy Glacier, in the southern Ross Sea Embayment, was approximately 1000 to 1200 m above modern sea level.

TABLE OF CONTENTS

	Page
List of Figures	ii
List of Tables	iv
Chapter 1: Introduction	1
Chapter 2: Surface-Exposure Ages of Glacial Deposits at Reedy Glacier	7
2.1. Introduction	7
2.2. Glacial Setting	8
2.3. Methods	17
2.4. Results	20
2.5. Discussion	28
2.6. Summary	33
Chapter 3: Forward Algorithm	64
3.1. Introduction	64
3.2. Previous Work	65
3.3. Forward Algorithm Description	66
3.4. Calibration to Present-day Surface Elevations	73
3.5. Discussion	77
Chapter 4: Inverse Algorithm	88
4.1. Introduction	88
4.2. Methods	89
4.3. Previous Work	92
4.4. Application to Reedy Glacier	93
4.5. Procedure	96
4.6. Results	97
4.7. Discussion	110
Chapter 5: Summary	113
References	108
Appendix A: Sliding Algorithm	117
Appendix B: Ice-temperatures at Reedy Glacier	122

LIST OF FIGURES

Figure Number	Page
1.1. Regional map of Reedy Glacier	6
2.1. Till-covered blue ice ablation area at the Quartz Hills	35
2.2. Ice-cored Reedy III deposit at the Quartz Hills	36
2.3. Upper limit of Reedy III deposit at the Quartz Hills	37
2.4. Results from the upper limit of Reedy III deposit at the Quartz Hills	38
2.5. Till-covered blue ice ablation area at the mouth of Reedy Glacier	39
2.6. Till-covered knoll at the margin of the mouth of Reedy Glacier	40
2.7. Erratic lodged in bedrock at the mouth of Reedy Glacier	41
2.8. "Drifting moraine" at the mouth of Reedy Glacier	42
2.9. Erratic deposited on compacted-till surface at the mouth of Reedy Glacier	43
2.10. The northeastern corner of the Quartz Hills	44
2.11. Glacial geologic map of the Quartz Hills	45
2.12. Reedy III deposit in a south-facing gully at the Quartz Hills	46
2.13. Mims Spur and Polygon Spur at the margin of McCarthy Glacier	47
2.14. Ice-cored moraine at Mims Spur	48
2.15. Reedy III deposit at Shapley Ridge	49
2.16. Till-covered blue ice ablation area at Hatcher Bluffs	50
2.17. Upper limit of Reedy III deposit at Hatcher Bluffs	51
2.18. Glacial geologic map of the Caloplaca Hills	52
2.19. USGS oblique air photo showing the Caloplaca Hills	53
2.20. Perched erratics at the Reedy III limit of the Caloplaca Hills	54
2.21. Results from the upper limit of the Reedy III deposit at Mims Spur	55
2.22. Results from the upper limit of the Reedy III deposit at Caloplaca Hills	56
2.23. Results from the recessional Reedy III deposit at the Quartz Hills	57
2.24. Nunataks at Lower Reedy Glacier	58
2.25. Summit of Langford Peak, 25 km from the mouth of Reedy Glacier	59
2.26. Reedy III deposit at Polygon Spur	60
3.1. Map of Reedy Glacier showing sampling sites, and tributary glaciers	79
3.2. Surface-exposure age constraints on ice-thicknesses at Reedy Glacier	80
3.3. Forward algorithm model space	81
3.4. Width of Reedy Glacier	82
3.5. Cross-glacier speed profiles from Reedy Glacier	82
3.6. Calculated bed elevations and observed surface elevations	83

3.7. Ice thicknesses from ice-penetrating radar traverses	83
3.8. Present-day surface mass-balance pattern at Reedy Glacier	84
3.9. Calculated present-day glacier-surface elevations	84
3.10. Mismatch between calculated and observed	85
3.11. Tuning-parameter values used for calculated glacier surface elevations	85
3.12. Calculated and measured ice velocities	86
3.13. Calculated glacier-surface elevations using different bed elevations	86
3.14. Tuning-parameter values using different bed elevations	87
4.1. Calculated ice-surface elevation history	103
4.2. 3.5 kyr B.P. surface	104
4.3. 7.5 kyr B.P. surface	104
4.4. 9 kyr B.P. surface	105
4.5. 10.5 kyr B.P. surface	105
4.6. 12.5 kyr B.P. surface	106
4.7. 15.5 kyr B.P. surface	106
4.8. Comparison of surfaces with number of data	107
4.9. Normalized mismatch	108
4.10. Comparison of surfaces with varying location of data	109
4.11. Calculated glacier surface elevations using modern values	109
A.1. Calculated glacier-surface elevations	119
A.2. Mismatch between calculated and observed glacier-surface elevations	120
A.3. Calculated sliding velocities	121
B.1. Calculated ice-softness parameter values using a conduction model	124

LIST OF TABLES

Table Number

2.1. Surface-exposure ages from the Quartz Hills	61
2.2. Surface-exposure ages from upper Reedy Glacier	62
2.3. Surface-exposure ages from lower Reedy Glacier	63

ACKNOWLEDGEMENTS

I acknowledge the efforts of my committee for their assistance in this project. Fellow graduate students in Earth and Space Sciences provided much-needed support and encouragement, especially Greg Balco, Michelle Koutnik, and Joe MacGregor. As always, I am most indebted to and appreciative of my family for their endless support.

DEDICATION

For my family.

Chapter 1: Introduction

The East Antarctic Ice Sheet (EAIS) and the West Antarctic Ice Sheet (WAIS) play an important role in global climate and ocean circulation, and are important factors in predictions of future sea-level change. The long-term history of the Antarctic ice sheets is not well known, but previous work indicates that past changes in the size of the ice sheets have had significant effects on global sea-level (e.g. Bindschadler, 1998). The EAIS and WAIS currently contain a volume of ice that is equivalent to 57 m of global sea-level rise (Lythe et al., 2001), but past configurations have held as much as 70 m of global sea-level equivalent (Bentley, 1999).

Unlike the EAIS, the WAIS is marine-based; areas of the bedrock beneath the WAIS are more than 2 km below sea level. Theoretical models suggest that marine-based ice sheets are more susceptible to sea-level rise than continental ice sheets (e.g., Weertman, 1974; Schoof, 2007), such as those in Greenland and East Antarctica, where most of the ice sheet is grounded above sea level.

We are motivated to study the WAIS because of its potential to contribute significantly to future sea-level rise. Radar and seismic-reflection data measuring West Antarctic ice thicknesses suggest that the volume of the ice sheet is 5 – 7 m of sea-level equivalent (Lythe et al., 2001). Retreat chronologies, primarily from the Ross Sea sector of the ice sheet, show that currently the WAIS is approximately two-thirds the size of its Last Glacial Maximum (LGM) configuration (Bindschadler et al., 1998). Numerical models of both the EAIS and the WAIS constrain the range of sea-level-rise contributions attributed to these ice sheets to 7.6 – 13.1 m since the LGM (Bentley, 1999). The majority of this contribution is due to ice loss from West Antarctica (Bentley, 1999).

Through this work, we aim to improve constraints on the timing and thickness of the WAIS at the LGM, and also on the timing and nature of subsequent ice-sheet retreat. By enhancing our understanding of the ice-thickness history of the ice sheet, we hope to improve predictions of future ice-sheet behavior.

Due to limited accessibility and availability of ice-free areas, efforts to understand the history of the WAIS have focused on the Ross Sea sector. Specifically, marine geologic studies and glacial geologic studies of glaciers flowing through the Transantarctic Mountains provided some of the earliest constraints on the size and timing of the LGM in West Antarctica. Denton et al. (1989) showed terrestrial evidence of grounded ice in the northwestern Ross Sea as early as 23.8 ± 0.2 k ^{14}C yr before present (B.P.), suggesting that ice advanced first in the western side of the embayment. Subsequent work by Licht et al. (1996) described a less extensive, but earlier ice-sheet maximum in the northwestern Ross Sea based on marine sediment cores. Marine sediment cores from the north central Ross Sea indicate that ice advanced across this area between 21.0 and 16.0 k ^{14}C yr B.P., and reached a maximum extent by approximately 13.5 k ^{14}C yr B.P. (Licht and Andrews, 2002).

Retreat from this maximum was underway by 11.0 ± 0.25 kyr B.P. when marine sediment cores reveal ice-shelf conditions in the northwestern Ross Sea (Licht et al., 1996; Domack et al., 1999; Licht et al., 2004). Conway et al. (1999) summarized additional work inferring grounding-line positions migrating toward the interior of the ice sheet until 3.2 kyr B.P., when ice stratigraphy suggests that the grounding line was still north of Roosevelt Island. The timing of subsequent retreat to the present grounding-line location is not yet known.

Deposits left by glaciers flowing through the Transantarctic Mountains are important indicators of past ice-thickness changes in the EAIS and WAIS. These glaciers drain the northwestern polar plateau in East Antarctica and flow into the Ross Sea Embayment (Figure 1.1). Currently, Reedy Glacier is the only large, Transantarctic-Mountains glacier that flows into grounded ice in the Ross Sea sector of the WAIS, but glacial geologic research shows that larger configurations of glaciers in the Transantarctic Mountains flowed into thick, grounded ice in the Ross Sea Embayment during the LGM (e.g., Mercer, 1968; Denton et al., 1989; Bockheim et al., 1989). Analyses of glacial sediments on the floor of the Ross Sea reveal that the contribution of these glaciers to LGM ice volume in the Ross Sea equaled the contribution of ice flowing from interior West Antarctica (Licht et al., 2005). When grounded ice in the Ross Sea began to retreat from its maximum position at the northern margin of the embayment, glaciers in the Transantarctic Mountains evolved in response to this grounding-line migration (e.g., Mercer, 1968; Denton et al., 1989; Bockheim et al., 1989). As the only large, Transantarctic-Mountains glacier south of the current grounding-line position, Reedy Glacier still responds to changes in ice thickness in the Ross Sea Embayment. In this work, I examine the late Quaternary evolution of Reedy Glacier in order to constrain the ice-thickness history in the southern Ross Sea through the Holocene. A complete ice-thickness history, will improve understanding of the current mass balance of the WAIS by establishing a long-term ice-sheet retreat trend against which short-term observations of ice-sheet mass-balance can be compared.

Surface-exposure-age studies of glacial environments can track the thinning of glaciers through time (e.g. Stone et al., 2003). Glacial deposits accumulate rare, cosmic-

ray-produced nuclides; concentrations of these nuclides can be used to determine the length of time that a rock surface has been exposed to the cosmic-ray flux.

Concentrations of these “cosmogenic nuclides” in erratics collected from different elevations above the glacier, and from different distances along the glacier, record a history of ice thickness. This history enables the reconstruction of glacier surfaces through time.

In this study, we measure cosmogenic ^{10}Be in glacial erratics from Reedy Glacier. Surface-exposure ages calculated from ^{10}Be concentrations in erratics track the history of ice thickness along Reedy Glacier from approximately 17 kyr B.P. through the late Holocene. This history reflects both changes in East Antarctic snow accumulation and changes in grounded-ice thickness downstream from the glacier in the southern Ross Sea. The ice-thickness history at Reedy Glacier provides insight into the deglaciation history of East and West Antarctica. However, due to limited availability of glacially-derived material at accessible and appropriate sampling sites, surface-exposure ages from lateral deposits at Reedy Glacier provide only partial ice-thickness histories for a limited number of locations along the length of the glacier. Specifically, at nunataks near the mouth of Reedy Glacier, where it becomes Mercer Ice Stream, deposits provide a history of ice thickness that begins approximately 7 kyr B.P. Surface-exposure ages from deposits elsewhere along Reedy Glacier show that maximum ice thicknesses occurred prior to this time.

Our goal is to determine the history of ice thickness at the glacier mouth that corresponds to our surface-exposure-age data, in order to constrain the LGM ice

thickness in the southern Ross Sea Embayment. To do so, we develop a numerical procedure to solve for this history.

Solving for an ice-thickness history from surface-exposure ages can be posed as an inverse problem. An inverse problem occurs when there are data that are produced by a known physical process, but the initial conditions or the parameters governing that physical process are unknown. Solving inverse problems requires (1) a forward algorithm that simulates a known physical process, given a set of parameters, (2) a set of observations or data that are the result of the known physical process, (3) an inverse algorithm that calculates estimates of the data by iteratively running the forward algorithm using estimates of the model parameters. The solution to an inverse problem is the set of model parameters that are physically reasonable and that yield results from the forward algorithm that best fit the data at a defined tolerance.

In this inverse procedure, our data are surface-exposure ages, which provide known ice thicknesses at discrete points on the glacier, at different times in the past. The forward algorithm is an ice-flow model that calculates ice thicknesses along the glacier, given a history of ice thickness at the mouth of the glacier. This history of ice thickness at the mouth of Reedy Glacier is our parameter set. Our inverse procedure finds the parameter set that (1) yields glacier surfaces that best match our surface-exposure-age data at a defined tolerance, and (2) is within a range of ice thicknesses that are physically reasonable. This history of ice thickness improves constraints on the LGM ice thickness in the southern Ross Sea.

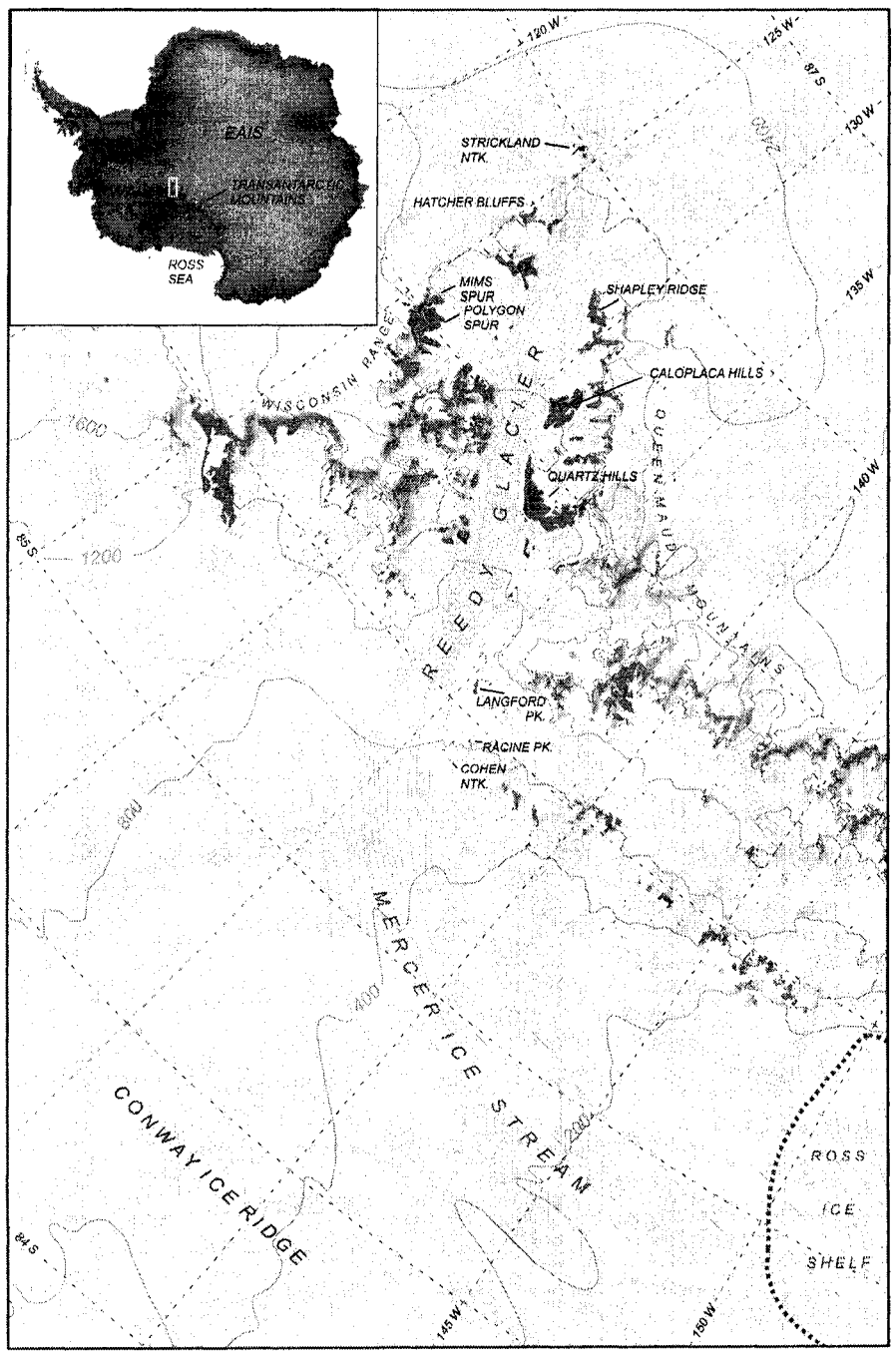


Figure 1.1. Area map of Reedy Glacier, its confluence with Mercer Ice Stream, and approximate grounding-line position. The box on the index map in upper left corner outlines the extent of the area map. Locations of glacial deposits sampled for surface exposure age analysis are labeled. Topography derived from the RAMP-DEM version 2 (Liu et al.,2001). Feature names provided by the Antarctic Digital Database (SCAR, 2002), and USGS topographic maps.

Chapter 2: Surface-exposure Ages from Reedy Glacier, Antarctica

2.1. Introduction

Reedy Glacier is the southernmost, large glacier draining ice from the polar plateau through the Transantarctic Mountains (Figure 1.1). Previous work indicates that the surface profiles of Transantarctic glaciers were strongly influenced by ice thickness in West Antarctica at the Last Glacial Maximum (LGM) (e.g., Bockheim et al., 1989); Mercer (1968) showed that Reedy Glacier been thicker by at least 250 m in the past, but could not date the deposits he described with absolute dating methods available at the time. In this work, we use surface-exposure ages of glacial deposits to constrain the timing of ice thickening and thinning at Reedy Glacier. Reedy Glacier is the only large, Transantarctic glacier still connected to the West Antarctic Ice Sheet (WAIS), and thus its thickness history may reflect changes in the ice sheet through the present day.

Evidence of the thickness and extent of grounded ice in the Ross Sea include deposits from glaciers flowing from the EAIS, through the Transantarctic Mountains, and into the Ross Sea Embayment. Early studies of these glaciers showed that elevations of glacial deposits in the Transantarctic Mountains exceed the current glacier surface by over 1200 m at some locations (Mercer, 1968; Denton et al., 1989; Bockheim et al., 1989), and that glacial thickening relative to the modern glacier surface increases toward the glacier outlet. This asymmetry suggests that the thickness of Transantarctic glaciers is controlled by the thickness of grounded ice in the Ross Sea Embayment, but recent work (e.g., Anderson et al., 2002; Licht et al., 2005) shows that the flux of East Antarctic ice delivered to the Ross Sea Embayment during the LGM was comparable to the flux of

ice delivered from interior West Antarctica. These results indicate that the LGM configuration of glaciers in the Transantarctic Mountains was also influenced by ice-flux from East Antarctica.

In this study, we measure cosmogenic ^{10}Be in glacial erratics from Reedy Glacier. Surface-exposure ages calculated from ^{10}Be concentrations in erratics track the evolution of the surface profile of Reedy Glacier from the LGM configuration to the modern ice surface. This evolution reflects both changes in East Antarctic accumulation and changes in grounded-ice extent in the southern Ross Sea. Thus, by constraining the evolution of the glacier profile from the LGM through the present day, we offer insight into the responses of the EAIS and of the WAIS to deglaciation, and the extent to which Transantarctic glacier profiles reflect these responses. Our ages also help to constrain LGM ice thickness in the southern Ross Sea and to improve constraints on the region's contribution to sea level since the LGM.

2.2. Glacial Setting

2.2.1. Field Area Description

Mercer (1968) established the significance of Reedy Glacier as an indicator of Antarctic Ice Sheet history. He identified three distinct deposits related to former glacial maxima, which he termed Reedy I, Reedy II, and Reedy III. Reedy I and II occur at elevations above Reedy III deposits, and are markedly older than Reedy III (Bromley et al., in prep.). The elevation of Reedy III deposits above the modern glacier surface decreases toward the head of the glacier. Surface exposure ages from this study confirm

the relative ages of the Reedy deposits; Reedy III corresponds to deposits described in Section 4 of this chapter.

Reedy Glacier flows through the southern Transantarctic Mountains, connecting the East and West Antarctic Ice Sheets (Figure 1.1). It originates at the edge of the polar plateau at 86° 30' S and 126° W, and becomes Mercer Ice Stream, in the southeastern corner of the Ross Sea Embayment, at 85° S and 140° W (Figure 1.1). The total length of the glacier is 140 km. Ice surface elevation ranges from nearly 2000 m above sea level (asl) at the head of the glacier, to 600 m asl at the glacier mouth.

The glacier is flanked by the Wisconsin Range on its eastern margins and by the Queen Maud Mountains to the west. Elevations in these mountain ranges exceed 2000 m asl. Glacier width varies from nearly 20 km at its head and mouth, to 9 km in the middle of the glacier's length. In this area, the glacier flows for 15 km past cliffs exceeding the elevation of the glacier's western margin by 200 to 600 m. Elsewhere along the glacier's length, ice-free peaks, known as nunataks, slope more gently toward the glacier margins. These nunataks closely flank the glacier at the head, but at the mouth of the glacier, in the foothills of the Transantarctic Mountains, there are fewer emerging peaks at the glacier margin. In this area, some of the nunataks that we sampled are more removed from the present glacier flow.

Analysis of the RAMP-DEM digital elevation dataset (Liu, et al. 2001) shows that Reedy Glacier drains approximately 25,000 km² of the polar plateau. The glacier catchment extends to within 200 km of the South Pole. We measured ice thicknesses at Reedy Glacier of up to 2 km using ground-penetrating radar. Repeat GPS measurements of survey poles indicate a center-line velocity of 170 m/yr at the Quartz Hills. Velocities

decrease only slightly in adjacent transect measurements, but fall sharply to less than 50 m/yr near the shear margin. Ice surface velocities measured from synthetic aperture radar data (Joughin et al., 2002) show centerline velocities of Reedy Glacier range from 100 – 200 m/yr.

Several tributary glaciers flow into Reedy Glacier (Figure 1.1). The largest tributary is the Kansas Glacier, which joins the glacier 100 km from the glacier head. Smaller tributaries also join Reedy Glacier, but contribute only a small fraction of the overall ice flux through Reedy Glacier. Repeat GPS measurements of a survey pole in Colorado Glacier, which meets the mid-point of Reedy Glacier at the Quartz Hills, indicated little surface ice-flow toward Reedy Glacier over one year; ice-penetrating radar measurements at Wotkyns Glacier, located at the northern edge of the Caloplaca Hills, reveal an ice thickness of only 750 m. Flowlines visible on aerial photos and satellite images, as well as the limited catchments of these tributaries, support these measurements, indicating that small tributaries make only a small contribution to the overall ice flux of Reedy Glacier.

Accumulation and ablation vary dramatically along the length and across the width of Reedy Glacier. Pole measurements in a blue-ice ablation area covering the middle 50 km of the glacier length show ablation values ranged from 19 - 25 cm over one year. However, aerial photos taken of the area in the 1950s and 1960s show areas of accumulation elsewhere on the glacier surface. We attribute these patterns to katabatic winds, which were observed during our field seasons, and reported from previous field campaigns (e.g. Mercer, 1968; Denton et al., 1989).

2.2.2. Depositional processes and modern-day deposits

Deposition of glacially-transported erratics at Reedy Glacier is dominated by delivery of sub-glacially transported material to the glacier margin by blue-ice ablation fields. In these ablation fields, convergence of flow lines concentrates thin layers of till on the glacier surface. When the glacier surface is in steady-state, ice loss due to ablation is replaced entirely by ice flow from the glacier trunk, causing transport of glacially-derived material to the glacier surface. When ice loss due to ablation exceeds replacement ice flow, the glacier surface lowers, stranding till on underlying topography. The lowered till-layer isolates glacier ice as the glacier margin retreats during ice thinning. This process produces drape-like, ice-cored deposits at elevations above the glacier surface.

At the foot of the Quartz Hills, 70 km from the head of the glacier, a medial moraine originates in a till-covered blue-ice ablation area at the confluence of Reedy and Colorado Glaciers (Figure 2.1). The till cover contains glacially-sculpted erratics that are unweathered and that range in size from sand to large boulders. Till-cover thickness ranges from cm at its margins, to up to 1 m-high moraines and mounds in its interior. An ice-cored drape-like deposit (Figure 2.2) covers a bedrock bench at elevations approximately 100 – 250 m above this till-covered blue-ice ablation area (Figure 2.3), and suggests that an analog to the deposit on the current glacier surface existed in the past. Surface exposure ages of erratics from the upper limit of the ice-cored deposit show ice remained at that elevation from 17.3 ± 1.1 until 14.3 ± 0.9 kyr B.P.; erratics collected from below the maximum elevation yield surface exposure ages both coincident with this maximum thickness, and indicative of ice-margin retreat (Figure 2.4). This result suggests that exposure of erratics during maximum ice thickness occurred in a blue-ice

ablation field similar to the blue-ice ablation field observed on the current glacier surface. This accumulation of material resulted in maximum-age erratics accumulating both at the margin, and at some distance from the margin of the maximum ice surface. Subsequent lowering of the ice surface stranded this maximum-age material at elevations below the maximum ice elevation.

At the mouth of Reedy Glacier, we observed three types of deposits: (1) drapes of glacially-derived material in blue-ice ablation areas between emerging nunataks (Figure 2.5), (2) drapes of glacially-derived material, indicative of accumulation in blue-ice ablation fields, covering low-elevation nunataks (Figure 2.6), and (3) sparsely scattered erratics lodged in bedrock on or near the peaks of nunataks (Figure 2.7).

We interpret the first type of deposit, drapes of glacially-derived material present on the ice surface or “drifting moraines,” to be precursors of the second, drapes of glacially-derived material covering low-elevation nunataks. Surface exposure ages of two erratics collected from a low-elevation nunatak at the glacier margin (Figure 2.7) show that the erratics emerged at 3.7 ± 0.3 kyr B.P., while analysis of two erratics from a “drifting moraine” located ~ 1 km from modern glacier margin (Figures 2.6, 2.9) yield surface exposure ages of 0.290 ± 0.05 kyr and 0.330 ± 0.05 kyr B.P.

These low-elevation, continuous, drape-like deposits contrast with deposits found at higher elevations at the mouth of the glacier. These higher-elevation deposits are characterized by isolated erratics lodged on bedrock and compacted till surfaces on nunatak peaks (Figure 2.10). We attribute these deposits to lodging of erratics by basal ice flow against obstructions at the glacier bed. This is consistent with the different flow regime and topography at the mouth of Reedy Glacier, where thick ice covered subglacial

topography and flowlines diverged as the glacier widened during maximum ice thickness. Subsequent ice thinning thus exposed a very sparse distribution of erratic material on nunatak flanks. Surface exposure ages show that the lowering glacier surface exposed erratics on nunatak peaks, 1060 – 745 m asl, ~ 7 kyr B.P.

The difference between deposits on nunatak peaks and deposits close to the present glacier surface suggest a Holocene shift in the deposition regime at the mouth of Reedy Glacier. Prior to the Holocene, Reedy Glacier was thicker and over 6 km wider at its mouth. This expanded version of the present-day glacier lodged a thin distribution of sub-glacially transported material on the summits and flanks of nunataks. During the Holocene, the surface of Reedy Glacier lowered below nunatak peaks, narrowing glacier flow to the eastern side of the nunataks (Figure 1.1).

2.2.3. Reedy III Deposits

Mercer (1968) described three different deposits related to former glacial maxima at Reedy Glacier: Reedy I, Reedy II, and Reedy III. Reedy I and II occur at elevations above Reedy III deposits, and are markedly older than Reedy III (Bromley et al., in prep.). The goal of our work is to date the most recent glacial high-stands at Reedy Glacier, and so we do not discuss Reedy I and II deposits in this thesis. In this section, we describe the Reedy III deposits; surface exposure ages from these deposits are reported in Section 4. We use the term 'Reedy III' to indicate deposits marking the most recent glacial high-stands at different locations at Reedy Glacier.

2.2.3.1. Quartz Hills

We collected samples from five glacial deposits that correspond to Mercer's Reedy III designation. The largest of these deposits is located at the Quartz Hills (Figure 1.1). The Quartz Hills border Reedy Glacier for 15 km on its western margin approximately 70 km from the glacier head. In this location, the Reedy III deposit covers a broad, bedrock bench that rises 200 m above the confluence of the Reedy and Colorado Glaciers (Figure 2.11). The interior of this deposit is ice-cored and is over ten centimeters thick in places, completely covering the surface beneath. Closer to the edge of the bench, near the modern margin of Reedy Glacier, the deposit thins. Here, Reedy III erratics are scattered across a compacted till surface. The extent of the deposit in the Quartz Hills shows that Reedy Glacier overtopped the bedrock bench and widened by over 1 km, covering the northeastern corner of the nunatak (Figure 2.12). The elevation of the upper limit ranges from 1410 m asl to 1359 m asl, which is 200 – 250 m above the modern glacier surface. These elevations decrease with distance away from the glacier trunk and show an expanded Reedy Glacier flowed into what is now the Colorado Glacier valley (Figure 2.12).

Erratics deposited at elevations below the upper limit are relatively well-preserved and unweathered. In contrast, at elevations above this limit, erratics are more sparsely distributed and heavily weathered, with surfaces that exhibit staining, spalling, and pitting. Reedy III material in a steep gully 1 km up the glacier from the margin described above shows that Reedy Glacier thickened over 200 m, overtopping a ~100 m-wide, south-facing gully (Figure 2.12, 2.13). We did not sample the margin of this southern maximum ice extent for surface-exposure-age analysis. However, surface-exposure ages

of erratics collected from a cliff face in the gully show that this material was deposited in concert with the deposit evidenced on the northeastern corner of the Quartz Hills.

2.2.3.2. Mims Spur

Mims Spur is a spur of the Wisconsin Plateau which descends along the northern margin of McCarthy Glacier, in the direction of its confluence with Olentangy Glacier (Figure 2.14). The Reedy III deposit at Mims Spur parallels the present-day surface of McCarthy Glacier and indicates glacier-surface elevations almost 200 m greater than present-day glacier-surface elevations. The upper limit of this deposit decreases from 2034 m asl at the head of McCarthy Glacier, to 1936 m asl at the front of the spur. The number of erratics present at this margin increases in the direction of glacier flow. As is the case on the glacier surface today, the number of erratics present at the paleo-margin is greatest where ice flowed around the front of the spur. At higher elevations, at the head of McCarthy Glacier, the deposit is defined by a line of single, sparsely distributed erratics; at the front of the spur, the margin is marked by a small, 2 m-high ice-cored moraine (Figure 2.15).

2.2.3.2. Shapley Ridge

The Reedy III deposit at Shapley Ridge, 20 km from the head of the glacier, is a less than one-clast thick, extensive, continuous deposit with a distinct upper limit (Figure 2.16). This deposit shows that the surface elevations of Reedy Glacier exceeded the modern ice surface by approximately 100 m, and that the glacier width expanded to fill a cirque now nearly 3 km from the present-day glacier shear margin. This deposit is nearly

homogenous in lithology, and this lithology was not observed at any other locations we studied. This observation, and the presence of more widely distributed lithologies found at other sampling sites, suggests that erosive basal conditions at Reedy Glacier are localized.

2.2.3.4. Hatcher Bluffs

Hatcher Bluffs is a nunatak near the head of Reedy Glacier (Figure 1.1). While the modern ice surface below the bluffs is covered with till, the only evidence of a formerly greater ice thickness is a few relatively unweathered erratics perched on a narrow, steep-sided, weathered bedrock ridge 50 m above the modern ice surface (Figures 2.17, 2.18). Above this elevation, we found no erratics or other evidence of glacial deposition. The absence of more Reedy III material at this location can be attributed to the narrow, steep-sided ridge, which would strand only a narrow section of a till-layer on a lowering ice-surface.

2.2.3.5. Caloplaca Hills

A Reedy III deposit is also present at Caloplaca Hills, a smaller nunatak located 45 km from the head of Reedy glacier, at the confluence of Wotkyns and Reedy Glaciers (Figure 2.19). This deposit indicates ice from Wotkyns Glacier flowed northeast around the Caloplaca Hills and into a valley parallel to Reedy Glacier (Figure 2.20). At the head of the valley, a continuous deposit of relatively unweathered, glacially-transported material is present up to 1529 m asl, approximately 130 m above the modern ice surface.

This upper limit is marked by weathered, embedded boulders topped with perched, relatively unweathered erratics (Figure 21).

2.2.3.6. Lower Reedy Glacier

At the mouth of Reedy Glacier, there are no deposits recording the upper limit of the past, thicker configurations evidenced by glacial deposits upstream. In this area, where Reedy Glacier flows through the foothills of the Transantarctic Mountains, the topography is more subdued than in the middle and upper sections of the glacier. The difference in elevation between Reedy III deposits and the modern glacier surface increases from Hatcher Bluffs to Quartz Hills, and likely continued to increase toward the mouth of the glacier. Thus, we infer that ice thicknesses at the mouth of the glacier must have exceeded the modern glacier surface by at least 250 m, the amount of thickening observed at the Quartz Hills. The presence of glacially sculpted erratics on nunataks currently located at the glacier margin and up to 7 km away from the glacier margin suggests Reedy Glacier was also much wider at its mouth during this maximum.

2.3. Methods

Cosmic-ray bombardment of rock surfaces produces rare nuclides within mineral lattices. Concentrations of these nuclides can be used to determine the length of time that a rock surface has been exposed to the cosmic-ray flux. In this study, we measured cosmogenic ^{10}Be concentrations in glacial erratics exposed by thinning or retreating ice at Reedy Glacier. Concentrations in erratics collected from different elevations above the glacier, and from different distances along the glacier, record a history of glacier-margin

positions. This history enables the reconstruction of glacier-profile evolution since the LGM.

Surface-exposure dating requires continuous exposure to the cosmic ray flux without prior exposure, burial, or change in the exposure geometry. These requirements can be problematic in polar glacial deposits due to delivery and deposition of erratic material in large blue-ice ablation fields at glacier margins. When ablation exceeds the replacement of ice from upstream, ice surface elevations decrease, often stranding an ice-core beneath erratic material accumulated at the ice surface. Slow ablation of this ice core, long after the ice margin has left the elevation of the deposit, can result in settling and disturbance of glacial deposits, and emergence of additional glacial erratics.

To avoid samples disturbed after deposition, we collected from flat, stable surfaces to ensure nuclide concentrations represent continuous exposure since deposition. We avoided areas showing evidence of post-depositional settling, sampling only erratics resting directly on bedrock, on compacted pre-existing pavements, or perched on the top faces of large boulders.

Snow cover can shield samples from the cosmic ray flux and cause a lower nuclide concentration than continuous exposure would otherwise produce. If snow cover occurred but is unaccounted for, surface exposure ages will be underestimated. We address this concern by sampling snow-free locations, and avoiding areas near the margins of snow tails or snow fields. Because most of the deposits we sampled are attributable to katabatic wind-driven ablation, we generally observed little snow accumulation in these exposed areas. Snow tails and snow fields are present in some shielded locations. Air photos taken in 1960 show only slight variation in the distribution

and size of these deposits over the last forty years. We have no information on the longer-term history of snow cover in this region, but the constancy of large-scale topographic features that establish the katabatic wind field, such as the polar plateau and the Transantarctic Mountains, may have preserved the modern accumulation and ablation patterns since the LGM (King & Turner, 1997; Bromwich & Parish, 1998).

There is no evidence of significant supraglacial transport of rocks at Reedy Glacier, but to ensure that we collected sub-glacially derived material with no prior exposure we sampled only faceted, shaped, and abraded erratics. Previous Antarctic surface exposure age datasets suggest it is difficult to avoid "pre-exposed" samples entirely because glacial deposits survive multiple glaciations (Stone et al., 2003; Sugden et al., 2004). Thus, we also evaluated potential samples based on relative surficial weathering. We preferentially selected samples that appeared to have survived only one post-glacial period of subaerial exposure.

We analyzed 81 glacial erratics. We selected coarse-grained samples, as this texture facilitates extraction of quartz for ^{10}Be analysis. Erratic thicknesses and the surrounding topography were recorded to correct for any shielding of samples from the cosmic ray flux; these corrections are shown in Tables 2.1-2.3. We measured surrounding topography using digitized images captured by a fisheye lens. To accurately quantify atmospheric shielding, sample elevations were measured using a barometer; these measurements were corrected using daily calibration to GPS measurements accurate to ± 1 m.

In preparation for ^{10}Be analysis, we isolated quartz using heavy-liquid mineral separation and by etching samples with dilute hydrofluoric acid, as described by Kohl

and Nishiizumi (1992). We extracted ^{10}Be from quartz using a procedure developed by Ditchburn and Whitehead (1994). Isotope ratios were measured at the Lawrence Livermore National Laboratory Center for Accelerator Mass Spectrometry and Purdue Rare Isotope Measurement Laboratory. We calculate exposure ages using production rates scaled with latitude and with altitude (Lal, 1991; Stone, 2000). Given the well-preserved, fractured and faceted surfaces of the samples, we assume that samples have not eroded since deposition.

2.4. Results

2.4.1. Surface-exposure ages of the upper limit of Reedy III deposits

Surface-exposure ages of glacial deposits show that Reedy Glacier and its tributaries reached maximum ice thickness at different times at different locations on the glacier (Tables 2.1-2.3). The earliest maximum had occurred by 17.3 ± 1.1 kyr B.P., and is recorded by deposits at the Quartz Hills, 70 km from the head of the glacier. Glacier thinning from this maximum ice thickness was underway during the early Holocene, when ice-surface elevations near the head of the glacier were increasing.

The Reedy III deposit at the Quartz Hills extends to 250 m above the modern glacier surface. Six of twelve surface exposure ages from the upper limit of this deposit indicate maximum ice thickness persisted for at least ~ 3 kyr, lasting from 17.3 ± 1.1 or earlier to 14.3 ± 0.9 kyr B.P. or later. The other six samples collected from the upper limit of the deposit yield surface-exposure ages that vary by over sixty thousand years and that greatly exceed the six ages ranging from $17.3 \pm 1.1 - 14.3 \pm 0.9$ kyr B.P. maximum (Figure 2.21). We interpret these disparate results as evidence of prior

exposure either in the Quartz Hills or at another location upglacier. The depth of this deposit also suggests that much of the material was present in the Quartz Hills prior to ice advance, and was simply reworked *in situ*. However, the tight cluster of the younger surface-exposure ages from the upper limit of the deposit confirms that ice stood at the upper limit of the Reedy III deposit in the Quartz Hills from at least $17.3 \pm 1.1 - 14.3 \pm 0.9$ kyr B.P.

Although we did not analyze samples from the Reedy III deposit at Shapley Ridge, 50 km up glacier from Quartz Hills, the extent and elevation of this deposit is similar to the Reedy III deposit at the Quartz Hills. Surface-exposure-age results from emerging nunataks at the mouth of the glacier suggest Reedy Glacier ice overrode these locations during this time period.

Surface exposure ages from the upper limit of the Reedy III deposit in the Caloplaca Hills show ice from Wotkyns Glacier, a 15 km-long tributary of Reedy Glacier, achieved a maximum thickness before 15.5 ± 1.0 kyr B.P. and remained at this maximum elevation until 10.8 ± 0.8 kyr B.P. (Figure 2.22). This timing lags the timing of the advance and retreat of Reedy Glacier evidenced at the Quartz Hills. Although these data provide only minimum age control for the onset of maximum ice thickness and only maximum age control for retreat from the maximum elevations, it is possible that ice advanced and retreated in these locations in response to the same forcing. Modern surface-velocity data and ice-penetrating radar show Wotkyns Glacier contributes only a small flux of ice to Reedy Glacier flow. Deposits in the Caloplaca Hills are derived from Wotkyns Glacier. The oldest ages here indicate that this glacier thickened at the same time as Reedy Glacier thickening measured at the Quartz Hills. The ~ 11 kyr B.P. age

indicates that Wotkyns Glacier remained at maximum thickness after Reedy Glacier ice began to thin at the Quartz Hills.

Results from the Reedy III deposit at Mims Spur (Figure 2.23) show that maximum ice thickness occurred at McCarthy Glacier several thousand years after the initial glacial maximum observed at the Quartz Hills. Surface-exposure ages from this maximum deposit at Mims Spur show that ice flowing off the Wisconsin Plateau into McCarthy Glacier reached a maximum thickness by 9.4 ± 0.7 kyr B.P. These data set a minimum timing constraint on the maximum ice thickness at Mims Spur. Exposure ages of samples collected further up the glacier show that this maximum ice thickness persisted as late as 8.0 ± 0.5 kyr B.P. There is no evidence of a contemporaneous maximum at $9.4 \pm 0.7 - 8.0 \pm 0.5$ kyr B.P. occurring elsewhere along the glacier. Surface-exposure ages of deposits at Quartz Hills and Caloplaca Hills show that ice had already retreated from maximum elevations by that time. Given the minimal contribution of McCarthy Glacier to present-day Reedy Glacier flow, it is possible that increased ice thicknesses at McCarthy Glacier might not cause thickening down glacier along the main trunk of Reedy Glacier. It seems unlikely, however, that an increase in accumulation on the Wisconsin Plateau large enough to cause 200 m of thickening at Mims Spur, would not also occur in Reedy Glacier's larger, adjacent catchment. Surface exposure ages discussed in the following section show that a slightly later maximum occurred at the head of Reedy Glacier; this maximum might reflect a delayed response at Reedy Glacier to the same accumulation increase that caused a 9,000 year B.P. maximum at McCarthy Glacier.

The most recent ice thickening apparent in surface-exposure age data from Reedy Glacier is evident at Hatcher Bluffs, a nunatak at the head of the glacier (Figure 1.1). An exposure age of one erratic collected there suggests that a maximum ice surface exceeded the modern ice surface by at least 50 m, at 7.5 ± 0.5 kyr B.P. A second sample shows that ice remained at this elevation until 3.7 ± 0.3 kyr B.P. These samples were the highest occurrence of glacially-derived material on a narrow, steep-sided, weathered bedrock ridge, which accumulated only a few relatively unweathered erratics during the maximum. On the modern ice surface below, a thick drape of erratic material covers a blue ice ablation area that surrounds the ridge (Figure 2.16). A sample collected 13 m below the highest erratics yielded a surface exposure age of 4.7 ± 0.5 kyr B.P. We attribute this result to exposure in the blue-ice ablation field during maximum ice thickness. When ice retreated and thinned from this maximum, the lowering ice surface stranded this sample on the emerging nunatak below.

We find no evidence of this recent ice thickening at other sampling locations along Reedy Glacier. Surface-exposure age data show that ice had retreated from maximum elevations at other locations by this time. Results discussed in the following section indicate that a steady retreat of ice at the mouth of Reedy Glacier was underway by approximately 7.8 ± 0.5 kyr B.P.

2.4.2. Surface-exposure ages of recessional deposits at Reedy Glacier

2.4.2.1. Recessional deposits at the Quartz Hills

In order to date the retreat of ice from its maximum position at the Quartz Hills, we collected erratics from elevations below the upper margin of the maximum deposit.

Surface-exposure ages of erratics collected from these lower elevations document two processes: (1) retreat of the glacier margin from its maximum extent, and (2) lowering of the large blue-ice ablation field that accumulated at the margin during the $17.3 \pm 1.1 - 14.3 \pm 0.9$ kyr B.P. maximum ice thickness (Figure 2.24). These two processes, glacier margin retreat and glacier thinning, co-mingle erratics with different surface-exposure ages at the same elevation. It is helpful to divide these surface-exposure ages into three groups. First, we interpret erratics yielding ages between $17.3 \pm 1.1 - 14.3 \pm 0.9$ kyr B.P. as evidence of a blue-ice ablation field that extended some distance from the glacier margin during the glacial maximum. These erratics were then exposed on the ice surface during the glacial maximum, but were not deposited until after the maximum when the ice ablated down to the elevation of bedrock below. Second, erratics with ages younger than the timing of the glacial maximum were exposed by ice-margin retreat, which uncovered a compacted-till surface and erratics as ice thinned from its maximum elevation. It is also possible that these younger surface-exposure ages are due to exposure on the thinning ice surface after the maximum ice thickness, and subsequent deposition on the compacted till surface as the ice thinned. Third, for surface-exposure ages that greatly exceed the age of maximum ice thickness in the Quartz Hills, we assume that previous exposure occurred prior to the maximum, either at the Quartz Hills or elsewhere up glacier.

The ages in the second group constrain the timing of retreat from the maximum position. At each elevation, the youngest surface-exposure age is a maximum limit on the age of ice retreat. Likewise, the highest erratic of a given age sets a minimum limit on ice thickness at that time. The range of ages at each elevation indicates that these rocks were

exposed before deposition. Thus, we can say that the minimum elevation of the ice margin decreased from 1310 m asl at 9.0 ± 0.9 kyr B.P., to 1272 m asl, at 7.1 ± 0.6 kyr B.P. This is not a tight constraint on the ice-margin location during retreat. Nevertheless, the lack of "young" exposure ages at the upper limit of the deposit, and the lack of ages younger than 7.1 ± 0.6 kyr B.P at elevations above 1272 m asl suggests that the ice surface had thinned by over 100 m from its maximum elevation in the Quartz Hills by 7.1 ± 0.6 kyr B.P.

2.4.2.2. Recessional deposits at lower Reedy Glacier

At nunataks near the mouth of Reedy Glacier (Figure 2.25), there are no deposits indicative of a maximum ice thickness. Our results show that these peaks were overrun by a thicker configuration of Reedy Glacier, as surface-exposure ages of erratics collected at the mouth of Reedy Glacier are younger than surface-exposure ages associated with the glacial maxima evidenced up glacier (Tables 2.1-2.3). Erratics stranded on nunatak flanks in this area yield surface-exposure ages indicative of mid- to late-Holocene ice thinning. These ages continue the thinning history described by surface-exposure ages of erratics at the Quartz Hills, which indicate ice had thinned by ~100 m from 14.3 ± 0.9 kyr to 7.1 ± 0.6 kyr B.P.

Surface-exposure ages of two erratics from Langford Peak (Figures 1.1, 2.26), located 110 km downglacier from the Quartz Hills and 30 km from the glacier outlet, show that the peak had emerged by 7.5 ± 0.5 kyr B.P. A sample collected from 120 m below the maximum ice elevation in the Quartz Hills yields a similar surface-exposure age of 7.6 ± 0.5 kyr B.P. Based on these results, we estimate an approximate surface

slope for lower Reedy Glacier of 5.5 m/km at this time. Comparison with the modern glacier slope of 7.9 m/km supports upstream evidence of asymmetric thinning, and suggests that this asymmetry extended to the glacier outlet. Thus, the post-glacial history recorded by erratics at Reedy Glacier show the surface profile of the glacier steepened through the mid-Holocene. This history is supported by results discussed in Chapter 4. Evidence for shallower glacier profiles during glacial maxima in the Transantarctic Mountains has been observed by others (e.g. Mercer, 1968; Denton et al., 1989; Bockheim et al., 1989), who also hypothesized that asymmetric thickening observed at the upper and middle section of these glaciers likely extended to the glacier outlets.

Erratics from nunataks further down glacier, at the confluence of Reedy Glacier and Mercer Ice Stream, reveal that a wider configuration of Reedy Glacier persisted through the mid-Holocene. Surface-exposure ages of erratics from Racine Nunatak and from an unnamed nunatak (Figure 1.1), located 6 and 2.5 km from the modern glacier margin, respectively, document ice thinning that is consistent with ice thinning recorded at the Quartz Hills and at Langford Peak. These ages show the summits of Racine Nunatak (853 m asl) and of the unnamed nunatak (898 m asl) emerged by 7.6 ± 0.5 kyr and 7.0 ± 0.5 kyr B.P., respectively. Subsequent glacier retreat from these elevations is best recorded at Cohen Nunatak, located ~ 5 km down glacier and only 2 km from the modern glacier margin (Figure 1.1). Erratics at the summit and on the flanks of Cohen Nunatak suggest that the glacier surface thinned from 745 m asl at 6.9 ± 0.5 kyr B.P., to the present ice margin (641 m asl) at 1.5 ± 0.2 kyr B.P. The emergence of nunatak peaks located 25 – 5 km from the mouth of the glacier within the past 1000 years indicates rapid, regional lowering of the glacier surface.

Surface-exposure ages of glacial erratics collected near the mouth of Reedy Glacier also indicate the preservation of a convex glacier transect profile since the mid-Holocene. The surface of the lower half of Reedy Glacier is currently marked by increases of tens of meters from the edge of glacier flow to the glacier centerline. Erratics collected from similar elevations at the mouth of Reedy Glacier yield different surface-exposure ages depending on the proximity of the sample location to the modern glacier centerline. For example, an erratic from the summit of Cohen Nunatak (745 m asl) yielded a surface-exposure age of 6.9 ± 0.5 kyr B.P., compared to surface-exposure ages of ~ 0.5 kyr B.P. for samples collected from similar elevations at the modern glacier margin. Thus, ages from the mouth of the glacier record not only thinning of the glacier surface, but also migration of the glacier margin as the glacier width decreased from at least 34 km to its current value of 28 km.

Surface-exposure ages of two erratics collected from the top of a knoll standing 7 m above the glacier margin show that the erratics emerged at the ice surface 3.7 ± 0.2 kyr B.P. Erratics at the glacier margin at this and other nunataks indicate a more recent change in the elevation of the glacier surface. Five erratics collected from four nunataks at the glacier margin yield surface-exposure ages ranging from 0.83 ± 0.08 kyr to 0.52 ± 0.07 kyr B.P. These erratics were collected at the base of nunataks in the glacier shear margin, at elevations ranging from 5 to 20 m above the local ice surface.

2.4.2.2. Recessional deposits at Polygon Spur

We also analyzed four erratics collected from a broad, fractured bedrock bench at Polygon Spur, located at the confluence of the McCarthy and Olentangy Glaciers

(Figures 1.1, 2.14). Samples were within a diffuse deposit of unweathered erratics; there is no geomorphic evidence of a maximum ice extent at this location (Figure 2.27). We assume that these erratics were exposed by ice-margin retreat across the bench from a maximum ice extent closer to the interior of Polygon Spur. The bench surface is at 1660 m asl, approximately 30 m above the ice margin at the foot of the bench. Two of the four erratics collected from this location yielded exposure ages greater than the glacial maximum that occurred from $9.4 \pm 0.7 - 8.0 \pm 0.5$ kyr B.P. at adjoining Mims Spur (Table 2.2). We assume that ^{10}Be concentrations in these two "older" samples result from previous exposure at Polygon Spur or at a location upglacier from this sampling site. Two of the four samples collected from the bench yielded ages of 6.7 ± 0.7 kyr and 5.6 ± 0.5 kyr B.P. This is consistent with evidence that retreat from the maximum ice thickness at Mims Spur occurred after 8.0 ± 0.5 kyr B.P.

2.5. Discussion

2.5.1. Glacier-profile evolution

Asynchronous ice thinning at Reedy Glacier contradicts previous work suggesting that glaciers in the Transantarctic Mountains equilibrate quickly to perturbations in glacier slope and accumulation (e.g., Anderson et al. 2005). It is possible that the mid-Holocene thickening documented at the head of Reedy Glacier is due to an increase in accumulation across the polar plateau, but this thickening is not recorded elsewhere on the glacier. It is also possible that this thickening signal was overwhelmed elsewhere along the glacier by significant ice retreat and thinning in the Ross Sea during this time. Indeed, surface-exposure ages at Quartz Hills and at nunataks at the mouth of the glacier

indicate substantial and rapid ice thinning during mid-Holocene ice sheet retreat in the Ross Sea Embayment (reviewed by Conway et al., 1999). These results show that the glacier profile steepened dramatically through the Holocene. This steepening could be due to simultaneous post-glacial increases in accumulation in East Antarctica and grounding-line retreat in West Antarctica. It is also possible that we did not capture the maximum age of maximum ice thickness at the head of Reedy Glacier, and the steepening of the glacier profile is due to propagation of thinning upglacier from the glacier mouth.

2.5.2. East Antarctic and West Antarctic Influence on Reedy Glacier

Surface-exposure ages of glacial deposits at Reedy Glacier indicate that ice thickness along the glacier is controlled by changes in the thickness of both the EAIS and the WAIS. The thickness of the WAIS has changed significantly during the late Quaternary. Flowlines inferred from reconstructions of the WAIS at the LGM (e.g., Denton & Hughes, 2002) suggest that ice originating from Reedy Glacier area at this time flowed into the central Ross Sea, where Licht et al. (2005) found evidence of both East and West Antarctic ice sources. Additional marine geologic evidence shows that grounded ice advanced to the inner shelf of the central Ross Sea Embayment 17.8 ± 1 ¹⁴C kyr B.P. (Licht et al., 2004). In the northwestern Ross Sea, marine geologic evidence shows that the maximum ice position was due to advance of East Antarctic ice through glacier valleys in the northern Transantarctic Mountains (e.g., Anderson et al., 2002; Licht et al., 2005). These advances may correlate with the $17.3 \pm 1.1 - 14.3 \pm 0.9$ kyr

B.P. maximum ice thickness observed at the Quartz Hills. However, uncertainties in both datasets prevent a definitive correlation.

Analysis of erratics collected from the mouth of Reedy Glacier offer additional insight into the LGM and post-LGM history of the WAIS. Surface-exposure ages show that (1) the ice surface was only approximately 100 m thicker approximately 7 kyr B.P. suggesting that the overall thickening attributed to the LGM was only a few hundred meters above the modern ice surface, and (2) nunatak peaks, ranging from 898 m asl to 745 m asl at the mouth of Reedy Glacier emerged at approximately the same time, suggesting a rapid thinning of the ice surface. Evidence of a relatively thin LGM configuration supports recent work by Waddington et al. (2005) that showed that the LGM ice surface at Siple Dome, located in the central Ross Sea Embayment, was only 200 – 400 m higher than the current ice surface. Evidence of rapid ice thinning at the glacier mouth supports results from a thermo-mechanical model of ice flow and ice thickness history at Siple Dome that suggest that ice stream acceleration led to 350 m of thinning at Siple Dome between 15 and 14 kyr B.P. (Price et al., *in press*).

The maximum ice thickness occurring at $9.4 \pm 0.7 - 8.0 \pm 0.5$ kyr B.P., at the margin of McCarthy Glacier, suggests a sensitivity of glaciers in the Transantarctic Mountains to changes in accumulation on the polar plateau. This maximum is not apparent elsewhere at Reedy Glacier; in fact, deposits show that ice is thinning at the lower half of Reedy Glacier during this time. The most recent maximum ice thickness at Reedy Glacier, occurring at $7.5 \pm 0.6 - 3.7 \pm 0.3$ kyr B.P., is evidenced in a sparse deposit at the head of Reedy Glacier, but is also not observed elsewhere at Reedy Glacier. The absence of evidence for a response to this thickening further down glacier is likely

due to significant grounding-line retreat in the Ross Sea Embayment during this time period. We are unable to confidently attribute either of these maxima to regional accumulation increases in East Antarctica because the accumulation history in interior East Antarctica is not well known.

2.5.3. West Antarctic Influence on Glacial Retreat at Lower Reedy Glacier

The glacial retreat history observed at the lower half of Reedy Glacier parallels mid- to late- Holocene retreat of the WAIS in the Ross Sea Embayment. Surface exposure ages from below the maximum ice limit in the Quartz Hills suggest that ice had left the maximum position by ~ 9 kyr B.P. By this time, grounded ice in the Ross Sea Embayment had also left its maximum position on the continental shelf (Conway et al., 1999). By 7.1 ± 0.6 kyr B.P., ice elevations at the Quartz Hills had decreased from a maximum of ~ 250 m above the modern ice surface to less than 150 m above the modern ice surface; the ice surface at the mouth of the glacier was less than 200 m above the modern ice surface by 7.0 ± 0.5 kyr B.P. The grounding-line in the Ross Sea Embayment also continued to retreat at this time, migrating south of McMurdo Sound. At this point, the grounding line in the Ross Sea was south of McMurdo Sound and north of Hatherton Glacier (Conway, et al., 1999). The emergence of the summit of Cohen Nunatak, which is 745 m asl and 104 m above the ice margin at the nunatak base, at 6.9 ± 0.5 kyr B.P. approximately coincides with the migration of the grounding line further south, past Hatherton Glacier. This shows that over half of the thinning that occurred at Reedy Glacier after the maximum ice thickness evidenced at the Quartz Hills, occurred by $6.9 \pm$

0.5 kyr B.P. when the grounding line in the Ross Sea was still 600 km away from the mouth of Reedy Glacier.

It is interesting to note that during this continuous retreat from the maximum position in the Ross Sea and from maximum ice thickness at the mouth of Reedy Glacier, two ice-thickness maxima were reached and sustained near the head of the glacier. These results reveal that areas of East Antarctica were thickening during the Holocene, while ice in West Antarctica retreated approximately 1300 km to its present position. This asynchronous glacial history at Reedy Glacier also suggests that glaciers in the Transantarctic Mountains have more complicated glacial histories than previously assumed, and those histories may help to constrain the differing glacial histories of the EAIS and the WAIS.

2.5.4. Recent ice surface lowering at Reedy Glacier

Younger exposure ages of erratics collected at the modern margin of Reedy Glacier suggest that glacier surface elevations may have responded more recently to ice-flow fluctuations in the Ross Sea Embayment. Surface-exposure ages < 1 kyr of erratics collected from the modern glacier margin suggest that Reedy Glacier may have responded to a recent change in the elevation of Mercer Ice Stream (Figure 1.1). Ice-penetrating radar shows that the flow rate of ice streams at the Siple Coast have changed on short timescales (e.g., Conway et al., 2002).

2.6. Summary

Our results show that ice achieved maximum thicknesses at different times at different locations at Reedy Glacier, and show the longitudinal glacier profile steepened through the Holocene. The earliest maximum, recorded by deposits at the Quartz Hills, had occurred by 17.3 ± 1.1 and persisted until at least 14.3 ± 0.9 kyr B.P. This maximum occurred during maximum ice extent in the Ross Sea. The maximum timing of its termination and the emergence of Langford Peak, ~ 30 km downglacier, by ~ 7 kyr B.P. supports evidence for early Holocene thinning of the WAIS (e.g., Price et al., in press).

Surface-exposure ages of erratics collected from the lower half of Reedy Glacier may reflect continuous Holocene grounding line retreat in the Ross Sea, and coincident ice thinning at the mouth of Reedy Glacier. Ages of samples from nunataks at the mouth of Reedy Glacier suggest that ice thinned rapidly there during the early Holocene; erratics from four nunatak peaks 5 – 25 km from the glacier mouth yield ages of 6.9 ± 0.5 - 7.8 ± 0.5 , respectively, and reveal that the ice surface was only ~ 100 m higher than the modern ice surface by this time.

While thinning ice at the mouth of Reedy Glacier reflected Holocene ice retreat in the Ross Sea, ice-surface elevations at the head of Reedy Glacier were increasing. Surface-exposure ages of erratics from Mims Spur show McCarthy Glacier was nearly 200 m thicker from 9.4 ± 0.7 to 8.0 ± 0.5 kyr B.P. A more recent maximum ice thickness was sustained at Hatcher Bluffs, a nunatak at the head of the glacier, from 7.5 ± 0.6 until 3.7 ± 0.3 kyr B.P. We attribute these maxima to increased accumulation rates on the polar plateau, but we need a millennial-scale climate history of interior East

Antarctica to confirm this interpretation. Our results suggest divergent post-glacial responses in East and West Antarctica during the Holocene.



Figure 2.1. Till-covered blue ice ablation area at the confluence of Reedy and Colorado Glaciers. Reedy Glacier is on the right side of the medial moraine, and is ten kilometers wide in this location. Photo taken facing approximately northeast.

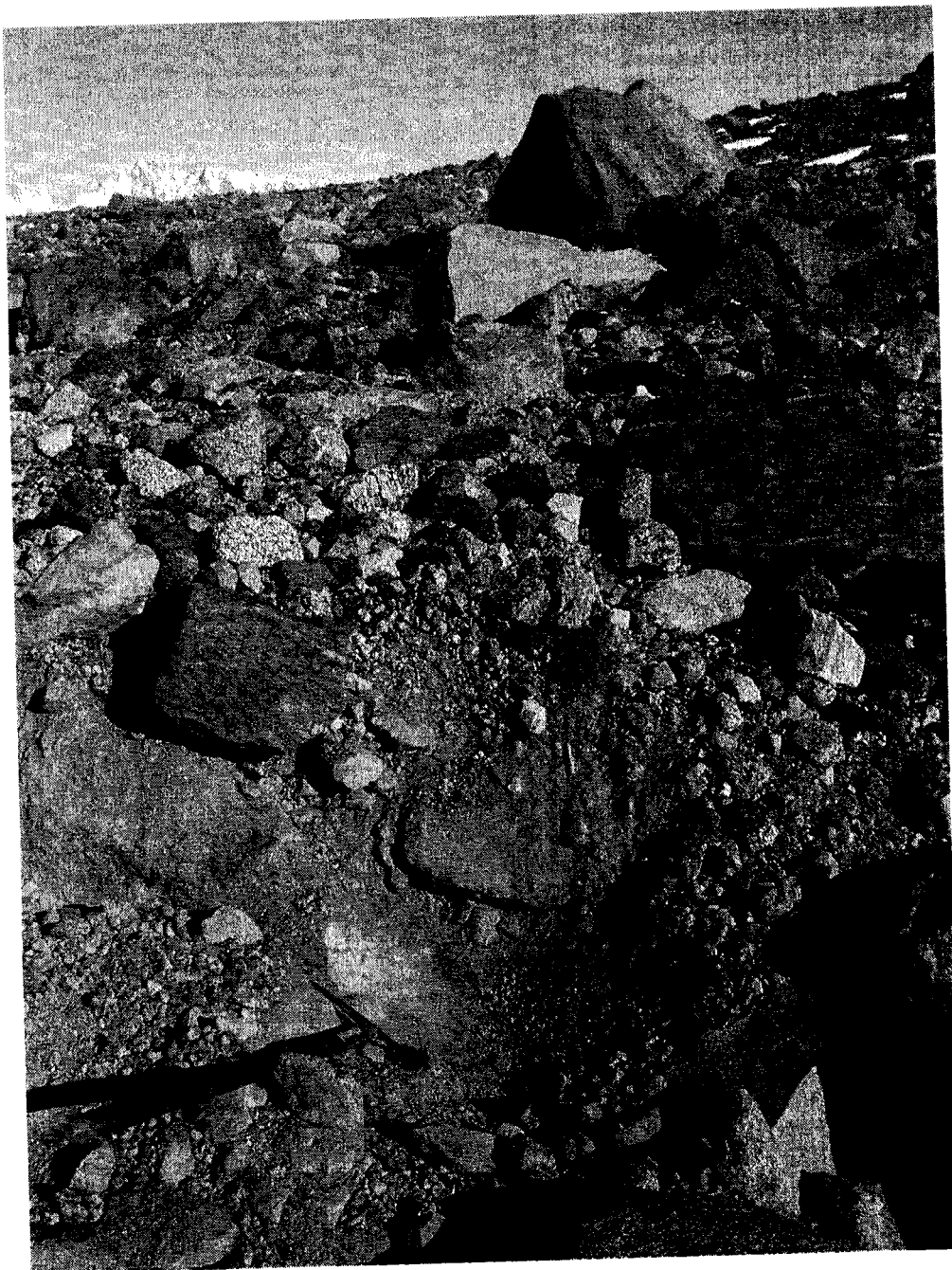


Figure 2.2. Ice-cored Reedy III deposit visible beneath ~ 10 cm of till in the Quartz Hills. This picture taken facing roughly east. Peaks of the Wisconsin Range are visible in the background. This location is ~1320 m asl, approximately 180 m above the modern glacier surface.



Figure 2.3. Upper limit of the Reedy III deposit in the Quartz Hills, ~ 1400 m asl. The margin of relatively unweathered, gray, Reedy III till is visible in the foreground. In contrast, the older, more weathered Reedy II deposit is visible in the background.

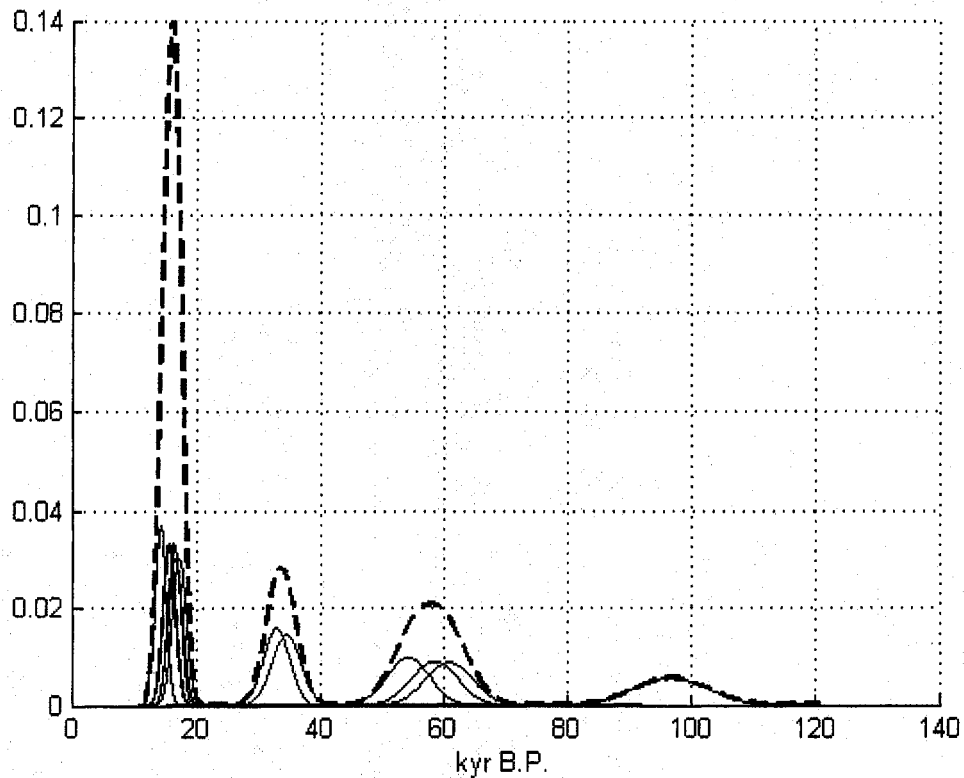


Figure 2.4: Probability density function of surface exposure age results from twelve erratics collected from the upper limit of the Reedy III deposit at the Quartz Hills. Errors in the age measurements are assumed to represent the standard deviations of a normal distribution of the error. Dashed line represents the total probability density function of all samples reported here. Six of the twelve erratics returned ages greatly exceeding the LGM, but the other six samples cluster tightly around ~ 17 kyr, suggesting that the most recent ice advance occurred at that time.



Figure 2.5. Blue ice ablation field at the foot of Cohen Nunatak, at the mouth of Reedy Glacier. Photo taken facing roughly northeast. Reedy Glacier flows to the northwest through the mid-ground of the photograph.



Figure 2.6. Drape deposit covering a recently emerged nunatak (730 m asl) at the mouth of Reedy Glacier.



Figure 2.7. Glacial erratic on the peak of an unnamed nunatak (893 m asl) at the mouth of Reedy Glacier. This deposit is typical of isolated erratics found on nunatak peaks at the mouth of Reedy Glacier, and contrasts with deposits formed in blue-ice ablation fields like the one visible on the ice surface between this unnamed nunatak and nunataks in the mid-ground of the photograph. Photograph taken facing east. Reedy Glacier flows to the left of the photograph beyond the nunataks in the mid-ground.



Figure 2.8. "Drifting moraine" deposit on the ice surface (630 m asl) at the mouth of Reedy Glacier.



Figure 2.9. Erratic on compacted till surface. Till accumulating on blue-ice ablation field and the Transantarctic Mountains are visible in the background.



Figure 2.10: South-facing view of the northeastern corner of the Quartz Hills. Photo taken from the Eblen Hills which is visible in the foreground. The confluence of Reedy Glacier (left) and Colorado Glacier is visible at the base of the Quartz Hills. Glacier flow is to the left of the photograph.

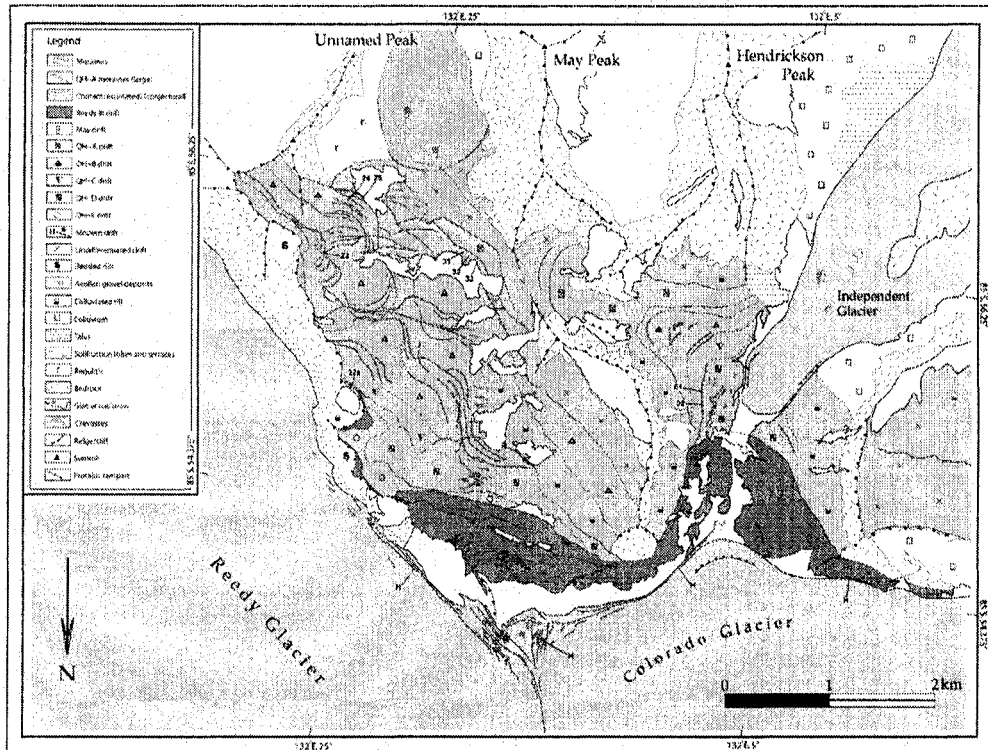


Figure 2.11. Glacial geologic map of the Quartz Hills. Dark orange areas denote the extent of Reedy III deposits at the Quartz Hills.



Figure 2.12: Reedy III deposit in a south-facing gully in the Quartz Hills. Till-covered shear margin is visible at the base of the gully. Reedy Glacier flows to the left margin of the photograph.

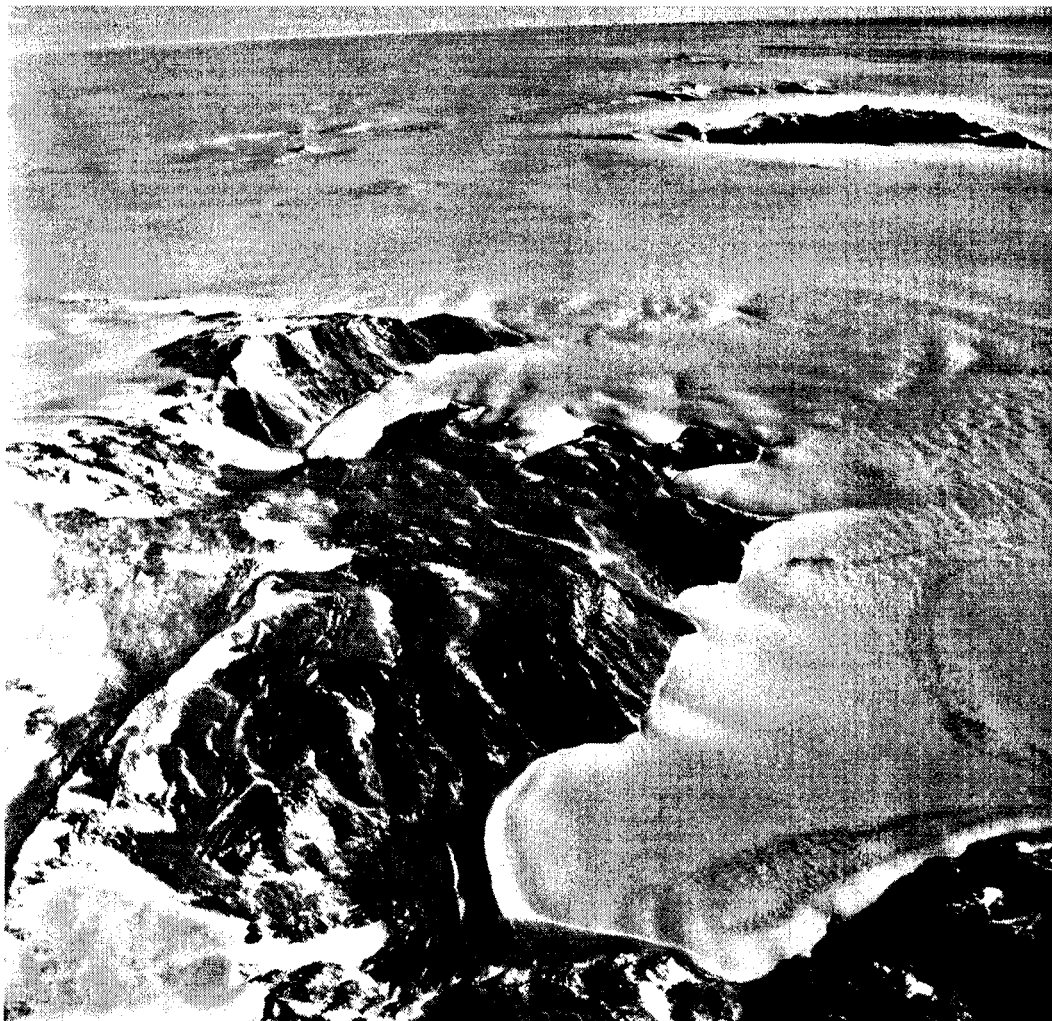


Figure 2.13. Polygon Spur (large spur in the center of the photograph) and Mims Spur (above Polygon Spur in the Photograph) at the margin of McCarthy Glacier, which flows roughly west (right) in this photograph to join Olentangy Glacier and ultimately Reedy Glacier. Reedy Glacier is visible in the upper right corner, flowing by Strickland Nunatak (southernmost, top nunatak in the upper right corner), Hatcher Bluffs (middle), and Metavolcanic Mountain, on the southern margin of McCarthy Glacier.



Figure 2.14. Ice-cored moraine (1920 m asl) at Mims Spur, facing northwest. The confluence of McCarthy Glacier and Oientangy Glacier is in the background. Reedy Glacier is visible in the upper left corner of the image.



Figure 2.15: Reedy III deposit in a cirque at Shapley Ridge. East-facing view across Reedy Glacier, which flows to the left of the image.



Figure 2.16: Northwest-facing image of till-covered ablation area at Hatcher Bluffs at the head of Reedy Glacier. Reedy Glacier flows toward the upper right corner of the photograph and is ~ 15 km wide in this location.



Figure 2.17: Upper limit of Reedy III deposit at Hatcher Bluffs, where erratic material is sparsely scattered on eroded bedrock.

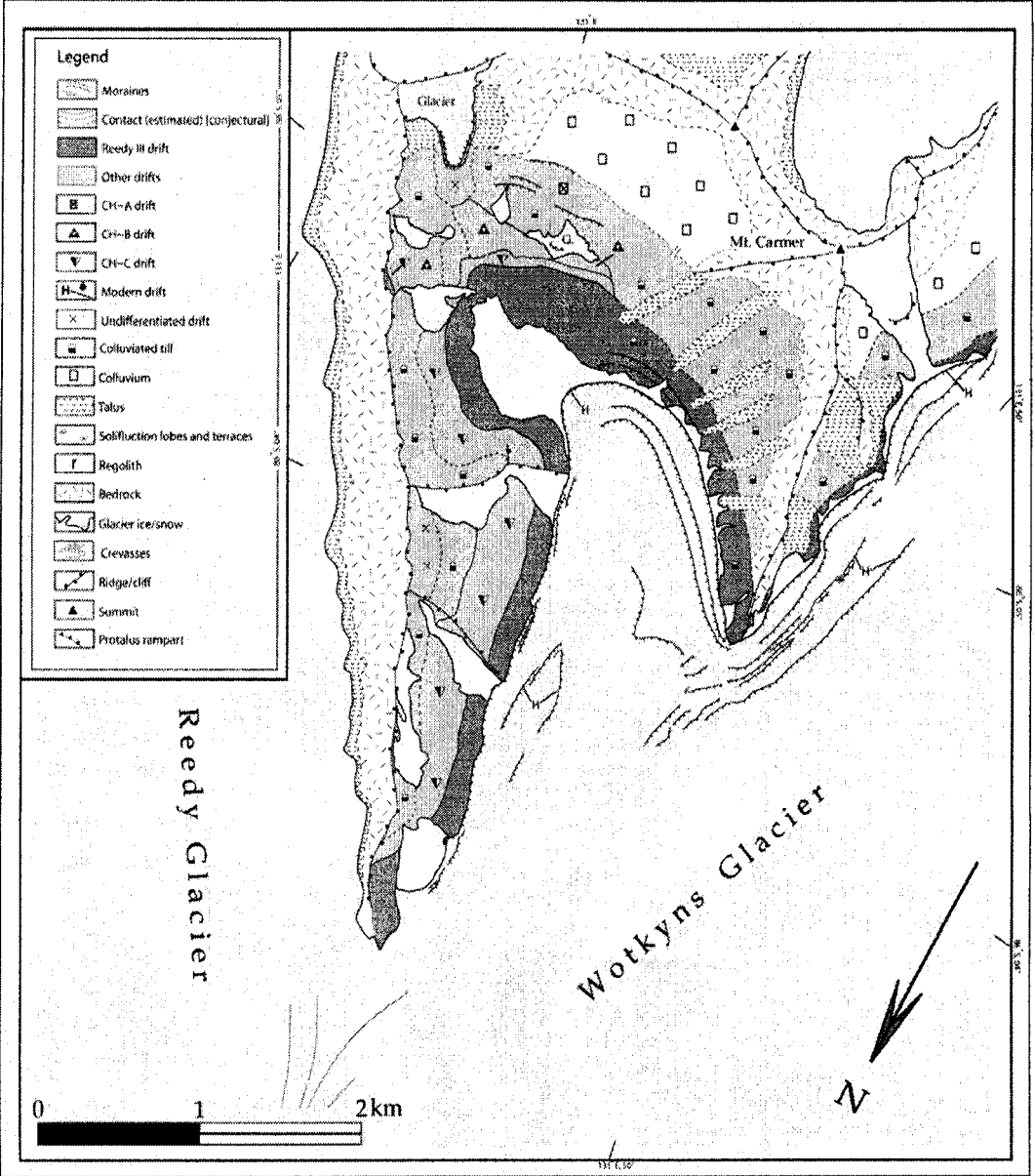


Figure 2.18. Glacial geologic map of the Caloplaca Hills. Reedy III deposits are denoted by dark orange areas.

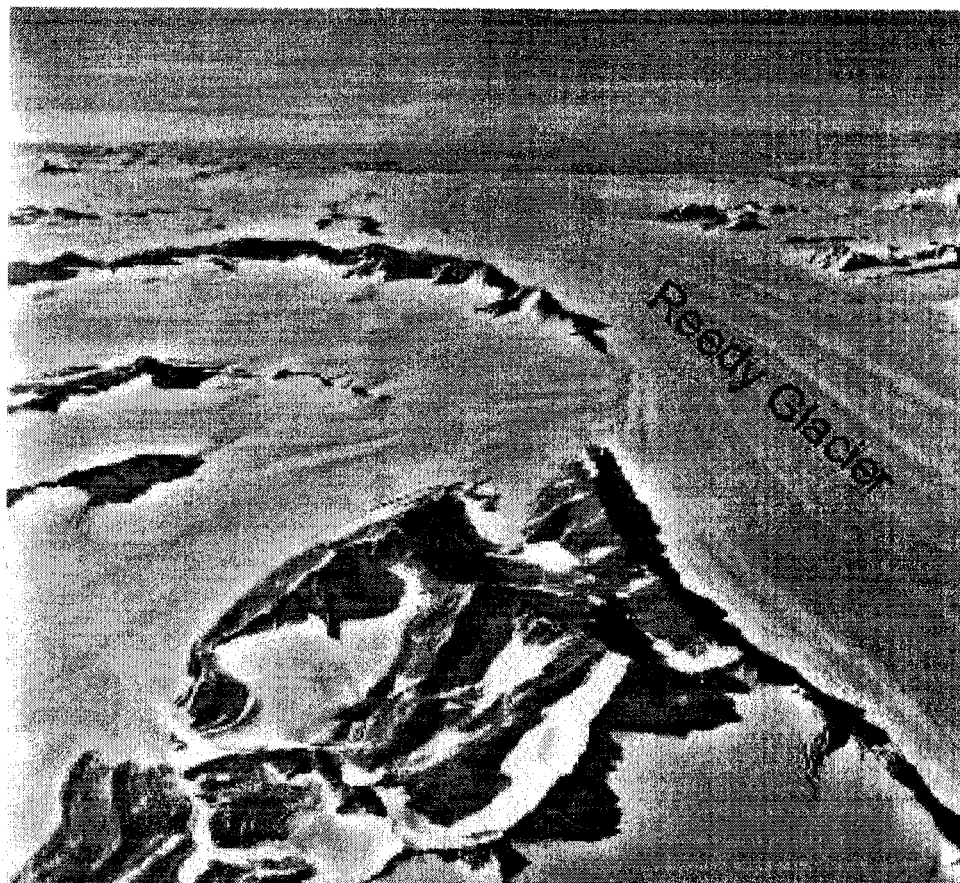


Figure 2.19. Confluence of Wotkyns (left) and Reedy Glaciers. Reedy Glacier is flowing to the top of the photograph. Caloplaca Hills is in the foreground. The Reedy III deposit sampled for this study is located at the head of northernmost valley in the Caloplaca Hills, right at the confluence.



Figure 2.20: Perched erratics at the limit of the Reedy III deposit at the Caloplaca Hills.

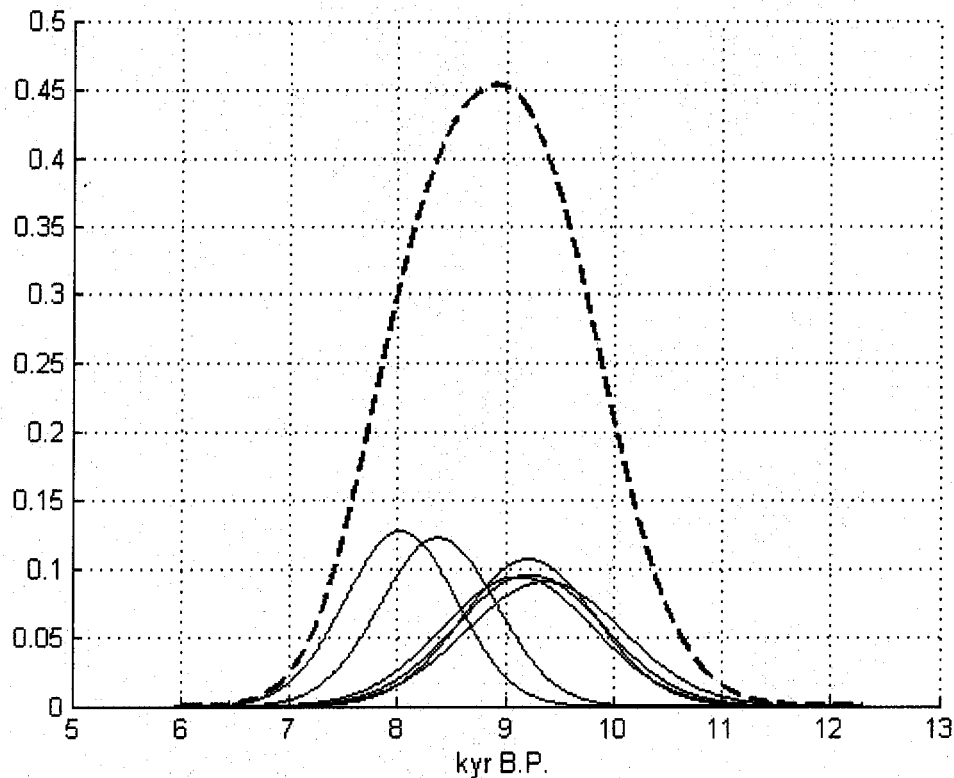


Figure 2.21: Probability density function of surface-exposure age results from six erratics collected from the upper limit of the Reedy III deposit at the Mims Spur. Errors in the age measurements are assumed to represent the standard deviations of a normal distribution of the error. Dashed line represents the total probability density function of all samples reported here. All six erratics return ages clustered tightly around ~ 9 kyr, confirming geomorphic evidence of ice thinning of ~ 200 m at Mims Spur.

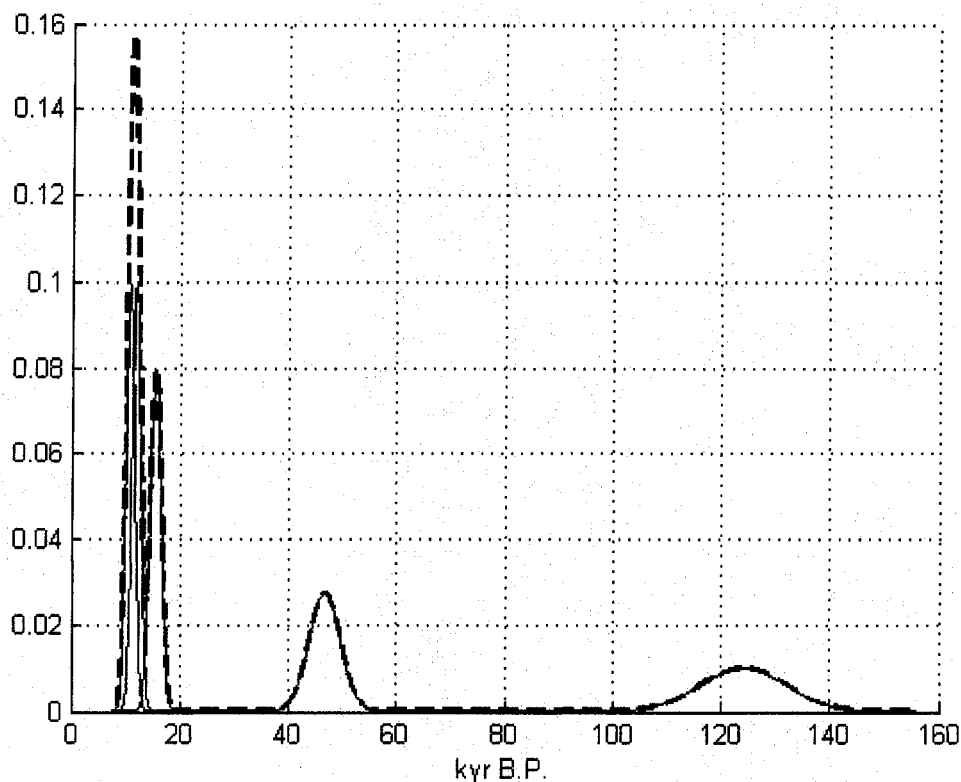


Figure 2.22: Probability density function of surface-exposure age results from five erratics collected from the upper limit of the Reedy III deposit at the Caloplaca Hills. Errors in the age measurements are assumed to represent the standard deviations of a normal distribution of the error. Dashed line represents the total probability density function of all samples reported here. Two of the five erratics returned ages greatly exceeding the LGM, but the other five samples cluster tightly around ~ 12 kyr, suggesting the most recent ice advance occurred at that time.

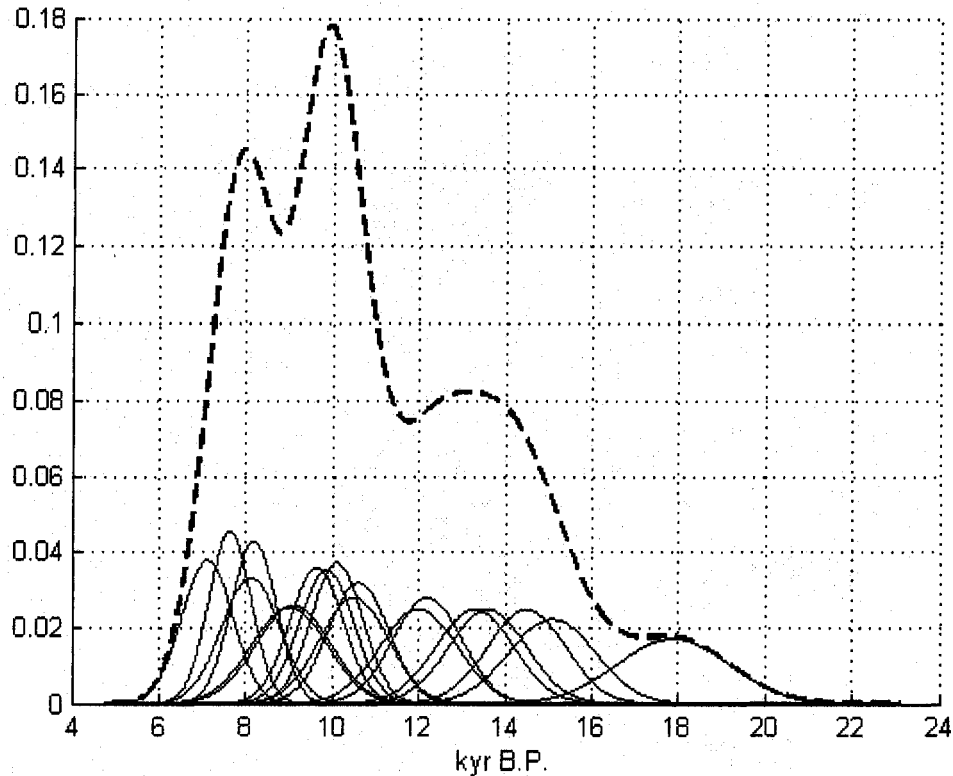


Figure 2.23: Probability density function of surface-exposure-age results from twelve erratics collected from the recessional Reedy III deposit at the Quartz Hills. Errors in the age measurements are assumed to represent the standard deviations of a normal distribution of the error. Dashed line represents the total probability density function of all samples reported here. Results show samples exposed during maximum ice thickness, when a blue-ice ablation field delivered material both to the glacier margin and to the ice surface some distance away from the glacier margin. These maximum-age erratics were subsequently lowered to elevations below the upper limit of the Reedy III margin during post-maximum glacier thinning.

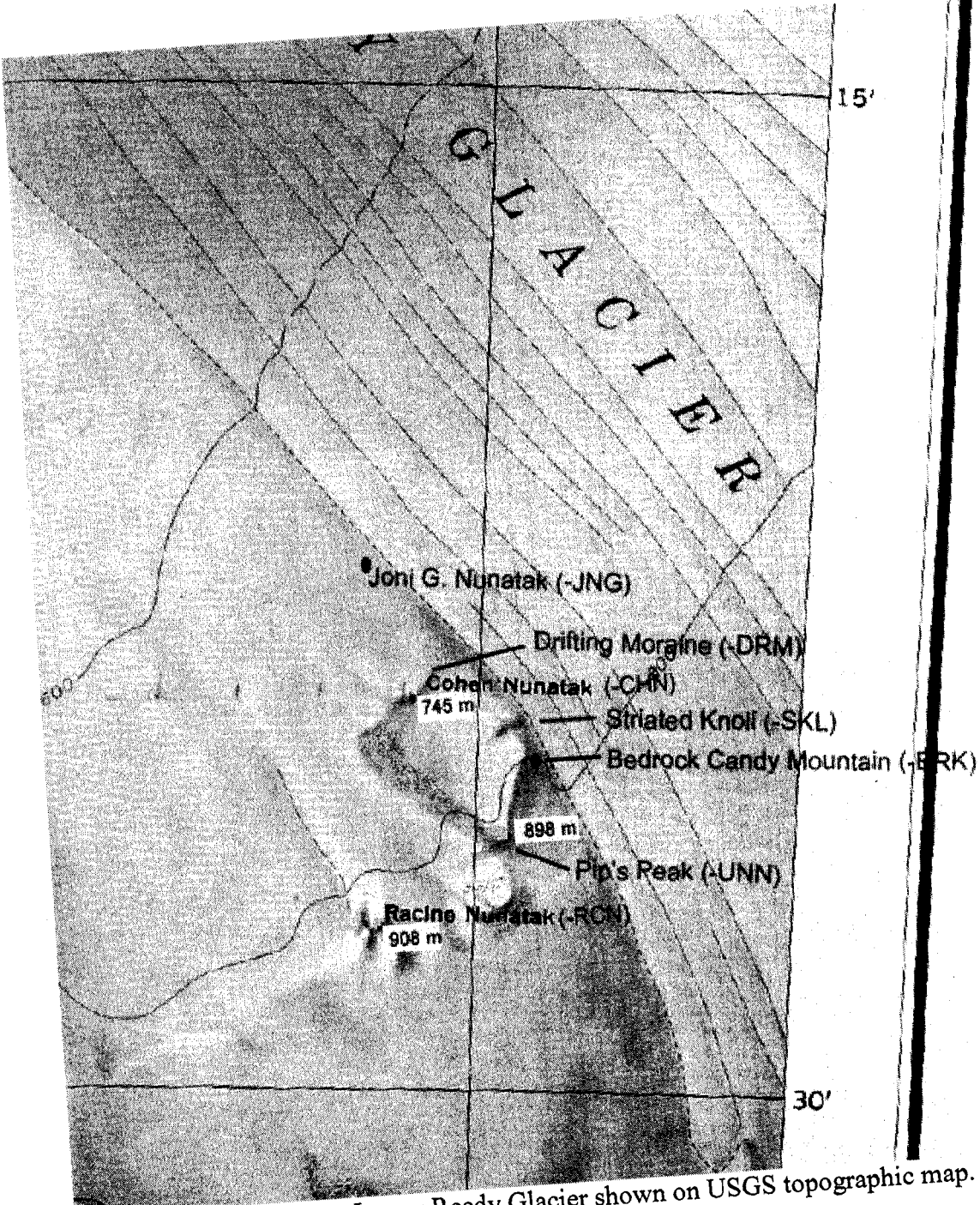


Figure 2.24. Nunataks at Lower Reedy Glacier shown on USGS topographic map.



Figure 2.25: South-facing photo of northern summit of Langford Peak. Reedy Glacier is visible flowing to the left side of the photograph. The Wisconsin Range is visible in the background. Unweathered, gray erratic is visible on the near summit.

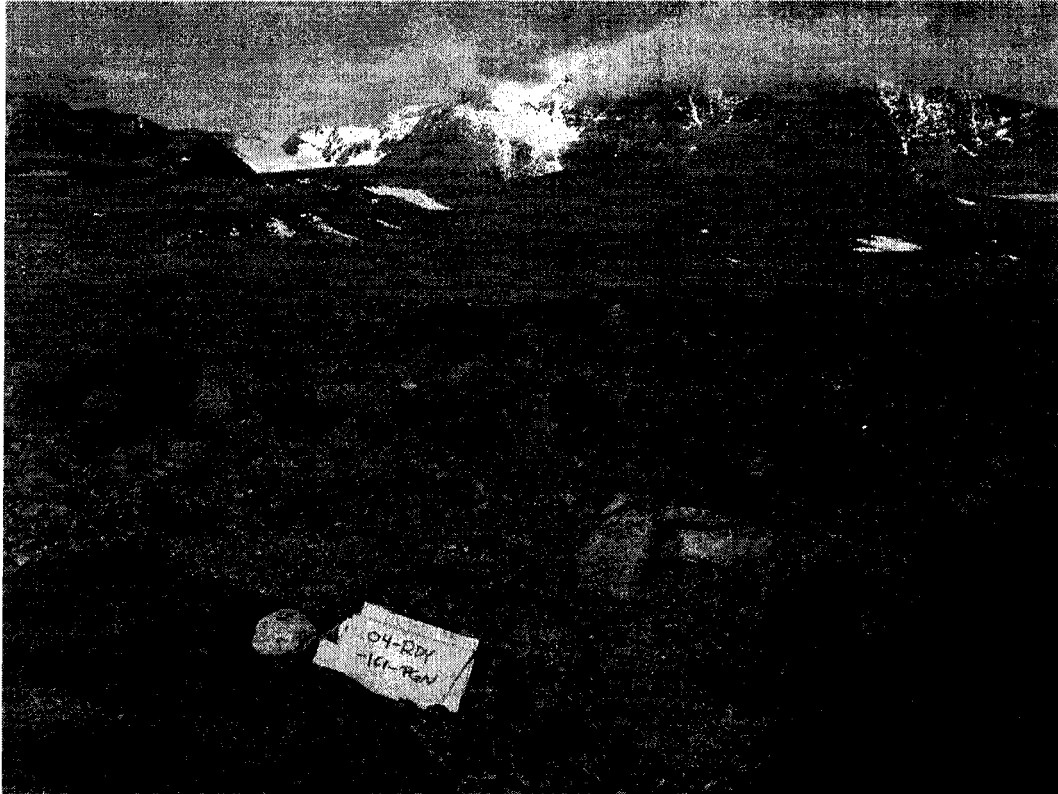


Figure 2.26: Erratic in sparse Reedy III deposit on a broad bedrock bench at Polygon Spur.

Table 2.1. Surface-exposure ages from the Quartz Hills, Reedy Glacier

Sample	Latitude (deg S)	Longitude (deg W)	Altitude (m)	Scaling (spallation)	Scaling (muons)	Thickness correction	Horizon correction	Be-10 prod'n rate (atoms/yr)	[Be-10] (10 ⁴ atoms/g)	Exposure age (kyr)	Internal error (kyr)	[Al] qtz ppm
Reedy Hill limit (glacial maximum deposits; W to E)												
03-RDY-005-QZH	85.90023	132.78708	1403	4.570	2.202	0.970	0.989	21.9 ± 1.3	71.8 ± 1.5	33 ± 2.1	0.71	22.3 ± 0.8
03-RDY-007-QZH	85.90123	132.75317	1401	4.562	2.200	0.941	0.981	21.3 ± 1.3	30.3 ± 0.7	14.3 ± 0.9	0.33	76.1 ± 0.5
03-RDY-008-QZH	85.90123	132.75317	1400	4.558	2.199	0.945	0.991	21.4 ± 1.3	123.7 ± 2.4	58.7 ± 3.7	1.2	70.9 ± 0.6
03-RDY-009-QZH	85.90322	132.69650	1363	4.424	2.162	0.929	0.983	20.2 ± 1.2	31.9 ± 0.7	15.8 ± 1	0.37	152.8 ± 2.4
03-RDY-021-QZH	85.90260	132.69640	1353	4.387	2.153	0.949	0.963	20.1 ± 1.2	68.8 ± 1.9	34.6 ± 2.3	0.97	225.2 ± 1.7
03-RDY-019-QZH	85.90360	132.68273	1359	4.408	2.158	0.929	0.990	20.3 ± 1.2	33.7 ± 1	16.7 ± 1.1	0.5	33.9 ± 0.5
03-RDY-024-QZH	85.90448	132.54638	1391	4.525	2.190	0.933	0.999	21.1 ± 1.3	36.3 ± 0.9	17.3 ± 1.1	0.41	49.2 ± 0.4
03-RDY-025-QZH	85.90448	132.54638	1391	4.525	2.190	0.949	0.999	21.5 ± 1.3	115.4 ± 2.2	54.4 ± 3.4	1.1	26.9 ± 0.2
03-RDY-026-QZH	85.90453	132.51820	1392	4.529	2.191	0.953	0.999	21.6 ± 1.3	130.1 ± 1.9	61.1 ± 3.8	0.89	35.6 ± 0.9
03-RDY-027-QZH	85.90453	132.49523	1399	4.553	2.197	0.937	0.989	21.1 ± 1.3	32.8 ± 0.8	15.6 ± 1	0.36	50.5 ± 2.5
03-RDY-077-QZH	85.90452	132.49380	1390	4.523	2.189	0.957	0.989	21.4 ± 1.3	35.3 ± 0.7	16.5 ± 1	0.35	256.9 ± 3.4
03-RDY-028-QZH	85.90452	132.49345	1394	4.537	2.193	0.943	0.962	20.6 ± 1.2	195.1 ± 2.7	96.9 ± 6	1.4	56.9 ± 1.2
Recessional deposits below Quartz Hills bench (by altitude)												
03-RDY-056-QZH	85.89955	132.57832	1310	4.235	2.111	0.945	0.999	20 ± 1.2	26.6 ± 0.8	13.3 ± 0.9	0.43	83.8 ± 1.5
03-RDY-057-QZH	85.89955	132.57832	1310	4.235	2.111	0.941	0.999	19.9 ± 1.2	17.9 ± 1.4	9.01 ± 0.88	0.7	27.1 ± 3.3
03-RDY-058-QZH	85.89955	132.57832	1310	4.235	2.111	0.925	0.999	19.6 ± 1.2	19.3 ± 0.5	9.86 ± 0.63	0.23	36.5 ± 0.5
03-RDY-059-QZH	85.89935	132.58710	1309	4.233	2.110	0.921	0.999	19.5 ± 1.2	26.4 ± 0.6	13.6 ± 0.9	0.32	54.4 ± 0.1
03-RDY-048-QZH	85.89832	132.58722	1302	4.210	2.104	0.974	0.999	20.5 ± 1.2	16.7 ± 0.4	8.18 ± 0.52	0.19	63.9 ± 0.8
03-RDY-045-QZH	85.89838	132.59863	1296	4.188	2.098	0.957	0.998	20 ± 1.2	20.2 ± 0.5	10.1 ± 0.6	0.24	37.6 ± 0.7
03-RDY-046-QZH	85.89838	132.59863	1296	4.188	2.098	0.949	0.999	19.9 ± 1.2	28.8 ± 0.5	14.5 ± 0.9	0.28	76.7 ± 0.7
03-RDY-053-QZH	85.89878	132.59013	1294	4.180	2.096	0.941	0.998	19.7 ± 1.2	479.9 ± 7.9	259 ± 16.9	4.6	73 ± 0.2
03-RDY-050-QZH	85.89867	132.58910	1293	4.178	2.095	0.949	0.998	19.8 ± 1.2	70.2 ± 1.2	35.7 ± 2.2	0.62	139.2 ± 0.8
03-RDY-052-QZH	85.89867	132.58910	1293	4.178	2.095	0.941	0.998	19.6 ± 1.2	20.8 ± 0.6	10.6 ± 0.7	0.3	57.8 ± 0.7
03-RDY-033-QZH	85.89733	132.60530	1290	4.169	2.093	0.974	0.998	20.3 ± 1.2	19.5 ± 0.5	9.63 ± 0.62	0.23	29.5 ± 0.5
03-RDY-036-QZH	85.89753	132.60825	1282	4.140	2.085	0.949	0.998	19.6 ± 1.2	100.3 ± 1.9	51.7 ± 3.3	1	54.4 ± 1.7
03-RDY-037-QZH	85.89753	132.60825	1282	4.140	2.085	0.957	0.998	19.8 ± 1.2	15.1 ± 0.4	7.63 ± 0.49	0.19	258.7 ± 2.4
03-RDY-032-QZH	85.89758	132.61042	1280	4.133	2.083	0.933	0.998	19.3 ± 1.1	28.9 ± 0.7	15.1 ± 1	0.35	22.4 ± 2
03-RDY-030-QZH	85.89788	132.61377	1280	4.132	2.082	0.933	0.998	19.3 ± 1.1	23.5 ± 0.6	12.2 ± 0.8	0.29	47.8 ± 1
03-RDY-029-QZH	85.89803	132.61128	1276	4.120	2.079	0.961	0.997	19.8 ± 1.2	16 ± 0.9	8.11 ± 0.67	0.47	32.8 ± 0.6
03-RDY-038-QZH	85.89690	132.62010	1272	4.107	2.075	0.945	0.998	19.4 ± 1.1	13.8 ± 0.8	7.11 ± 0.59	5.1	43.5 ± 0.3
03-RDY-041-QZH	85.89717	132.61902	1266	4.087	2.070	0.953	0.998	19.5 ± 1.2	493 ± 8.8	269.4 ± 17.8	5.1	25.7 ± 0.5
03-RDY-042-QZH	85.89627	132.63007	1246	4.019	2.051	0.953	0.998	19.1 ± 1.1	17.4 ± 1.3	9.1 ± 0.86	0.68	37 ± 0.7
03-RDY-043-QZH	85.89627	132.63007	1246	4.019	2.051	0.949	0.998	19.1 ± 1.1	19.9 ± 1.1	10.5 ± 0.8	0.56	94.6 ± 0.4
Recessional deposits on bluff overlooking glacier (by altitude)												
04-RDY-105-QZHL	85.91008	132.34532	1310	4.236	2.111	0.941	0.908	18.1 ± 1.1	21.7 ± 0.8	12 ± 0.9	0.47	75.3 ± 0.3
04-RDY-102-QZHL	85.90997	132.34222	1284	4.147	2.087	0.929	0.808	15.6 ± 0.9	67.1 ± 1.7	43.5 ± 2.8	1.1	72.9 ± 1
04-RDY-103-QZHL	85.90997	132.34222	1284	4.147	2.087	0.929	0.791	15.3 ± 0.9	27.2 ± 1	17.9 ± 1.3	0.69	22.9 ± 0.4

Table 2.2: Surface exposure ages from upper Reedy Glacier

Sample	Latitude (deg S)	Longitude (deg W)	Altitude (m)	Scaling (spallation)	Scaling (muons)	Thickness correction	Horizon correction	Be-10 prod'n rate (atom/g/yr)	[Be-10] (10 ⁴ atom/g)	Exposure age (kyr)	Internal error (kyr)	[Al] qtz ppm
Caloplaça Hills												
Reedy III limit (glacial maximum deposits; W to E)												
03-RDY-117-CPH	86.08975	130.96432	1528	5.048	2.327	0.949	0.934	22.4 ± 1.3	24.1 ± 0.9	10.8 ± 0.8	0.4	315.7 ± 2.4
03-RDY-128-CPH	86.09003	130.96353	1529	5.052	2.328	0.945	0.942	22.5 ± 1.3	271.7 ± 4.4	124.2 ± 7.9	2.1	52.7 ± 0.9
03-RDY-127-CPH	86.08998	130.95963	1525	5.035	2.324	0.945	0.944	22.5 ± 1.3	34.7 ± 0.8	15.5 ± 1	0.36	59.6 ± 1.4
03-RDY-124-CPH	86.08908	130.93792	1516	4.999	2.314	0.949	0.949	22.5 ± 1.3	26.7 ± 0.6	11.9 ± 0.8	0.28	55.2 ± 0.9
03-RDY-121-CPH	86.08825	130.90778	1517	5.005	2.316	0.951	0.956	22.8 ± 1.3	105.2 ± 2	46.7 ± 2.9	0.91	54.9 ± 0.3
Polygon Spur												
Recessional deposits (by distance from glacier margin; farthest to closest)												
04-RDY-154-PGN	86.01080	126.24662	1654	5.569	2.459	0.970	0.986	26.6 ± 1.6	56.1 ± 2.8	21.2 ± 1.7	1.1	46.1 ± 0.7
04-RDY-157-PGN	86.01013	126.24988	1660	5.595	2.465	0.957	0.987	26.4 ± 1.6	17.6 ± 1.6	6.69 ± 0.74	0.62	141.3 ± 9.7
04-RDY-159-PGN	86.01117	126.25185	1656	5.578	2.461	0.949	0.984	26 ± 1.5	119.8 ± 2.7	46.5 ± 3	1.1	168.6 ± 2.3
04-RDY-160-PGN	86.01145	126.25898	1657	5.582	2.462	0.953	0.967	25.7 ± 1.5	14.1 ± 0.8	5.5 ± 0.46	0.33	108.1 ± 0.4
Mim's Spur												
Reedy III limit (glacial maximum deposits; approx. N to S along moraine)												
04-RDY-168-MIM	86.04250	125.74313	1924	6.820	2.758	0.937	0.971	31 ± 1.8	28.2 ± 1.4	9.12 ± 0.7	0.44	94.4 ± 1.4
04-RDY-169-MIM	86.04247	125.74425	1923	6.815	2.757	0.970	0.949	31.3 ± 1.9	28.9 ± 1.3	9.23 ± 0.69	0.42	88.8 ± 1.4
04-RDY-170-MIM	86.04237	125.74607	1917	6.785	2.750	0.929	0.972	30.6 ± 1.8	28.6 ± 1.4	9.37 ± 0.73	0.47	100 ± 1
04-RDY-174-MIM-RPT	86.04386	125.70660	1988	7.145	2.832	0.970	0.971	33.6 ± 2	28.1 ± 0.7	8.38 ± 0.54	0.2	47.7 ± 2.3
04-RDY-178-MIM-RPT	86.04395	125.71752	1966	7.032	2.806	0.953	0.959	32.1 ± 1.9	25.7 ± 0.6	8.03 ± 0.52	0.2	61.2 ± 0.8
04-RDY-179-MIM	86.04405	125.71328	1970	7.052	2.811	0.953	0.964	32.4 ± 1.9	29.8 ± 0.9	9.22 ± 0.62	0.29	106.3 ± 0.9
Recessional deposits (by distance below Reedy III limit)												
04-RDY-181-MIM	86.04250	125.75835	1895	6.676	2.724	0.921	0.996	30.6 ± 1.8	23.8 ± 0.7	7.78 ± 0.52	0.24	69.4 ± 1
04-RDY-183-MIM	86.04262	125.75902	1892	6.662	2.721	0.945	0.994	31.2 ± 1.9	52.2 ± 1.7	16.8 ± 1.1	0.53	71.2 ± 0.6
04-RDY-186-MIM	86.04400	125.80575	1826	6.344	2.646	0.961	0.991	30.2 ± 1.8	420.2 ± 18	143.8 ± 10.9	6.4	67.7 ± 0.4
Hatcher Bluffs												
Reedy III limit (upper limit of deposit on N spur)												
04-RDY-210-HCH	86.32798	126.08850	1956	6.981	2.795	0.983	0.989	33.9 ± 2	25 ± 1.2	7.39 ± 0.57	0.37	260 ± 2
04-RDY-211-HCH	86.32798	126.08850	1956	6.981	2.795	0.945	0.943	31.1 ± 1.8	11.3 ± 0.7	3.63 ± 0.32	0.23	59.6 ± 0.6

Table 2.3: Surface exposure ages from nunataks at lower Reedy Glacier

Sample	Latitude (deg S)	Longitude (deg W)	Altitude (m)	Scaling (spallation)	Scaling (muons)	Thickness correction	Horizon correction	Be-10 prosth rate (atom/gyr)	[Be-10] (10 ⁴ atom/g)	Exposure age (kyr)	Internal error (kyr)	[Al] qtz (ppm)
Langford Peak												
Summit erratics												
04-RDY-074-LNG	85.54638	135.38480	1060	3.434	1.882	0.949	0.989	16.3 ± 1	12.2 ± 0.4	7.46 ± 0.49	0.22	44.5 ± 0.6
04-RDY-076-LNG	85.54642	135.37515	1050	3.405	1.873	0.957	0.981	16 ± 1	12.5 ± 0.3	7.8 ± 0.5	0.19	27 ± 0.5
Racine Nunatak												
Recessional deposits (by altitude)												
04-RDY-061-RCN	85.46152	136.24397	853	2.865	1.706	0.949	1.000	13.6 ± 0.8	9.9 ± 0.29	7.27 ± 0.48	0.21	56.7 ± 0.5
04-RDY-064-RCN	85.46327	136.23030	806	2.747	1.668	0.945	0.989	12.9 ± 0.8	8.4 ± 0.27	6.53 ± 0.44	0.21	47.7 ± 0.8
Pip's Peak												
Recessional deposits (by altitude)												
04-RDY-041-UNN	85.43522	135.93657	898	2.982	1.743	0.949	1.000	14.2 ± 0.8	10.6 ± 0.3	7.48 ± 0.48	0.18	37.7 ± 1.6
04-RDY-040-UNN	85.43520	135.93548	896	2.977	1.741	0.961	1.000	14.4 ± 0.9	10.1 ± 0.2	7.03 ± 0.45	0.17	42.7 ± 0.5
04-RDY-042-UNN	85.43533	135.94978	896	2.977	1.741	0.941	1.000	14 ± 0.8	10.2 ± 0.2	7.26 ± 0.46	0.17	41.6 ± 0.5
04-RDY-039-UNN	85.42890	135.88902	811	2.759	1.672	0.953	1.000	13.2 ± 0.8	8.92 ± 0.28	6.77 ± 0.45	0.21	62.4 ± 1.5
04-RDY-038-UNN	85.42870	135.88933	810	2.757	1.671	0.941	1.000	13 ± 0.8	8.79 ± 0.22	6.76 ± 0.44	0.17	23.6 ± 0.8
04-RDY-036-UNN	85.42590	135.88608	773	2.666	1.641	0.937	0.995	12.5 ± 0.7	8.56 ± 0.21	6.88 ± 0.44	0.17	74.1 ± 1
04-RDY-037-UNN	85.42660	135.88468	773	2.666	1.641	0.937	0.986	12.4 ± 0.7	4.89 ± 0.15	3.96 ± 0.26	0.12	69.4 ± 0.3
04-RDY-035-UNN	85.42443	135.88128	745	2.599	1.619	0.949	0.975	12.1 ± 0.7	0.63 ± 0.07	0.52 ± 0.07	0.06	28.1 ± 0.5
Cohen Nunatak												
Recessional deposits (by altitude)												
03-RDY-139-CHN	85.39980	136.22203	745	2.599	1.619	0.949	1.000	12.4 ± 0.7	8.54 ± 0.31	6.9 ± 0.48	0.25	50.4 ± 1.1
03-RDY-151-CHN	85.39982	136.21527	724	2.551	1.603	0.961	0.997	12.3 ± 0.7	8.24 ± 0.22	6.72 ± 0.44	0.18	68.2 ± 0.6
03-RDY-146-CHN	85.39970	136.19603	680	2.448	1.568	0.937	0.991	11.4 ± 0.7	5.68 ± 0.17	4.98 ± 0.33	0.15	64.8 ± 0.7
03-RDY-141-CHN	85.39973	136.18645	641	2.363	1.538	0.949	0.966	10.9 ± 0.6	1.63 ± 0.17	1.49 ± 0.18	0.16	52.6 ± 2.6
03-RDY-142-CHN	85.39973	136.18645	641	2.363	1.538	0.937	0.966	10.7 ± 0.6	1.89 ± 0.09	1.76 ± 0.13	0.08	58.8 ± 1.1
Outcrops in glacier shear margin (by altitude)												
04-RDY-031-BRK	85.41232	135.84777	750	2.611	1.623	0.978	1.000	12.8 ± 0.8	0.75 ± 0.08	0.59 ± 0.07	0.06	59.8 ± 0.9
04-RDY-032-BRK	85.41232	135.84782	749	2.609	1.622	0.941	1.000	12.3 ± 0.7	0.83 ± 0.05	0.68 ± 0.06	0.04	52.9 ± 0
04-RDY-016-SKL	85.40540	135.91125	736	2.578	1.612	0.953	0.989	12.3 ± 0.7	4.56 ± 0.14	3.7 ± 0.25	0.11	36 ± 0.3
04-RDY-015-SKL	85.40537	135.91193	735	2.576	1.611	0.987	1.000	12.8 ± 0.8	4.66 ± 0.15	3.66 ± 0.25	0.12	37.3 ± 0.2
04-RDY-022-SKL-RPT	85.40572	135.86155	728	2.559	1.605	0.949	0.998	12.2 ± 0.7	1.01 ± 0.08	0.83 ± 0.08	0.06	164.3 ± 2
04-RDY-003-JGN	85.38615	136.27515	633	2.345	1.532	0.933	0.972	10.7 ± 0.6	0.57 ± 0.05	0.54 ± 0.06	0.05	74.6 ± 0.3
Drifting moraine below Cohen Nik												
04-RDY-068-DRM	85.38845	136.19483	637	2.354	1.535	0.949	0.989	11.1 ± 0.7	0.32 ± 0.05	0.28 ± 0.05	0.04	32.8 ± 0.5
04-RDY-070-DRM	85.39452	136.19140	631	2.341	1.531	0.945	0.986	11 ± 0.6	0.36 ± 0.05	0.33 ± 0.05	0.05	65.3 ± 0.7

Chapter 3: Forward Algorithm

3.1. Introduction

Surface-exposure ages of lateral glacial deposits at Reedy Glacier (Tables 2.1-2.3, 3.1; Figures 1.1, 3.1, 3.2) provide a chronology of ice thickness at various locations along the length of the glacier, but sampling of glacial deposits is limited by the availability of glacially-derived material at exposed and accessible sampling sites. Thus, the surface-exposure ages described in Chapter 2 provide only a fragmented ice-thickness history for Reedy Glacier. Specifically, nunataks at the mouth of Reedy Glacier do not record a maximum ice thickness; surface-exposure-age data show that these peaks were overrun by the glacier when maximum ice thicknesses occurred upglacier.

Ice thickness at Reedy Glacier is influenced by the thickness of grounded ice in the southern Ross Sea, and by the surface mass-balance of the polar plateau. Thus, a history of ice thickness at Reedy Glacier can help to constrain (1) the history of ice thickness in the Ross Sea Embayment, and (2) the history of accumulation rates in East Antarctica. In this work, we use surface-exposure ages from Reedy Glacier to constrain the history of ice thickness in the Ross Sea Embayment, as there is disagreement regarding the LGM configuration of the Ross Sea sector of the WAIS (e.g. Price et al., 2007; Waddington et al., 2005). Improved constraints on the elevation of the LGM in the Ross Sea will help to constrain estimates of past and future sea-level contributions from this region.

In order to most effectively constrain the elevation of the LGM in the Ross Sea, we need a complete ice-thickness history at the mouth of Reedy Glacier. Surface-exposure ages of glacial deposits located upglacier constrain this history. We want to determine the history of ice thickness at the mouth of Reedy Glacier that is most consistent with our surface-exposure-age data.

Solving for an ice-thickness history from surface-exposure ages is an inverse problem. An inverse problem consists of a forward algorithm and an inverse algorithm (Parker, 1994; Aster et al., 2005). In this chapter, I describe a forward algorithm developed for use with the inverse algorithm described in Chapter 4. The forward algorithm is a steady-state, flow-band model that calculates ice thickness along the length of Reedy Glacier, given an elevation at the glacier mouth. We use this forward algorithm together with an inverse algorithm (Chapter 4) to reconstruct the history of ice thickness at the mouth of Reedy Glacier. This history will constrain the LGM configuration and subsequent thinning of the WAIS.

3.2. Previous Work

Anderson et al. (2004) showed that numerical models of Transantarctic glaciers can improve constraints on LGM ice thickness in the Ross Sea by calculating glacier surface profiles from existing geologic data sets. They used a transient glacier-flowline model and dated lake deposits from the Hatherton-Darwin glacier system, located approximately 600 km north of Reedy Glacier, and determined that LGM ice thickness at

the outlet of Darwin glacier in the Ross Sea was 800 m higher than the modern ice-shelf surface.

Anderson et al. (2004) also calculated the response of the Hatherton-Darwin glacier system to thinning of LGM ice in the Ross Sea. They calculated response times of 300 and 1100 ± 200 years, given linear and stepwise retreat scenarios, respectively, in the Ross Sea. Because this response time is less than or equal to uncertainties in our surface-exposure age data, we are unable to resolve the response time of Reedy Glacier using surface-exposure ages. Thus, we use a steady-state forward algorithm in our inverse procedure, in order to infer glacier surfaces between contemporary surface-exposure age data.

Anderson et al. (2004) acknowledged the difficulties of modeling glaciers in the Transantarctic Mountains, including unknown glacier-bed topography, and the lack of data constraining ice-flow parameters. For our work on Reedy Glacier, we address these difficulties as follows: (1) we use ice-surface speeds calculated from synthetic aperture radar together with ice thickness measured by ice-penetrating radar to better estimate the glacier-bed topography, and (2) we use a single flow parameter as a tuning parameter in order to best fit our modeled ice-surface elevations to observed ice-surface elevations.

3.3. Forward Algorithm Description

3.3.1. Calculation of ice-surface elevations

We calculate ice-surface elevations using a steady-state, flow-band model. The constitutive relation for ice flow is

$$\dot{\epsilon}_{ij} = A(T)\tau^{n-1}\tau_{ij}, \quad (1)$$

where $\dot{\epsilon}$ is the strain rate, τ is the shear stress, $A(T)$ is the temperature-dependent ice-softness parameter, and n is the flow-law exponent (Glen, 1955; Paterson, 1994). The length of the Reedy Glacier greatly exceeds the glacier thickness. Thus, we assume that the longitudinal stress gradients are small relative to vertical stress gradients. This assumption is called the shallow ice approximation (e.g., Hutter, 1983). This approximation provides a simplified expression of strain rate,

$$\dot{\epsilon}_{xz} = \frac{1}{2} \left(\frac{\partial u}{\partial z} \right), \quad (2)$$

which considers only the vertical gradient of the horizontal velocity, $\frac{\partial u}{\partial z}$.

We define the shear stress, τ_{xz} , as,

$$\tau_{xz} = \rho g h(x) \frac{dS}{dx}, \quad (3)$$

where g is acceleration due to gravity, ρ is ice density, h is ice thickness, and $\frac{dS}{dx}$ is the

surface slope. Substituting equations (2) and (3) into equation (1) gives:

$$\frac{\partial u}{\partial z} = 2A(T) \left(\rho g \frac{dS}{dx} \right)^n h(x)^n. \quad (4)$$

Integrating this equation twice over the depth of the ice, z , yields the depth-averaged velocity:

$$\bar{u}(x) = \frac{1}{n+2} 2A(T) \left(\rho g \frac{dS}{dx} \right)^n h(x)^{n+1}. \quad (5)$$

The average velocity, \bar{u} , can also be expressed as

$$\bar{u}(x) = \frac{q(x)}{w(x)h(x)}, \quad (6)$$

where q is ice flux, and w is width. We can find the ice-thickness profile, $h(x)$ using,

$$h(x) = S(x) - B(x). \quad (7)$$

where S_o is the ice-surface elevation, and B is the glacier-bed elevation. Using conservation of mass, ice flux can be described kinematically as:

$$q(x) = q_{in} + \int_{x_m}^x (\dot{b}(x) - \dot{h}(x))W(x)dx, \quad (8)$$

where q_{in} is the ice flux entering the model domain at x_{in} . Substituting Equations (6), (7), and (8) into equation (5), and setting $\dot{h}(x) = 0$ gives:

$$\frac{dS}{dx} = \left[\frac{(n+2)q(x)}{2A(T)(\rho g)^n W(x)(S-B)^{n+2}} \right]^{\frac{1}{n}}. \quad (9)$$

We can account for enhanced ice flow caused by non-isotropic ice-fabrics using an enhancement factor, E (Van der Veen, 1999):

$$\frac{dS}{dx} = \left[\frac{(n+2)q(x)}{2E(x)A(T)(\rho g)^n W(x)(S-B)^{n+2}} \right]^{\frac{1}{n}}. \quad (10)$$

Equation (10) is a non-linear ordinary differential equation. We solve this equation numerically using a control-volume method (Patankar, 1980). The surface elevation at the glacier mouth is a boundary condition, and we set n equal to 3 (Paterson, 1994).

3.3.2. Glacier Geometry

The forward algorithm requires glacier width and bed elevation at nodes that are uniformly spaced every 5 km along the 140-km glacier length (Figure 3.3). Width and bed-elevation values are then linearly interpolated between nodes.

We measure glacier width using topographic maps published by the United States Geologic Survey (USGS). These widths range from 9 to 22 km, and are shown in Figure 3.4. We check these measurements using ice-surface speeds calculated from synthetic aperture radar (Joughin et al, 2002). Synthetic-aperture radar shows that shear-margin surface speeds range from 25 to 45 m/a (Figure 3.5). These values are consistent with a field measurement of ice-surface speed at the Quartz Hills (Figure 3.1) that showed 45 m of down-glacier movement between December 2003 and December 2004. To check measurements of glacier width from topographic maps, we also measured glacier width using cross-glacier surface-speed profiles. Based on synthetic-aperture radar data, we considered the edge of the glacier to be where ice-surface speeds are below 25 m/a. Glacier widths measured using this method agree with measurements of glacier width from topographic maps to within 1 km.

Glacier-bed elevations (Figure 3.6) are calculated using ice-penetrating radar profiles, ice-surface speeds (Joughin et al., 2002), glacier-surface mass-balance and present-day ice-surface elevations. Ice-penetrating radar profiles are used to calculate the cross-sectional area of the glacier (Figure 3.7) in two locations: Quartz Hills and Cohen Nunatak (Figure 1.1). The ice-penetrating-radar profile at Cohen Nunatak is not perpendicular to glacier flow. Thus, we scale the cross-sectional area calculated from that

profile by the ratio of the glacier width at the mid-point of the profile to the length of the profile.

We calculate depth-averaged glacier velocity from ice-surface velocity data. We average ice-surface velocities across the width of the glacier. Velocities across the width of the head, middle, and mouth of the glacier are shown in Figure 3.5. Width-averaged surface velocities range from 80 to 120 m/a. We calculate depth-averaged velocity from these average surface velocities using a factor of 0.8 (Paterson, 1994). By making this calculation, we assume that Reedy Glacier is isothermal and that there is no velocity due to basal sliding.

At the Quartz Hills and at Cohen Nunatak, the product of the cross-sectional area of the glacier with the depth-averaged velocities at those locations yields the local ice flux. The calculated ice flux at Quartz Hills is approximately $1.5 \times 10^9 \text{ m}^3/\text{a}$. The calculated ice flux at Cohen Nunatak is approximately $3.0 \times 10^9 \text{ m}^3/\text{a}$. These fluxes are the result of (1) influx of ice from the polar plateau at the head of the glacier, (2) surface mass-balance upglacier of these locations, and (3) influx of ice from tributary glaciers. Based on the surface mass-balance pattern shown in Figure 3.8 and the glacier width (Figure 3.4), we calculate an ice flux at each node by adjusting ice fluxes at the Quartz Hills and at Cohen Nunatak to account for variations in ice flux due to variations in surface mass balance along the glacier length. The calculated ice flux at the Quartz Hills includes ice flux from McCarthy Glacier and Wotkyns Glacier (Figure 3.1), but we do correct ice fluxes upglacier of these confluences because of additional uncertainty introduced by estimating ice flux from these tributaries. This simplification results in an overestimation of ice fluxes in the upper 30 km of Reedy Glacier, and bed elevations

calculated based on these ice fluxes are underestimated. The calculated ice flux at Cohen Nunatak accounts for ice flux from Kansas Glacier and part of Horlick Ice Stream. Ice fluxes calculated downglacier from Cohen Nunatak are not corrected for additional ice flux from Horlick Ice Stream, resulting in an underestimation of ice flux for the lower 10 km of the glacier. For the 10 km of the glacier length that spans the confluence of Kansas Glacier and Reedy Glacier, we linearly interpolate between ice fluxes calculated for the upper 90 km of the glacier and ice thicknesses calculated for the lower 30 km of the glacier.

To summarize, we solve for ice thickness at each node in the model domain (Figure 3.3) using Equation (6), which requires glacier width, average velocity, and ice flux. We measure glacier width at each node using USGS topographic maps. We average ice-surface velocities across the glacier width at each node, and calculate a depth-averaged ice velocity by multiplying the average ice-surface velocity by 0.8 (Paterson, 1994). We use the calculated ice fluxes as described above. We subtract the calculated ice thicknesses from surface elevations to get glacier-bed elevations at each node. This method underestimates ice thicknesses, because it oversimplifies bed geometry by ignoring changes in ice thickness across the glacier width. The effect of this uncertainty on the calculation of bed elevations is explored in Section 3.4.4.

3.3.3. Assumptions and simplifications

We assume that the surface-exposure ages of glacial deposits sampled for this study are associated with steady-state glacier surfaces. We chose a steady-state approach because previous work suggests that a similar glacier, Hatherton Glacier, equilibrates to

changes in ice-surface elevation at the glacier mouth in several hundred years (Anderson et al., 2004). Measurements of ice-surface speeds at Reedy Glacier support this suggestion. GPS-based position measurements of poles installed across Reedy Glacier indicate a centerline, ice-surface speed of approximately 170 m/a in the middle of the glacier length. Synthetic aperture radar data (Joughin et al., 2002) show that centerline, ice-surface speeds range from approximately 100 to 190 m/a along the glacier length; width-averaged ice-surface speeds range from approximately 80 – 120 m/a along the glacier length. The average of these width-averaged, ice-surface speeds over the glacier length is approximately 100 m/a. These velocities suggest that the residence time of ice in the Reedy Valley is approximately 1400 - 1750 years. This residence time is within uncertainties in some of our surface-exposure-age data. Surface-exposure ages used to constrain the history of ice thickness at Reedy Glacier range from approximately 3.5 kyr B.P. to 16 kyr B.P., and are generally known to within 8% of these ages. Available data are also temporally sparse (Figure 3.3; Table 3.1), which, combined with uncertainty in the data, prohibits us from resolving transient behavior of Reedy Glacier. Thus, we calculate a sequence of steady-state glacier surfaces to interpolate between contemporary surface-exposure-age data at different times.

The forward algorithm does not explicitly parameterize side-wall drag. We approximate the effect of side-wall drag on ice-velocities at Reedy Glacier by averaging measured surface-speeds across the glacier width for use in the bed-elevation calculation. We also do not directly account for ice-flux contributions to Reedy Glacier from tributary glaciers, but by deriving bed elevations from ice fluxes at the Quartz Hills and Cohen Nunatak (Section 3.3.2) we include ice-flux contributions from the two largest tributary

glaciers, Kansas Glacier and McCarthy Glacier (Figure 3.1). We also neglect variations in ice density expected near the surface and the bed of the glacier, as these volumes are small relative to the overall ice volume.

In addition, the forward algorithm does not explicitly parameterize basal sliding. The presence of large, subglacially derived deposits at Reedy Glacier suggests that there is basal melt, and thus basal sliding may occur, but input parameters required to accurately calculate sliding velocities are not known. In Appendix A, we derive and show calculated surfaces from a forward algorithm that approximates ice velocity due to basal sliding.

3.4. Calibration to Present-day Surface Elevations

3.4.1. Surface mass-balance

The modern surface mass balance at Reedy Glacier is marked by a blue-ice ablation field midway along the glacier. Stake measurements show that 0.19 to 0.24 m of ablation occurred at the Quartz Hills from December 2003 to December 2004. A stake in the center of Colorado Glacier, which joins Reedy Glacier at the base of the Quartz Hills, showed that 0.25 m of ablation occurred over the same time period. We use these measurements to characterize the surface mass balance midway along the glacier. We use accumulation measurements compiled by Vaughan et al. (1999) and compiled and calculated by Monaghan et al. (2006) to specify accumulation rates elsewhere along Reedy Glacier. The surface mass-balance pattern is shown in Figure 3.8.

3.4.2. Boundary Conditions

The forward algorithm requires the specification of two boundary conditions: (1) the ice flux into the head of Reedy Glacier, and (2) the elevation of ice at the glacier mouth. The ice flux into the head of the glacier is assumed to be the same as the ice flux calculated at the Quartz Hills. This ice flux is equivalent to assuming an accumulation rate of 0.06 m/a over the catchment area of Reedy Glacier. This accumulation rate is less than plateau accumulation measurements of 0.1 m/a compiled and reported by Vaughan et al. (1999), but it is consistent with estimates made by Monaghan et al. (2006). We calculate a catchment area of 25,000 km² using the RAMP DEM (Liu et al, 2001).

We use Geoscience Laser Altimetry System (GLAS) elevation measurements (Smith, 2006) for the ice-surface-elevation boundary condition at the glacier mouth in order to calculate modern ice thicknesses at Reedy Glacier.

3.4.3. Tuning parameter

Both internal deformation and basal sliding likely contribute to ice flow at Reedy Glacier, but the input parameters required to calculate these components of ice flow separately are not well known. The value of the ice-softness parameter, $A(T)$, at Reedy Glacier, is not well known because ice temperatures are not well known. One approach to calculating ice temperatures is to assume that ice-temperatures vary linearly from the surface to the bed by heat conduction, but this calculation overestimates ice temperatures at Reedy Glacier because it does not account for the advection of cold ice from the polar plateau (Appendix B). Péclet numbers of approximately 2.5 confirm the importance of advection of ice from the polar plateau for ice temperatures deep in Reedy Glacier

(Appendix B). However, the temperature history of ice from the polar plateau is also not well known. Thus, we cannot characterize the effect of advection of polar plateau ice on ice temperature at Reedy Glacier.

It is common to use the enhancement factor, $E(x)$, to account for non-isotropic ice-fabrics at depth that can enhance ice flow (van der Veen, 1999), but most measurements of enhancement factors are made in ice characterized by ice flow at an ice divide. Given (1) the uncertainties in determining input values for ice-flow parameters $A(T)$ and $E(x)$, and (2) the uncertainties in calculating ice velocity due to basal sliding (Section 3.2.3; Appendix A), we rewrite Equation (10) by defining a tuning parameter, f :

$$\frac{dS}{dx} = \left[\frac{(n+2)q(x)}{2f(x)(\rho g)^n W(x)(S-B)^{n+2}} \right]^{\frac{1}{n}}, \quad (11)$$

This parameter has units of $\text{yr}^{-1} \text{Pa}^{-3}$, and we use it as a tuning parameter to account for physical processes such as ice softness, ice-fabric enhancement, and basal sliding.

Without more information about basal conditions at Reedy Glacier and the temperature of the glacier ice, we cannot justify a more complicated algorithm. Also, this simplification makes the inverse procedure described in Chapter 4 more tractable. The inverse algorithm runs the forward algorithm iteratively, and thus a simple forward algorithm reduces the computation time required to run inverse algorithm experiments.

We use this tuning parameter to calculate the present-day glacier surface by varying f to minimize the difference between calculated and observed glacier-surface elevations. Figure 3.9 compares calculated glacier-surface elevations to observed glacier-surface elevations. By using this deformation factor, f , we are able to match the observed glacier-surface elevations to within 20 m (Figure 3.10). The tuning-parameter values used

in this calculation are shown in Figure 3.11. We compare depth-averaged velocities calculated using the tuning-parameter to width-averaged surface velocities measured by synthetic-aperture radar in Figure 3.12. Calculated depth-averaged velocities follow the trend of width-averaged surface velocities shown for the upper 85 km of the glacier, but calculated average velocities are nearly half of observed width-averaged surface velocities for the lower 50 km of the glacier. This discrepancy is likely due to ice flux from Kansas Glacier and from Horlick Ice Stream that is not accounted for in these calculations.

3.4.4. Effect of uncertainties in bed elevation

Ice-penetrating radar measurements of ice thickness at Quartz Hills and Cohen Nunatak provide important constraints on glacier-bed elevation at Reedy Glacier, but simplifications in the calculation of glacier-bed elevations could result in errors up to 20% at other locations along the glacier length. Comparison of calculated ice velocities to measured surface velocities shows we are underestimating glacier-bed elevations near the mouth of the glacier. We also underestimate bed elevations near the head of the glacier because we do not correct for ice flux from tributary glaciers located downstream but included in the calculated ice-flux at the Quartz Hills. Figures 3.13 and 3.14 show calculated glacier-surface elevations and corresponding tuning parameters using glacier-bed elevations that are 100 m higher than glacier-bed elevations calculated as described in Section 3.3.2; the tuning parameter scales with increases in glacier-bed elevation in order to match observed glacier-surface elevations. Thus, the tuning parameter is an effective means of accounting uncertainties in calculated bed elevations.

3.5. Discussion

The tuning parameter is used to account for all physical processes that contribute to ice flow at Reedy Glacier. Thus, without additional knowledge of ice temperature, basal conditions, or enhanced ice flow, we cannot determine what fraction of the net ice flux (Figure 3.11) corresponds to each process contributing to ice flow. However, the spatial pattern of f values reveals where increased ice flow is needed to calculate modern glacier-surface elevations. Peaks in the spatial pattern of the tuning parameter indicate areas of increased ice flow. Thus, Figure 3.11 shows that the spatial pattern of f reflects the bed topography shown in Figure 3.9, with higher values of f corresponding to areas where the slope of the glacier bed decreases. One exception to this pattern is the sharp decrease in f 100 km downglacier (Figure 3.11), where Kansas Glacier joins Reedy Glacier (Figure 3.3). We attribute this decrease to an overestimation of bed elevations at this confluence. Although we use ice-flux calculations to calculate glacier-bed elevations, we linearly interpolate glacier-bed elevations across the confluence of Kansas and Reedy Glaciers based on ice-fluxes measured at Cohen Nunatak and Quartz Hills (Figure 3.3). The tuning-parameter pattern suggests that this linear interpolation may not account for higher bed topography in this area.

Our approach to calculating glacier-surface elevations is similar to the methods described by Anderson et al. (2004). In that work, the authors calculated surface elevations of the Hatherton-Darwin glacier system using flow parameters f_s , for sliding velocity, and f_d , for deformation velocity. They calibrated their ice-flow model to present-

day glacier-surface elevations, by holding the deformation parameter constant and varying the sliding parameter. As in this study, the authors used their ice-flow model to calculate past glacier-surface elevations. To do so, they iteratively ran the ice-flow model to match past surface-elevation data from dated lake deposits at the glacier margins.

In the following chapter, I describe an inverse algorithm that we use with our forward algorithm to solve for the history of ice-surface elevations at the mouth of Reedy Glacier. This inverse algorithm iteratively runs the forward algorithm to find the ice-thickness history at the mouth of Reedy Glacier that varies smoothly in time, and that also best fits surface-exposure ages data at a defined tolerance. This inverse method allows us to apply surface-elevation constraints from surface-exposure age data, while maintaining physically reasonable ice thicknesses at the mouth of Reedy Glacier. The resulting ice-thickness history will help to constrain the ice-thickness history in the southern Ross Sea. These constraints will improve our understanding of the history of the WAIS.

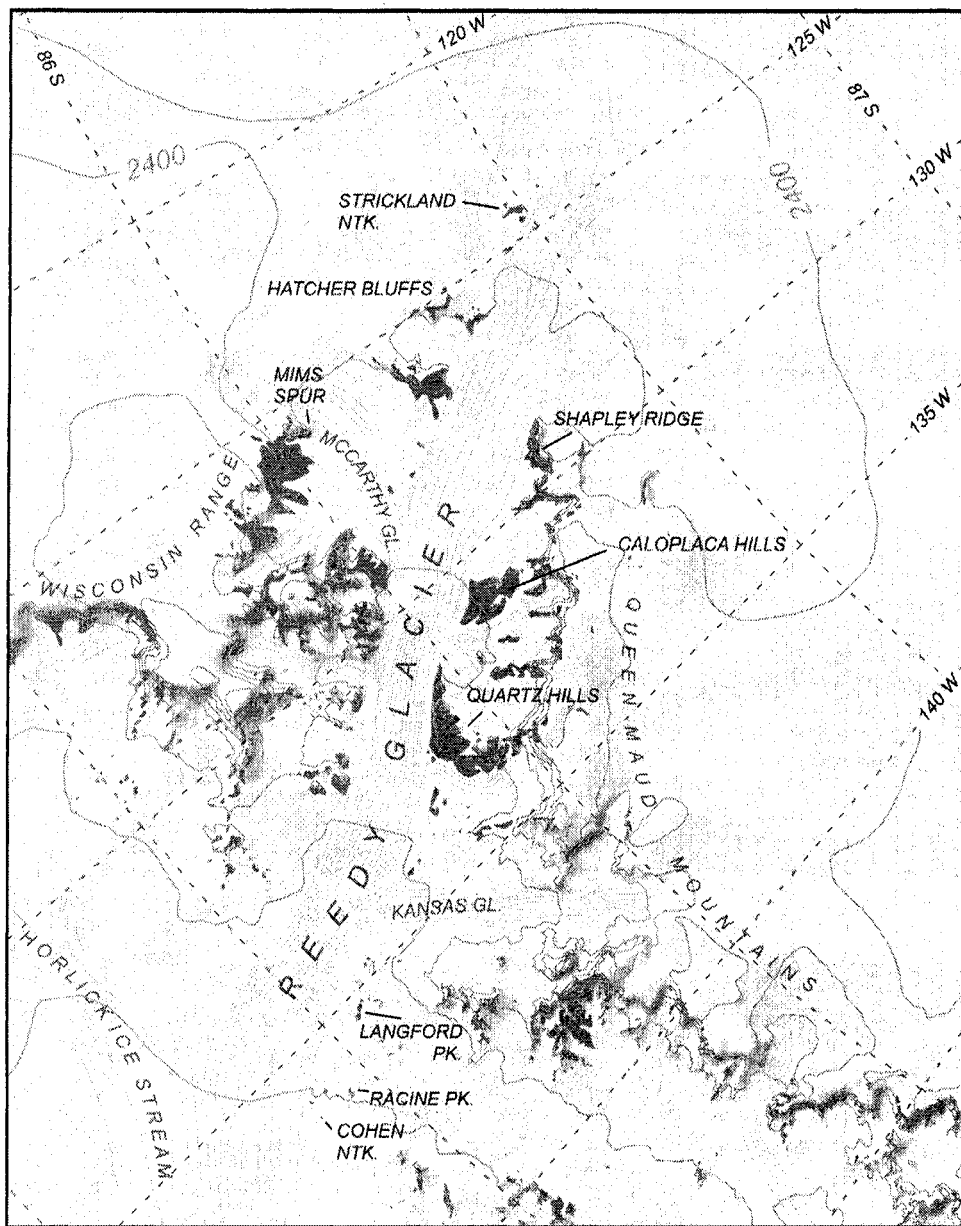


Figure 3.1. Map of Reedy Glacier showing sampling sites, and tributary glaciers. Topography derived from the RAMP-DEM version 2 (Liu et al., 2001). Feature names provided by the Antarctic Digital Database (SCAR, 2002), and USGS topographic maps.

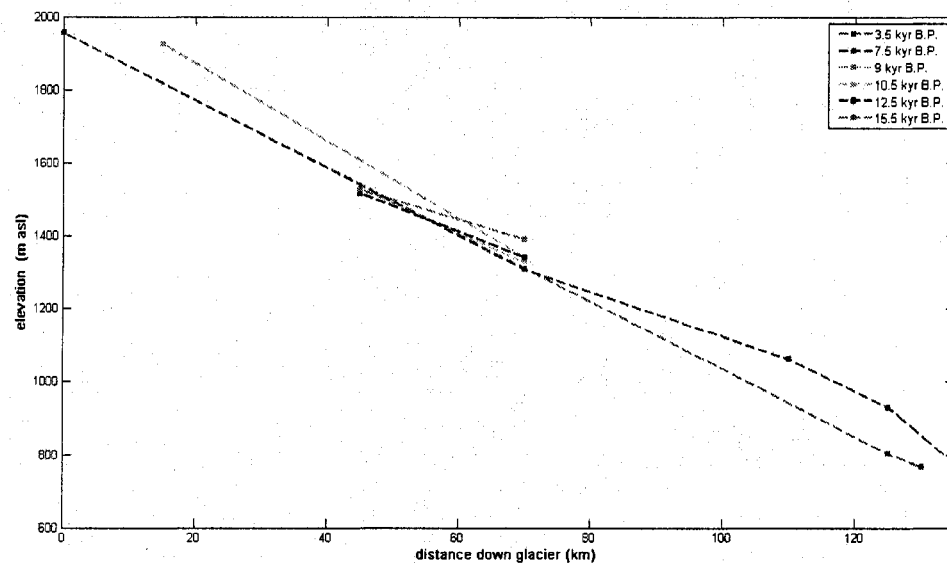


Figure 3.2. Surface-exposure age data used to constrain forward-algorithm calculations of surface elevations at Reedy Glacier.



Figure 3.3. Forward algorithm domain shown on a Moderate-resolution Imaging Spectroradiometer Mosaic of Antarctica) image (Haran et al., 2005). Nodes are located every 5 km.

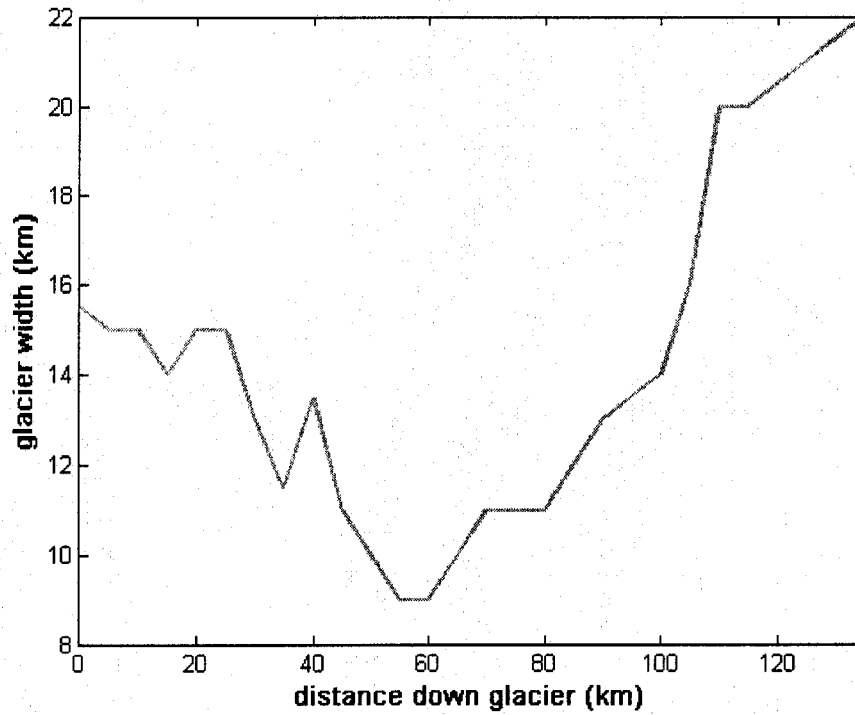


Figure 3.4. Width of Reedy Glacier.

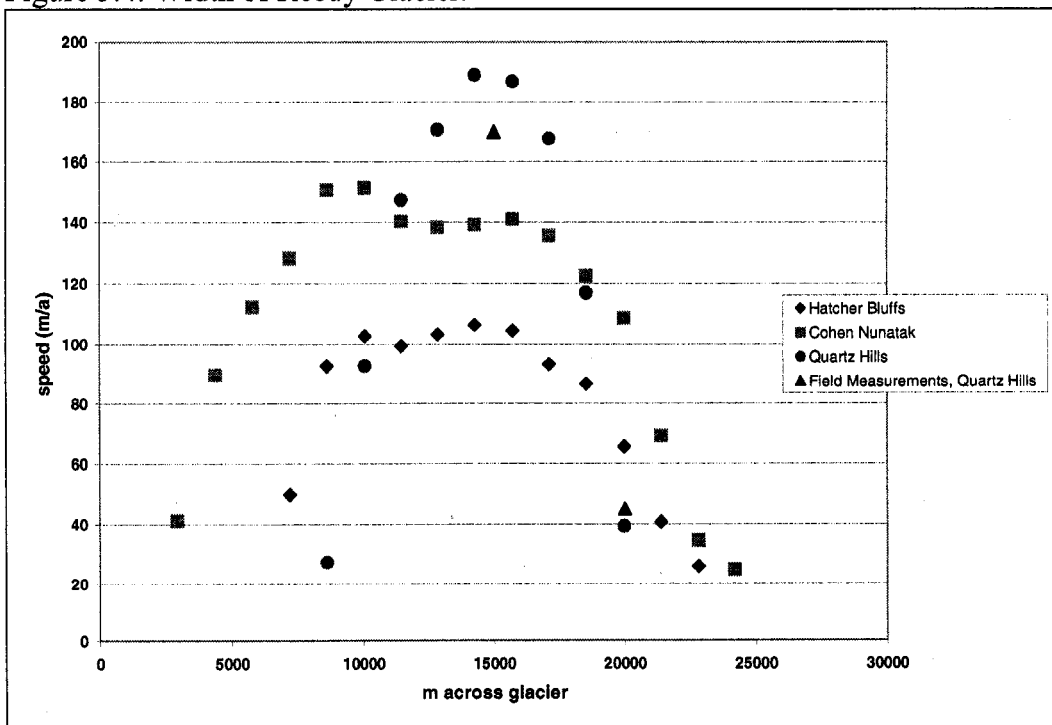


Figure 3.5. Cross-glacier speed profiles from the head of Reedy Glacier (blue diamonds; Hatcher Bluffs), from the middle of the glacier length (purple circles; Quartz Hills), and from the mouth of the glacier (pink squares; Cohen Nunatak), compared to two stake measurements from the Quartz Hills.

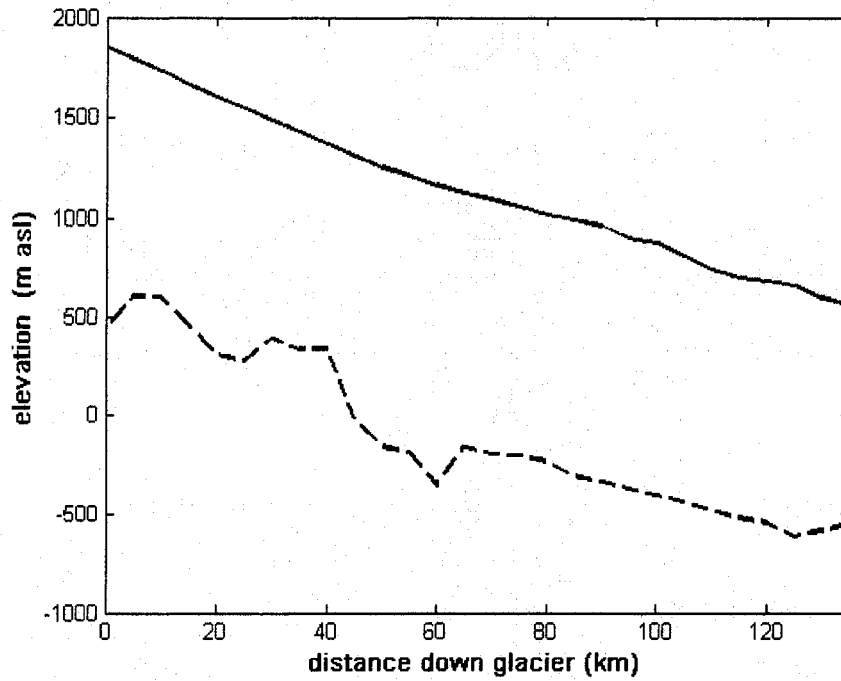


Figure 3.6. Calculated bed elevations (black dashed line), and observed surface elevations (blue solid line) at Reedy Glacier.

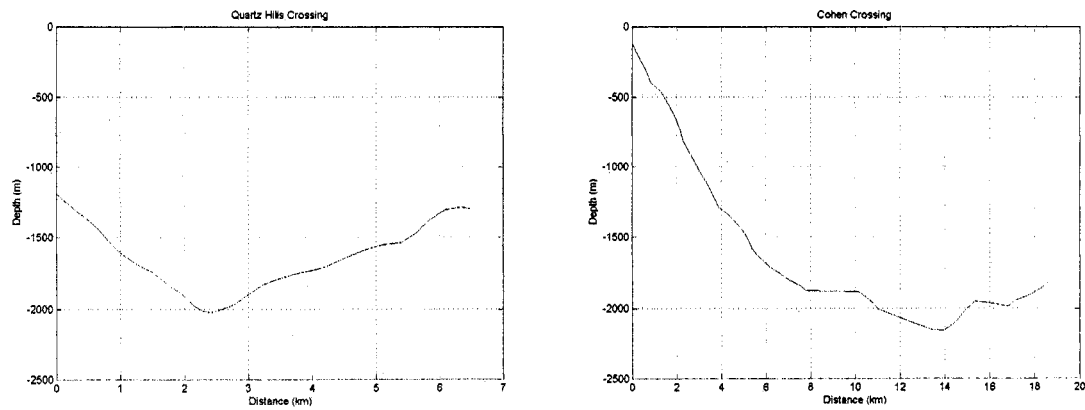


Figure 3.7. Ice thicknesses at Quartz Hills and Cohen Nunatak from ground penetrating radar traverses.

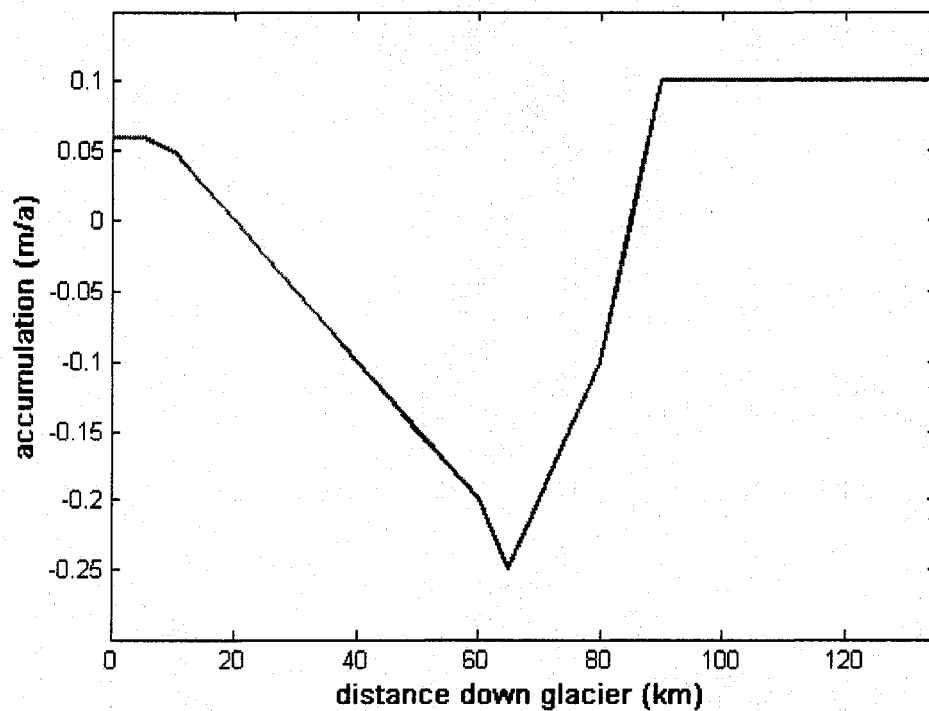


Figure 3.8. Estimated present-day surface mass-balance pattern at Reedy Glacier. Values are derived from stake measurements and modeled values reported by Monaghan et al., (2006).

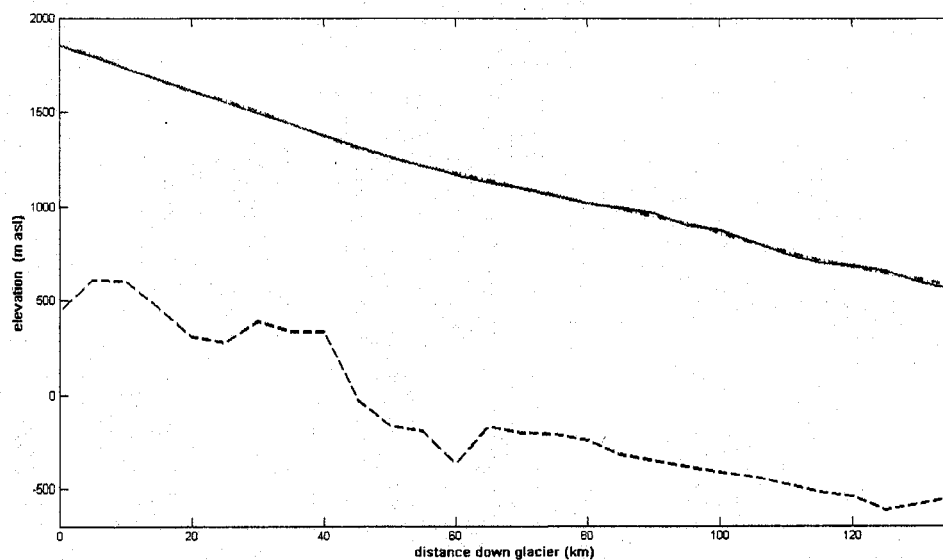


Figure 3.9 Calculated present-day glacier-surface elevations (dashed line), using tuning parameter f_d , compared to observed surface elevations (solid line).

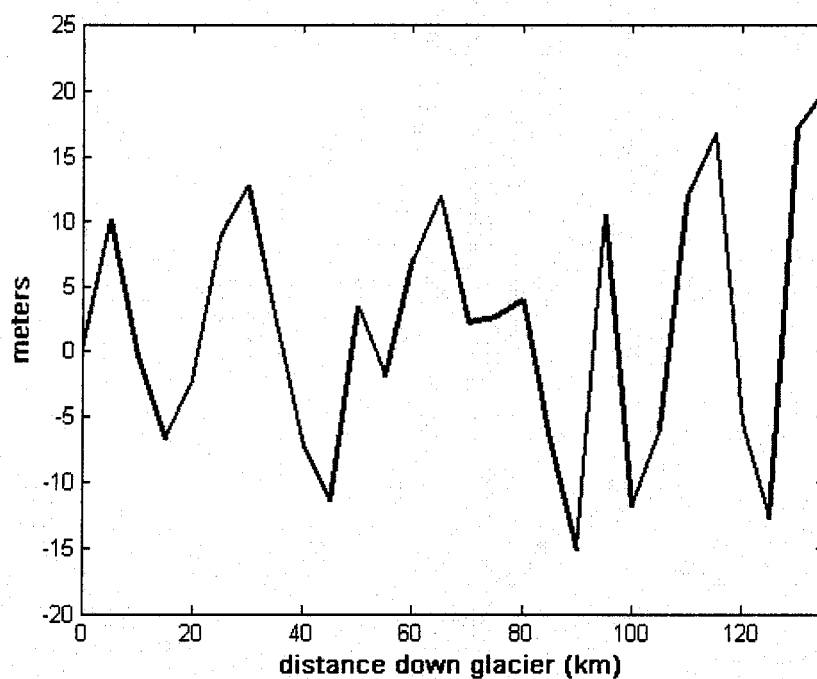


Figure 3.10. Difference between calculated present-day glacier-surface elevations, and observed glacier-surface elevations, using tuning parameter f_d .

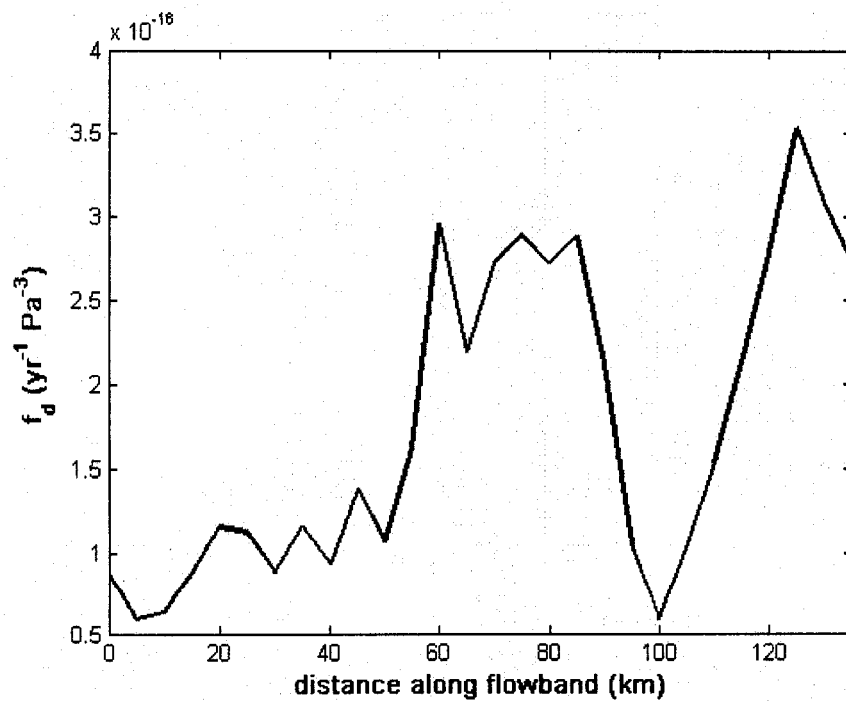


Figure 3.11. Tuning parameter values used to calculate present-day glacier-surface elevations.

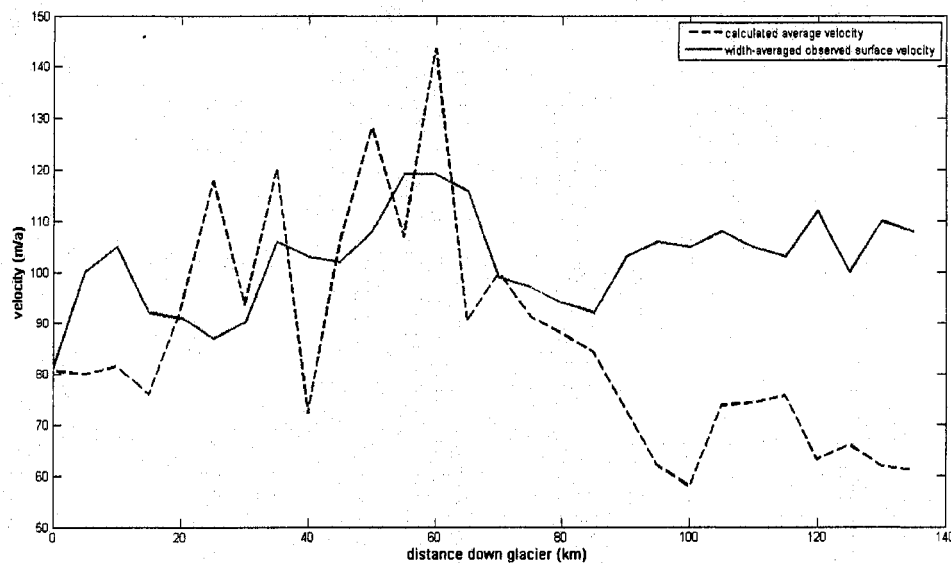


Figure 3.12. Calculated average velocities using the tuning-parameter values shown in Figure 3.11., compared to width-averaged, observed surface velocities.

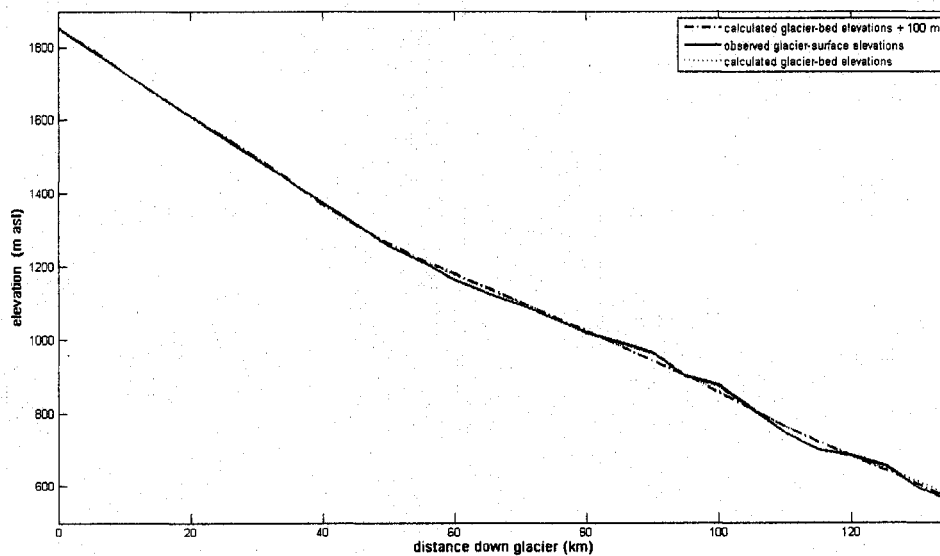


Figure 3.13. Calculated glacier-surface elevations using calculated glacier-bed elevations and calculated glacier-bed elevations increased by 100 m, compared to observed glacier-surface elevations.

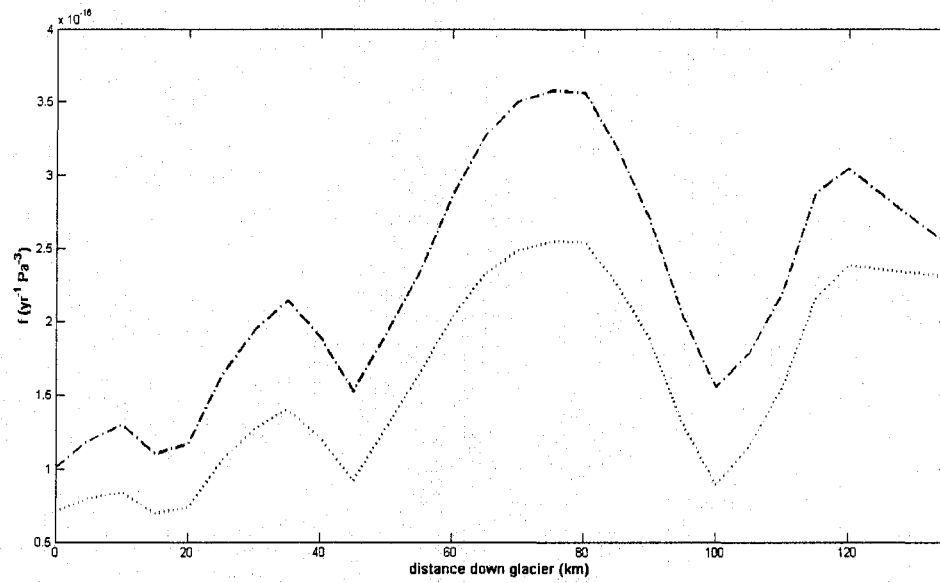


Figure 3.14. Tuning-parameter values corresponding to calculated glacier-surface elevations using calculated glacier-bed elevations (dotted line) and calculated glacier-bed elevations increased by 100 m (dashed line).

Chapter 4: Inverse Problem

Section 4.1. Introduction

The WAIS is a potential source of future sea-level rise (e.g., Weertman, 1974; Lythe et al., 2001). In order to estimate the future sea-level contribution from the WAIS, researchers have first attempted to determine the sea-level contribution from west Antarctica since the LGM. Reconstructions of ice-sheet volume and extent help to quantify past sea-level contribution from the WAIS (e.g., Denton and Hughes, 2002), but additional data are needed to constrain these calculations. Specifically, there is disagreement about the elevation of grounded ice in the Ross Sea Embayment at the LGM (e.g., Waddington et al., 2005).

Existing marine and terrestrial geologic data describing ice retreat in the Ross Sea have been used to reconstruct WAIS elevations at the LGM. Denton and Hughes (2000) used glacial deposits in the Transantarctic Mountains to reconstruct LGM ice elevations in the Ross Sea Embayment. The authors set a minimum ice elevation of 1700 m at the mouth of Reedy Glacier, or approximately 1100 m higher than the present-day ice surface. Anderson et al. (2004) used a transient glacier-flowline model together with dated marginal lake deposits to show that LGM ice thickness at the outlet of Hatherton Glacier was 800 m higher than the current ice-shelf surface, approximately 200 m less than LGM ice-surface elevations calculated by Denton and Hughes (2000). Evidence of a thinner configuration supports recent work by Waddington et al. (2005) that showed that the LGM ice-surface at Siple Dome, located in the central Ross Sea Embayment, was only 200 – 400 m higher than the current ice surface. Additional evidence is needed to

improve constraints on this maximum configuration, and to better quantify the post-LGM sea-level contribution from West Antarctica. In this study, we use surface-exposure ages from Reedy Glacier together with inverse methods, to solve for a history of ice elevations in the southern Ross Sea Embayment at the lower end of Reedy Glacier. Our results constrain WAIS thickness near Reedy Glacier at the LGM.

Section 4.2. Methods

Solving for an ice-thickness history from surface-exposure ages is an inverse problem. In both forward problems and inverse problems, a well-understood physical process is simulated with a forward algorithm. The forward algorithm requires a set of parameters or boundary conditions to predict observable quantities. In a forward problem, these parameters or boundary conditions are known, and are used to calculate unknown observables. In an inverse problem, data have been observed, but the parameters or boundary conditions required by the forward algorithm to produce the data are unknown. Inverse problems comprise an inverse algorithm and a forward algorithm. The forward algorithm makes a prediction of the data. The inverse algorithm iteratively runs the forward algorithm to find the parameter set or boundary conditions that fit the data at an appropriate tolerance.

There are challenges to solving inverse problems. Specifically, if the forward algorithm does not contain all of the physics necessary to reproduce the data, the inverse algorithm may not be able to calculate the observed data at the defined tolerance. Also, if few observed data are available, it is possible that many different sets of parameters or boundary conditions will be consistent with the data. We can address some of these

challenges by using a regularized inverse algorithm. Regularization stabilizes the inverse algorithm by allowing us to define a range of physically possible solutions, and thus limit the solutions deemed to be acceptable by the inverse algorithm. In this study, we use Tikhonov regularization (Aster et al., 2005). This regularization method allows us to account for uncertainty in the data and for physical limitations on the model parameters. This method prevents us from overfitting the data and from selecting a solution that is physically unreasonable.

To do this, we minimize a performance index, I_p ,

$$I_p = \|m\|^2 + \nu(\|d\|^2 - T^2), \quad (1)$$

where $\|m\|^2$ is the model norm, $\|d\|^2$ is the data norm, T is the tolerance, and ν is a tradeoff parameter. The model norm, $\|m\|^2$, discriminates against physically unreasonable solutions. The formulation of $\|m\|^2$ can be different for each inverse problem. In this study, the model norm is

$$\|m\|^2 = \sum_{j=1}^M \left[\frac{(m_j - m_j^{(char)})}{m_j^{(conf)}} \right]^2, \quad (2)$$

where m_j is an estimate of a model parameter, $m_j^{(char)}$ is the characteristic value of the model parameter, and $m_j^{(conf)}$ specifies a physically reasonable range of parameter values.

The data norm, $\|d\|^2$, measures mismatch between predictions of the data and the observed data and is defined by:

$$\|d\|^2 = \sum_{i=1}^N \left[\frac{(o_i^{(m)} - o_i^{(d)})}{\sigma_i^{(d)}} \right]^2, \quad (3)$$

where $o_i^{(m)}$ are predictions of the data, $o_i^{(d)}$ are observed data, $\sigma_i^{(d)}$ are the standard deviations of the data, and N_d is the total number of data. T defines how closely we want to fit the data and is based on the number of data (Parker, 1994). The tradeoff parameter, ν , determines the relative importance of minimizing the model norm and fitting the data (Parker, 1994).

The goal of the inverse algorithm is to find a set of parameters that minimizes the performance index by fitting the data at a specified tolerance, and minimizing the model norm. The inverse algorithm does this by minimizing the performance index for a range of ν values (Equation (1)). For each value of ν , there is a set of model parameters that minimizes the performance index. The appropriate value of ν and corresponding set of model parameters are the values that satisfy:

$$\frac{\partial I_p}{\partial m_j} = 0 \quad (4)$$

and,

$$\frac{\partial I_p}{\partial \nu} = 0. \quad (5)$$

This second criterion is met when

$$\|d\|^2 - T^2 = 0. \quad (6)$$

The mismatch criterion in Equation (6) determines when the data have been fit at a defined tolerance, T . The set of model parameters corresponding to the value of ν that satisfies Equation (6) is the solution to the inverse problem.

In this study, our data are surface-exposure ages from Reedy Glacier. Our forward algorithm is a steady-state ice-flow model that calculates glacier-surface elevations, given

boundary conditions of ice flux entering from the polar plateau, and the glacier-surface elevation at the glacier mouth. We specify the ice-flux boundary condition and use the inverse algorithm to solve for the history of ice thickness at the outlet of Reedy Glacier in order to constrain the history of ice thickness in the southern Ross Sea Embayment.

Section 4.3. Previous Work

Anderson et al. (2004) minimized mismatch between calculated glacier surface elevations and the elevation of marginal lake deposits to find unknown model parameters. We use a different method for determining ice-thickness history from surface-exposure ages. Rather than minimizing mismatch between the data and calculated ice-thicknesses to find unknown model parameters, we apply formal inverse methods (e.g. Menke, 1989; Parker, 1994; Aster et al., 2005) to constrain unknown model parameters by not only matching glacier surfaces to geologic data, but by also selecting for only physically reasonable values of model parameters.

Inverse methods have proven useful for other glaciological applications. Truffer (2004) applied a similar inverse procedure to calculate basal velocities of valley glaciers. He used a forward algorithm that calculated glacier-surface speeds from glacier-valley geometry and basal velocities. In his inverse procedure, he solved for basal velocities by requiring basal velocity patterns to be smooth along the length of the glacier. Waddington et al. (in press) use a similar inverse procedure described here to infer an accumulation-rate history from shapes of internal layers detected by ice-penetrating radar.

4.4. Application to Reedy Glacier

In this study, our forward algorithm is a steady-state ice-flow model that requires an ice-thickness boundary condition at the glacier mouth (Chapter 3). The forward algorithm calculates ice-surface elevations, based on this boundary condition. Our parameter set consists of the history of ice-thickness at the glacier mouth together with the corresponding history of the longitudinal profiles of the tuning parameter. Our data are surface-exposure ages that provide known ice-surface elevations at discrete points on the glacier at different times in the past.

Our inverse algorithm iteratively solves for histories of the ice-thickness boundary condition and of the tuning parameter. The inverse algorithm selects the history of these parameters that corresponds to a sequence of glacier surfaces that (1) best fits surface-exposure-age data at a specified tolerance, and (2) falls within physically reasonable values.

Inverse problems can be represented by the following equation:

$$\mathbf{G}(\mathbf{m}) = \mathbf{d}, \quad (7)$$

where \mathbf{G} represents a forward algorithm, and \mathbf{m} represents the forward-algorithm parameters that yield a given data set, \mathbf{d} , when used in the forward algorithm (Menke, 1989; Aster et al., 2005). Our forward algorithm is non-linear, making it difficult to solve Equation (7) directly for our parameter set, \mathbf{m} (Parker, 1994, Aster et al., 2005). To simplify our problem, we linearize Equation (4) and solve for a change in the parameter values.

For application to Reedy Glacier, we use a data norm defined by Equation (3),

where $o_i^{(m)}$ are predicted ice-surface elevations, $o_i^{(d)}$ are measured ice-surface elevations, and $\sigma_i^{(d)}$ are uncertainty in those data. N_d is the total number of ice-surface elevations that we use to constrain the history of ice thickness.

We use surface-exposure age data to define ice-surface elevations at six times: 3.5, 7.5, 9, 10.5, 12.5 and 15.5 kyr B.P. (Figure 3.2). Ice-surface elevations are assumed to be contemporary, if the surface-exposure ages from two or more elevations are equal within the uncertainty of the surface-exposure ages. Uncertainties in these elevations are derived from (1) modern elevation differences between the glacier margin, where we have data, and the glacier centerline, where we calculate ice thickness, (2) extrapolations of ice-surface elevations measured at the margins of tributary glaciers, and (3) glacial deposits in which samples arrived at the ice surface prior to deposition at the glacier margin. The total number of ice-surface elevations used is $N_d = 17$.

The model norm discriminates against physically unreasonable estimates of the model parameters. In this study, our model norm includes: the boundary condition of the forward algorithm, ice-surface elevations at the glacier mouth; and the tuning parameter, f , through space and time (Chapter 3, Equation (11)). We can use our surface-exposure-age data to define a range of physically possible ice-surface elevations at the mouth for each time. For each time, we specify the maximum possible ice-surface elevation at the mouth as the observed ice-surface elevation closest to the glacier mouth, minus the difference in the elevation of that location and of the glacier mouth on the modern glacier surface. For times with data available at the glacier mouth, present-day, 3.5, and 7.5 kyr B.P., we specify the minimum possible ice-surface elevation at the mouth as the elevation at the mouth on the modern glacier surface. For times prior to 7.5 kyr B.P., for which we

have no observed ice-surface elevations near the glacier mouth, we use the observed ice-surface elevation closest to the glacier mouth at 7.5 kyr B.P., as the minimum possible ice-surface elevation.

These minimum and maximum possible ice-surface elevations define a range within which we expect parameter estimates to fall. To quantify this range for the inverse algorithm, we define a model norm in which we specify a characteristic value at the midpoint of the range, and define a confidence interval as the difference between this midpoint and the end-members of the range. We call this model norm the preconception model norm. We also include the tuning parameter in our model norm, but we define a large confidence interval for these values because we have no information about the values of this parameter in the past. We use a temporally and spatially uniform pattern of the tuning parameter values as characteristic values. Our model norm is defined by Equation (2):

$$\|m\|^2 = \sum_{j=1}^{M_f} \left[\frac{(f_j - f_j^{(char)})}{f_j^{(conf)}} \right]^2 + \sum_{j=1}^{M_{S_o}} \left[\frac{S_{oj} - S_{oj}^{(char)}}{S_{oj}^{(conf)}} \right]^2, \quad (8)$$

where N_m is the number of model parameters, f_j is an estimate of the tuning parameter, $f_j^{(char)}$ is the characteristic value of the tuning parameter, and $f_j^{(conf)}$ is our specified confidence in the tuning-parameter estimates. S_{oj} , $S_{oj}^{(char)}$, and $S_{oj}^{(conf)}$ are estimates, characteristic values, and confidence intervals of the ice-surface elevation at the glacier mouth.

The inverse procedure requires the bed elevation and width of Reedy Glacier. These values are held constant at all times. A pattern of accumulation rates is specified at each time. The modern pattern of accumulation rates (Figure 3.6) is used for the 3.5, 7.5,

and 9 kyr B.P. times. Accumulation rates are scaled to 85%, 66% and 50% of the modern values for the 10.5, 12.5 and 15.5 kyr B.P. times, respectively, to account for lower accumulation rates before the Holocene and during the LGM (Steig et al., 2000).

4.5. Procedure

For times with few observed data near the glacier mouth, the solution will be sensitive to the pre-conceived characteristic value of ice-surface elevation at the glacier mouth. To determine this sensitivity, we (1) run the inverse procedure for each time, individually, using the corresponding characteristic value for the ice-surface elevation at the glacier mouth, $S_{oj}^{(char)}$, plus half of the confidence interval, $S_{oj}^{(conf)}$, and (2) run the inverse procedure for each time, individually, using the corresponding characteristic value for the ice-surface elevation at the glacier mouth, $S_{oj}^{(char)}$, minus half of the confidence interval, $S_{oj}^{(conf)}$. These calculations define the range of possible ice-surface elevations at the glacier mouth that are consistent with observed ice-surface elevations at that time. At times with observed data near the glacier mouth, the inverse algorithm may not be able to find solutions for the minimum and maximum elevations, defined by the confidence interval, that also fit observed data at that time. If this occurs, we use the minimum and maximum characteristic values for which the inverse algorithm can find a solution to define the range of possible ice-surface elevations at the glacier mouth that are consistent with observed ice-surface elevations at that time.

For each time, we then define a first estimate of S_o as the maximum possible ice-surface elevation at the glacier mouth. These maximum values are determined by the first

experiment described above. We run the inverse algorithm to solve for a history of ice thickness at the glacier mouth using the following model norm,

$$\|m\|^2 = \sum_{j=1}^{M_f} \left[\frac{(f_j - f_j^{(char)})}{f_j^{(conf)}} \right]^2 + \sum_{j=1}^{M_{S_o}} \left[\frac{S_{o_j} - S_{o(j-1)}}{t_j - t_{j-1}} \right]^2, \quad (9)$$

where t represents the time. This model norm selects for a history of ice thickness at the glacier mouth that is as flat as possible in time, while still being consistent with the surface-exposure age data. We repeat this procedure using the minimum possible ice-surface elevation at the glacier mouth.

4.6. Results

4.6.1 Calculated ice-surface elevations at the mouth of Reedy Glacier

Figure 4.1 shows the calculated histories of ice-surface elevation at the mouth of Reedy Glacier using the model norms described by Equations (8) and (9). The maximum ice-surface elevation calculated for 15.5 kyr B.P. using the preconception model norm (Equation (8)) is 1200 m. Our results using the preconception model norm show that ice-surface elevations of 1200 – 1010 m asl are consistent with surface-exposure-age data from 15.5 kyr B.P. Calculation of the history of ice thickness at the mouth of Reedy Glacier using a model norm that selects for a history that is flat in time yields an ice-surface elevation of 1060 m at 15.5 kyr B.P. This history corresponds to a minimum thinning rate at the mouth of Reedy Glacier of approximately 3 cm/a. The mean ice-surface elevation history calculated using the preconception model norm suggests that the thinning rate varied in time, increasing between 10.5 kyr B.P. and 7.5 kyr B.P.

4.6.2. Sensitivity of ice-thickness history to preconception values

We use one model norm that solves for ice-surface elevations at the glacier mouth that minimize deviation from pre-conceived characteristic values of ice-surface elevation at the glacier mouth. For times when we have no observed data near the glacier mouth, the results are sensitive to the choice of the characteristic value. Figure 4.1 compares the maximum and minimum preconception values with resulting calculated ice-surface elevations. At 7.5 and 3.5 kyr B.P., we have data near the mouth of the glacier which constrain calculated ice-surface elevations to a narrow range, despite using a wide range of pre-conceived characteristic values for these calculations. At 9 kyr B.P., there are no data near the glacier mouth but data upglacier require a steep glacier-surface slope which limits the calculated ice-surface elevations at the glacier mouth to a narrow range, despite using a wide range of pre-conceived characteristic values.

Figures 4.2 through 4.7 show the series of glacier surfaces and tuning-parameter patterns that best fit our surface-exposure-age data, and meet constraints imposed by the preconception model norm. Minimum and maximum ice thicknesses plotted in these figures correspond to calculations made using minimum and maximum preconception values.

Our results support evidence from surface-exposure ages suggesting that the slope of the glacier surface has steepened since 15.5 kyr B.P. While the history of the tuning parameter, f , does not differentiate between velocity due to deformation and velocity due to sliding, the patterns of f can identify sections of the glacier where increases or decreases in ice velocities are required to achieve surface slopes implied by surface-exposure-age data. At 10.5, 12.5 and 15.5 kyr B.P., tuning-parameter values in the lower

half of the glacier increase by a factor of three between the minimum and the maximum calculated glacier-surface elevations that correspond to minimum and maximum preconception values. Maximum preconception values cause the preconception model to solve for a glacier surface with a lower surface slope near the mouth of the glacier. In order to achieve this low surface slope, f values increase to increase ice flow.

4.6.3 Sensitivity of glacier-surface profiles to location of data

Calculated glacier-surface elevations at Reedy Glacier are influenced by the location of available surface-elevation data used to constrain the calculations (Figures 4.8 – 4.9). In order to determine where data are most effective for constraining calculated glacier-surface elevations at Reedy Glacier, we performed our inverse procedure using known, present-day glacier-surface elevations from different locations along the glacier length. Our results show that data located in the middle of the glacier provide the most effective constraints on glacier-surface elevations along the glacier length. Solving for present-day glacier-surface elevations using surface-elevation data located in the middle 30-km of the glacier length yields a maximum mismatch between calculated glacier-surface elevations and observed glacier-surface elevations of 30 m. Solving for present-day glacier-surface elevations using three surface-elevation data points, one at the head, middle, and mouth of the glacier, reduce mismatch at the head and the mouth of the glacier by approximately 10 m, but does not improve mismatch with known elevations in the middle of the glacier. In comparison, using data from all nodes in the model space yields glacier-surface elevations within 20 m of observed present-day glacier-surface

elevations. Using data constraints solely from the head or from the mouth of Reedy Glacier, results in mismatch between calculated and observed glacier-surface elevations of over 50 m in the middle of the glacier.

4.6.4 Sensitivity of glacier-surface profiles to number of data

Calculated glacier-surface elevations at Reedy Glacier are influenced by the number of available surface-elevation data used to constrain the calculations (Figures 4.10 and 4.11). In order to determine how the number of data influences the accuracy of the solution, we performed our inverse procedure using 3, 7, 14, and 28 known, present-day glacier-surface elevations evenly spaced along the glacier length. Using 14 data points spaced at 10 km increases mismatch between calculated and observed glacier-surface elevations from mismatch between calculated and observed glacier-surface elevations using 28 data points at one location near the mouth of the glacier by only 10 m, but mismatch changes by only a few meters elsewhere along the glacier length. A more realistic scenario is simulated by calculations using 3 evenly-spaced data, which results in mismatch of up to 30 m between data points.

4.7. Discussion

Our results agree with evidence for a thinner LGM configuration of the Ross Sea sector of the WAIS (e.g. Anderson et al., 2004; Waddington et al., 2005; Price et al., 2007). The maximum ice-surface elevation at the mouth of Reedy Glacier that is consistent with our surface-exposure age data is 1200 m, or approximately 500 m less than the ice-surface elevations calculated by Denton and Hughes (2000) in this region.

Using this inversion procedure to solve for modern-day surface elevations using different number and locations of data shows that three data points evenly spaced along the glacier can result in calculated glacier-surface elevations within 30 m of observed glacier-surface elevations. That mismatch decreased by half near the head of the glacier and by 25% near the mouth of the glacier when seven evenly-spaced data points are used. Data from the middle of the glacier are most useful in calculating ice-surface elevations along the glacier profile. This result may be specific to Reedy Glacier, because Reedy Valley narrows by 5 km from the head of the glacier to the midpoint of the glacier length. Thus, using data only near the head or the mouth of the glacier would not capture the effect of this narrowing on the glacier profile.

Our inverse procedure shows that data near the mouth of the glacier can limit calculated ice-surface elevations near the mouth of the glacier to within 10 m. At times with no data near the mouth of the glacier, we can constrain calculated ice-surface elevations at the mouth of the glacier to within approximately 300 m. The range of calculated glacier surfaces that corresponds to this range of ice-surface elevations at the glacier mouth, also corresponds to a spatial pattern of the tuning parameter, f (Figures 4.2 – 4.8). With improved understanding of ice temperatures at Reedy Glacier, we could limit the range of calculated glacier-surfaces by defining a more limited range of physically reasonable values of the tuning parameter. Macgregor et al. (2007) suggest that it may be possible to determine ice temperatures using ice-penetrating radar. If this possibility can be realized, we could use modern ice temperatures to limit values of the tuning parameter, and thus limit the number of calculated glacier surfaces consistent with surface-exposure age data at a given time.

We apply a model norm that minimizes the rate of ice-surface lowering for comparison to results calculated using the characteristic-value model norm. However, the rate of change of ice-surface elevation at the mouth of Reedy Glacier is not necessarily uniform. Constraints on tuning-parameter values could also determine if requiring a flat ice-surface elevation history at the glacier mouth is physically reasonable. If tuning-parameter values required to make the flat ice-surface-elevation history at the glacier mouth (Figure 4.1) could be deemed physically unreasonable by new constraints on ice temperatures, we could place tighter constraints on the minimum rate of thinning at the mouth of Reedy Glacier.

This method can be applied to existing and future geologic datasets in the Transantarctic Mountains. However, the strength of the resulting constraints on ice-surface elevations at the glacier mouth is limited by the availability of data near the glacier mouth. Also, this method requires an estimation of glacier-bed elevations. In this application, we used ice-penetrating radar measurements of glacier thickness and ice-surface speeds to calculate glacier-bed elevations. Future glacial geologic studies of glaciers in the Transantarctic Mountains should include similar measurements of glacier thickness. Future applications of this method to glaciers further north in the Transantarctic Mountains would provide a series of ice-surface elevation histories around the eastern coast of the Ross Sea. The spatial variation in these histories could provide valuable insight into the retreat dynamics of the WAIS from its LGM extent to its present position.

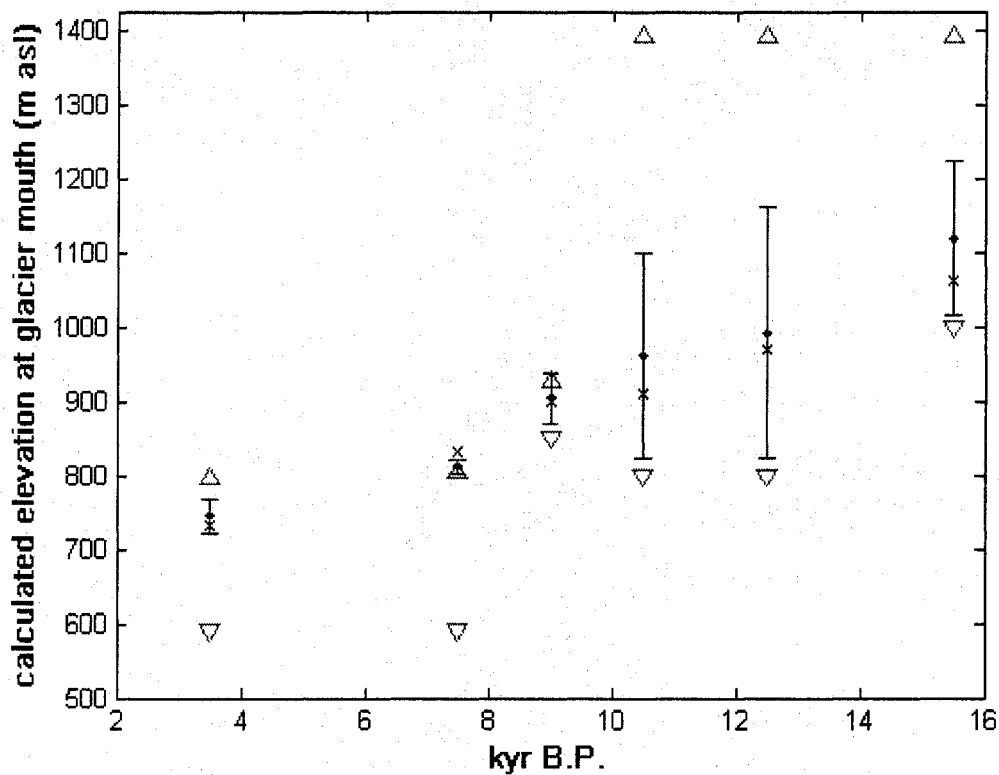


Figure 4.1 Calculated ice-surface elevation histories at the mouth of Reedy Glacier. Red triangles show maximum and minimum preconception values used in the preconception model norm (Equation (8)). Blue lines indicate the range of elevations calculated using the range of preconception values defined by the red triangles. Blue dots indicate mean glacier-mouth elevations calculated using the preconception model norm. Black 'x's indicate glacier-mouth elevations calculated using a model norm that minimizes the rate of ice-surface elevation change (Equation (9)).

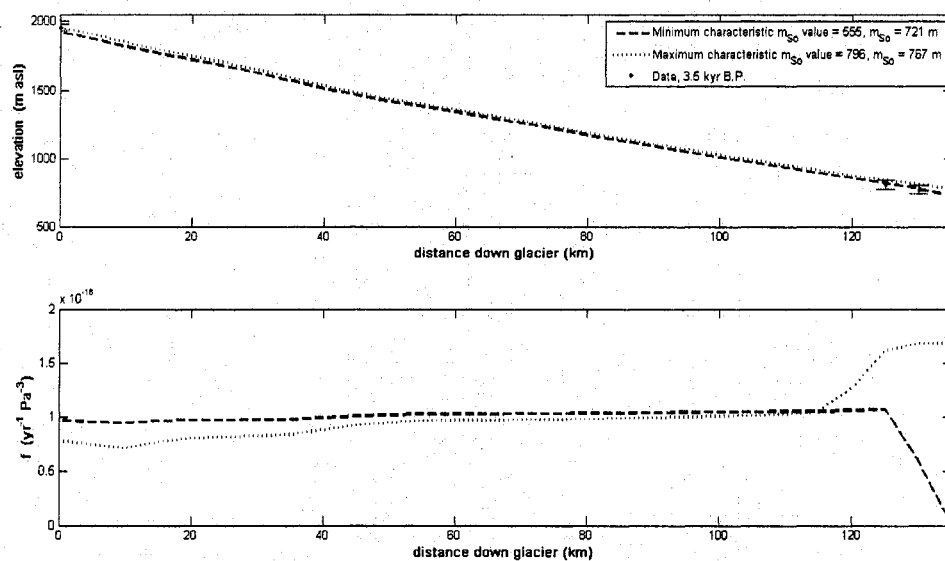


Figure 4.2: In the top graph: Surface-exposure ages and uncertainties from 3.5 kyr B.P. shown with minimum and maximum calculated glacier surfaces. In the bottom graph: corresponding tuning-parameter values.

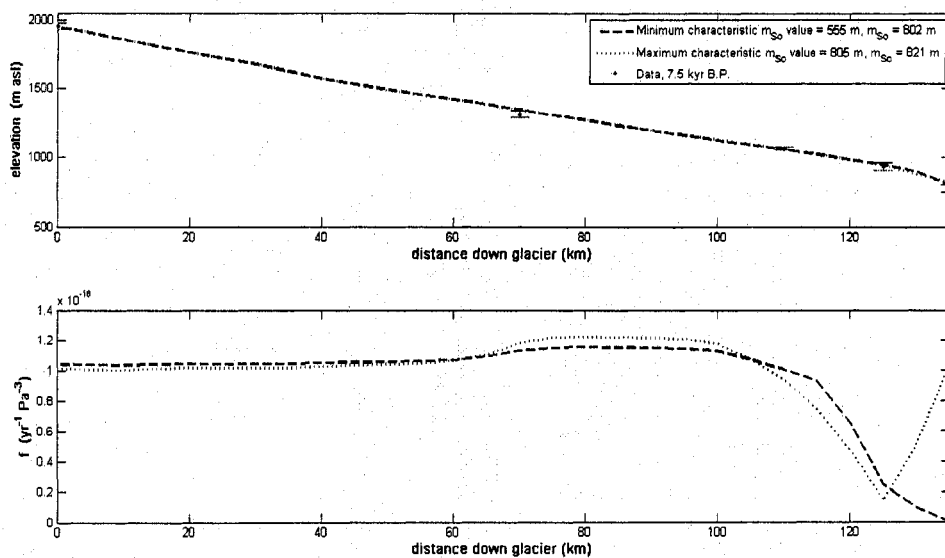


Figure 4.3: In the top graph: Surface-exposure ages and uncertainties from 7.5 kyr B.P. shown with minimum and maximum calculated glacier surfaces. In the bottom graph: corresponding tuning-parameter values.

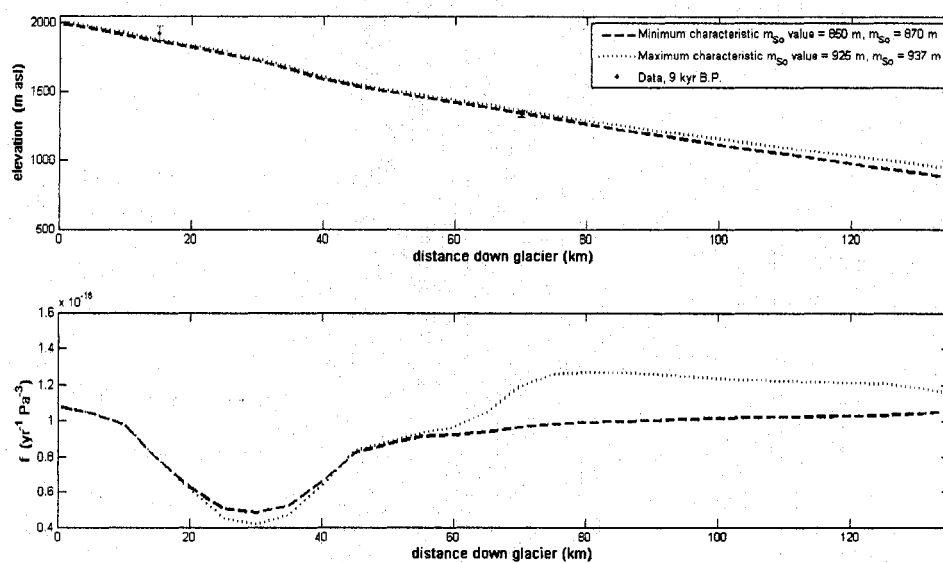


Figure 4.4: In the top graph: Surface-exposure ages and uncertainties from 9 kyr B.P. shown with minimum and maximum calculated glacier surfaces. In the bottom graph: corresponding tuning-parameter values.

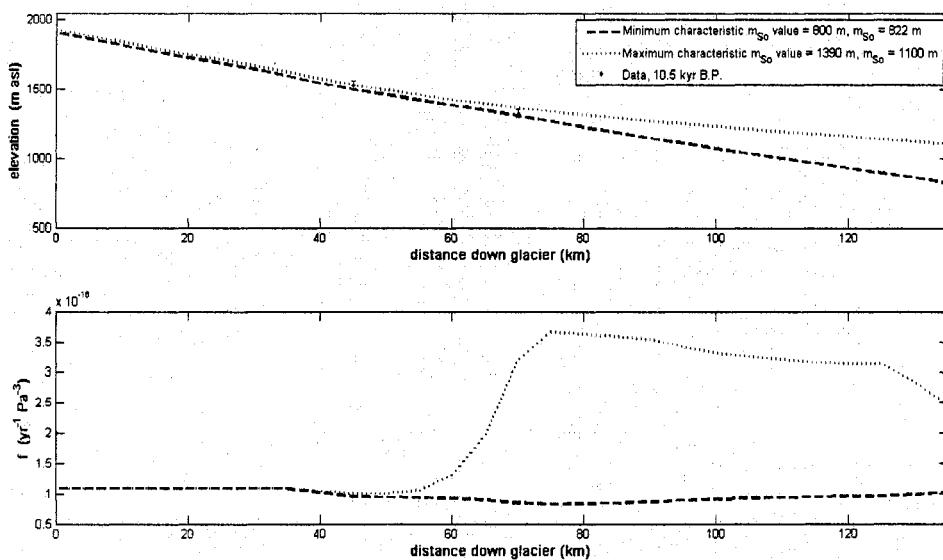


Figure 4.5: In the top graph: Surface-exposure ages and uncertainties from 10.5 kyr B.P. shown with minimum and maximum calculated glacier surfaces. In the bottom graph: corresponding tuning-parameter values.

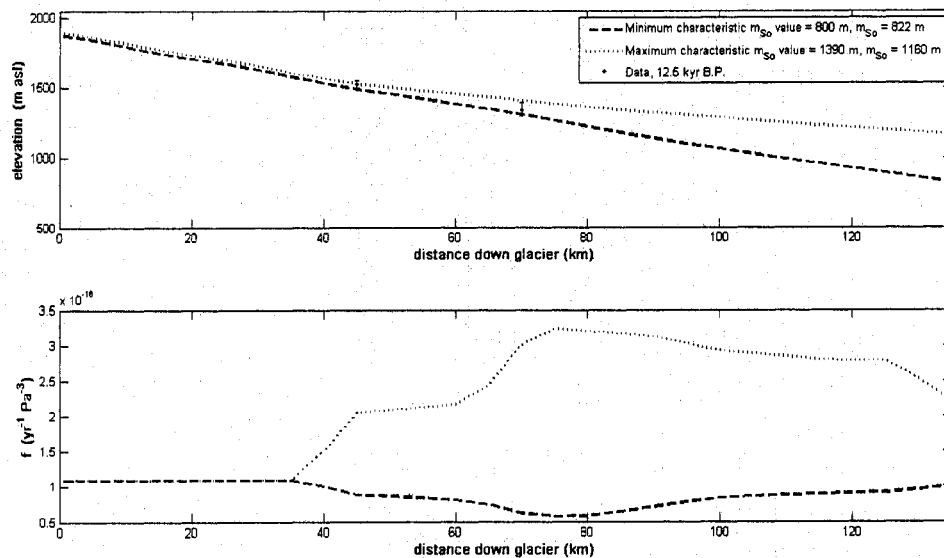


Figure 4.6: In the top graph: Surface-exposure ages and uncertainties from 12.5 kyr B.P. shown with minimum and maximum calculated glacier surfaces. In the bottom graph: corresponding tuning parameter values.

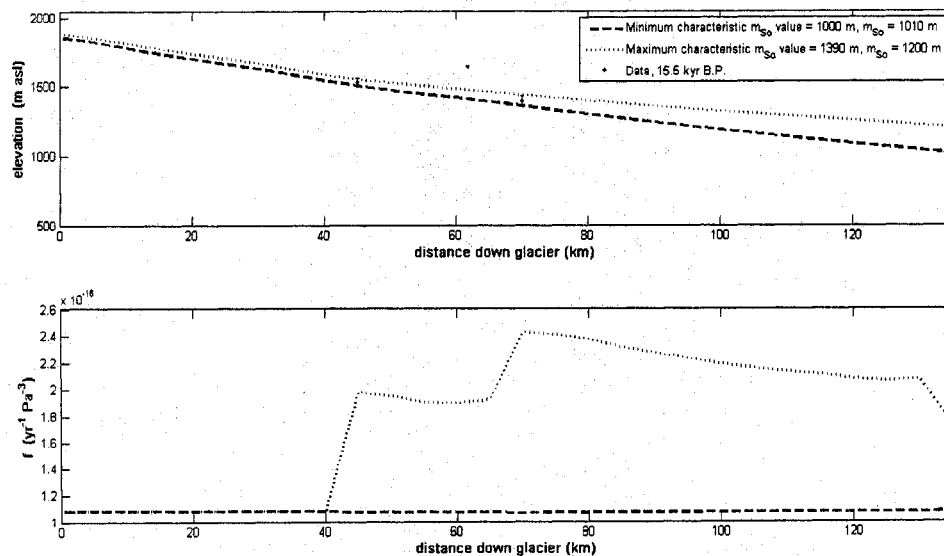


Figure 4.7: In the top graph: Surface-exposure ages and uncertainties from 15.5 kyr B.P. shown with minimum and maximum calculated glacier surfaces. In the bottom graph: corresponding tuning parameter values

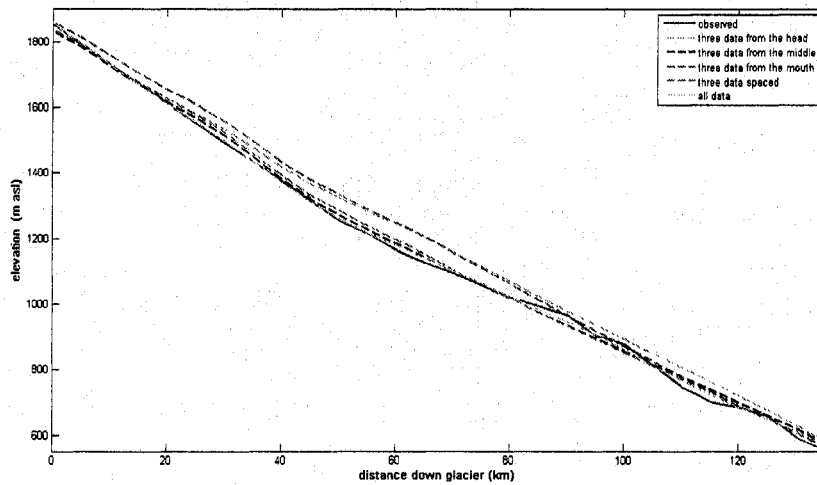


Figure 4.8: Comparison between present-day (blue solid-line) and calculated glacier-surface elevations showing effect of location of constraining data. Calculated glacier-surface elevations using (1) three data located in the top 30-km of the glacier length (green dashed-line), (2) three data located in the lower 30 km (red dashed-line) of the glacier length, (3) three data in the middle 30-km of the glacier length (black dashed-line), and (4) three data: one at the head, one at the middle and one at the mouth of the glacier (magenta dashed-line). These surfaces are compared to calculated glacier-surface elevations using all data (cyan dashed-line).

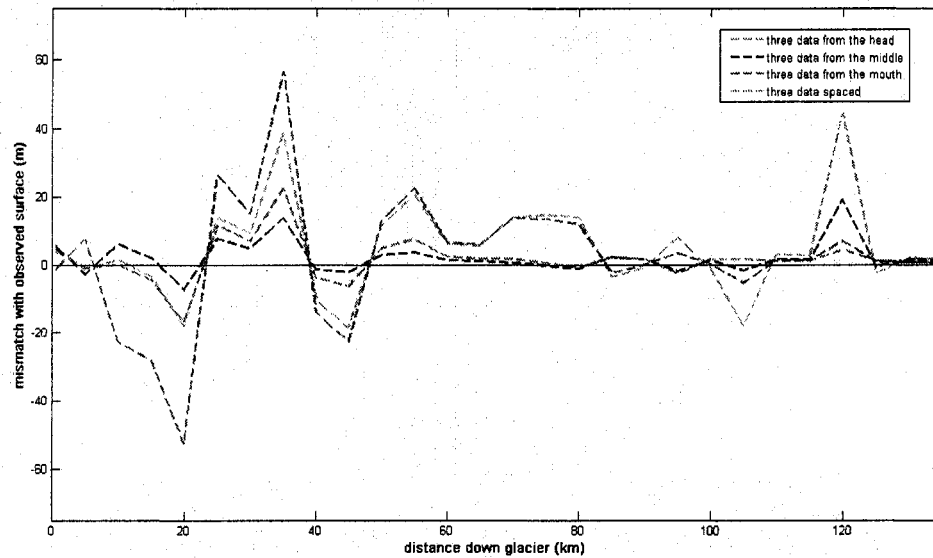


Figure 4.9. Normalized mismatch between calculated glacier-surface elevations and present-day glacier surface elevations. Mismatch using (1) three data located in the top 30-km of the glacier length (green dashed-line), (2) three data located in the lower 30 km (red dashed-line) of the glacier length, (3) three data in the middle 30-km of the glacier length (black dashed-line), and (4) three data: one at the head, one at the middle and one at the mouth of the glacier (magenta dashed-line). These mismatches are normalized by dividing by the mismatch that results from calculated glacier-surface elevations using all data points.

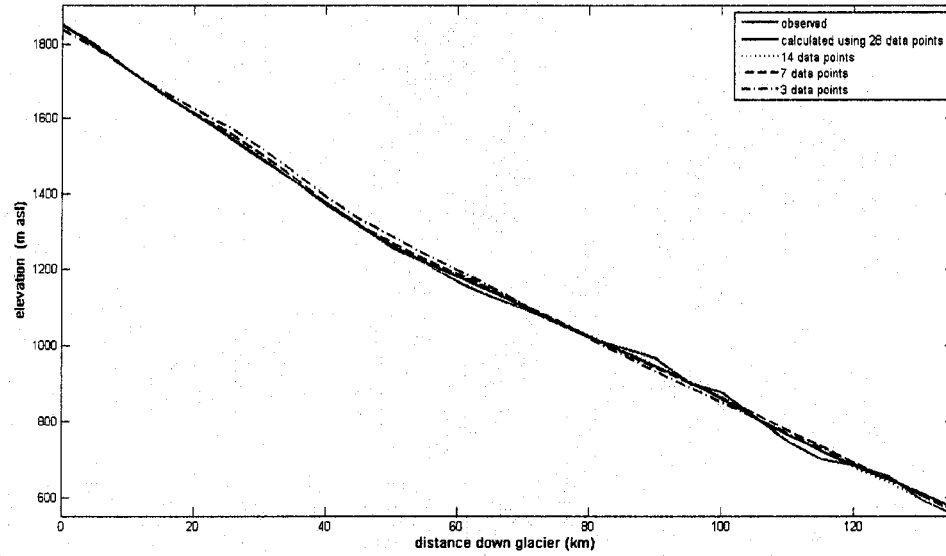


Figure 4.10. Comparison between observed and calculated glacier-surface elevations showing effect of number of constraining data.

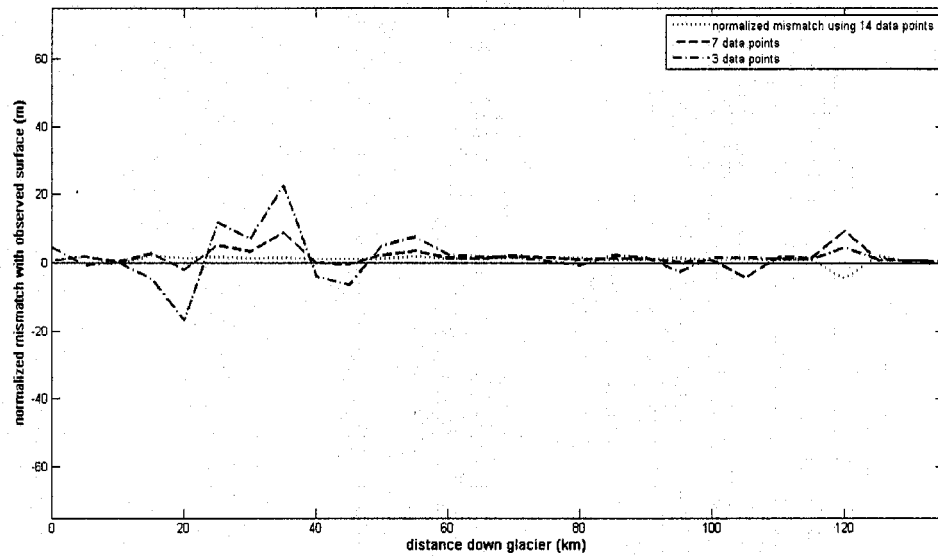


Figure 4.11. Normalized mismatch between calculated glacier-surface elevations using different number of constraining data and present-day glacier surface elevations.

Chapter 5: Summary

This work enhances existing deglaciation chronologies in East and West Antarctica by providing a history of ice-surface elevation at Reedy Glacier. Results of our inverse procedure provide new constraints for use in ice-sheet reconstructions, and this procedure can be adapted for use with other datasets in the Transantarctic Mountains which could extend these constraints.

Surface-exposure ages from Reedy Glacier show that ice achieved maximum thicknesses at different times at different locations. The earliest maximum, recorded by deposits at the Quartz Hills, had occurred by 17.3 ± 1.1 and persisted until at least 14.3 ± 0.9 kyr B.P. The maximum timing of its termination provided by this youngest age, and the emergence of Langford Peak, ~ 30 km downglacier, by ~ 7 kyr B.P., supports evidence for early Holocene thinning of the WAIS (e.g., Price et al., 2007).

Although surface-exposure age data are temporally sparse, our results suggest divergent post-glacial responses in East and West Antarctica during the Holocene. Surface-exposure ages of erratics collected from the lower half of Reedy Glacier show Holocene thinning at the mouth of Reedy Glacier and may reflect Holocene grounding-line retreat in the Ross Sea Embayment. Ages of samples from nunataks at the mouth of Reedy Glacier suggest that ice thinned rapidly there during the early Holocene; erratics from four nunatak peaks 5 – 25 km from the glacier mouth yield ages of 6.9 ± 0.5 - 7.8 ± 0.5 , respectively, and reveal that the ice surface was less than 200 m higher than the modern ice surface by this time. While the mouth of Reedy Glacier was thinning, our data suggest that ice-surface elevations near the head of Reedy Glacier were increasing. Surface-exposure ages of erratics from Mims Spur show McCarthy Glacier was nearly

200 m thicker than present from 9.4 ± 0.7 to 7.7 ± 0.5 kyr B.P. A more recent maximum ice thickness was sustained at Hatcher Bluffs, a nunatak at the head of the glacier, from 7.5 ± 0.6 until 3.7 ± 0.3 kyr B.P.

Maxima recorded at the head of the glacier could be caused by increased accumulation rates on the polar plateau, but a millennial-scale climate history of interior East Antarctica is needed to confirm this hypothesis. It is possible that our data do not reveal the complete duration of maximum ice thickness at Hatcher Bluffs, at the head of Reedy Glacier; we cannot rule out the possibility that this maximum ice thickness was coincident with maximum ice thickness recorded at the Quartz Hills. Nevertheless, the young surface-exposure ages at Hatcher Bluffs combined with ice thinning documented by erratics at the mouth of Reedy Glacier, show that maximum ice thickness at Hatcher Bluffs persisted for approximately three thousand years after ice thinning was underway at the mouth of the glacier.

We improve constraints on the ice-surface-elevation history of the southern Ross Sea Embayment using a new inverse procedure together with surface-exposure ages from Reedy Glacier. Results show that LGM ice thickness at the mouth of the glacier was between 1000 – 1200 m above modern sea level. This elevation is approximately 600 m less than the LGM ice-surface elevation calculated by Denton and Hughes (2000), and supports existing evidence for a relatively thinner LGM configuration of the WAIS (e.g., Anderson et al., 2004; Waddington et al., 2005, Price et al., 2007). Evidence for a thinner but extensive ice-sheet (e.g. Conway et al., 1999), suggests that ice streams may have remained active during the LGM.

The inverse procedure holds promise for application to existing and future geologic data from the Transantarctic Mountains, and perhaps to data from other locations. Despite a temporally and geographically sparse dataset, we are able to constrain the range of possible ice-surface elevations at the mouth of Reedy Glacier to ~200 m. By varying a tuning parameter, we are able to calculate steep surface slopes observed on the modern glacier surface and suggested by surface-exposure-age data, and approximate non-steady-state behavior by accounting for temporal and spatial variations in basal sliding or ice temperatures. Our procedure requires the estimation of many quantities that are not well known, such as glacier-bed elevation, and current and past accumulation rates on the polar plateau, and future applications would also require estimations of those quantities. However, a significant limiting factor to constraining ice-surface elevations at the mouth of Reedy Glacier is the availability of age-constraints at the lower half of the glacier. Subdued topography near the mouth of the glacier is a challenge likely to be encountered in other glacial settings, but this method is still effective at constraining a range of possible ice-surface elevations at the glacier mouth. Further application of this method to Reedy Glacier and to synthetic glacier geometries will improve sampling strategies for future surface-exposure age studies.

REFERENCES

- Anderson, J. B., Shipp, S. S., Lowe, A. L., Wellner, J. S., and Mosola, A. B. 2002. The Antarctic Ice Sheet during the Last Glacial Maximum and its subsequent retreat history: a review. *Quaternary Science Reviews* 21, 49-70.
- Anderson, B.M., Hindmarsh, R.C.A., and Lawson, W.J. 2004. A modeling study of the response of Hatherton Glacier to Ross Ice Sheet grounding line retreat. *Global and Planetary Change*. 42. 143-153.
- Aster, R., Borchers, B., Thurber, C. 2005. *Parameter Estimation and Inverse Problems*, Elsevier Academic Press.
- Bentley, M.J., 1999. Volume of Antarctic ice at the last glacial maximum, and its impact on global sea-level changes. *Quaternary Science Reviews* 18, 1569-1595.
- Bindschadler, R.A.1998. Future of the West Antarctic Ice Sheet, *Science*, 282(5388), 428-429.
- Bockheim, J.G., Wilson, S.C., Denton, G.H., Anderson, B.G. and Stuiver, M. 1989. Late Quaternary fluctuations of Hatherton Glacier, Transantarctic Mountains. *Quaternary Research* 31, 229-254.
- Bromley, G.R.M. 2005. Reconstructing the History of Reedy Glacier, Antarctica. Master's Thesis. University of Maine.
- Bromwich, D. and Parish, T. 1998. Meteorology of the Antarctic. In *Meteorology of the Southern Hemisphere*, edited by D. Karoly and D. Vincent, 27(49), 175-220.
- Conway, H., Hall, B.L., Denton, G.H., Gades, A.M. and Waddington, E.D. 1999. Past and future grounding-line retreat of the West Antarctic Ice Sheet. *Science* 286, 280-283.
- Denton, G.H., Bockheim, J.C., Wilson, S.C. and Stuiver, M., 1989a. Late Wisconsin and Early Holocene glacial history, inner Ross Embayment, Antarctica. *Quaternary Research* 31, 151-182.
- Denton, G.H. and Hughes, T.J. Reconstruction of the Ross ice drainage system, Antarctica, at the last glacial maximum. *Geografiska Annaler* 82 A (2000), 143-166.
- Denton, G.H. and Hughes, T.J., 2001. Reconstructing the Antarctic Ice Sheet at the last glacial maximum. *Quaternary Science Reviews* 21, 193-202.
- Ditchburn R. G. and Whitehead N. E., 1994. The separation of ^{10}Be from silicates. *3d Workshop of the South Pacific Environmental Radioactivity Association*, 4-7.

- Domack, E.W., Jacobson, E.A., Shipp, S., Anderson, J.B. 1999. Late Pleistocene-Holocene retreat of the West Antarctic ice-sheet system in the Ross Sea; Part 2, Sedimentologic and stratigraphic signature. *Geological Society of America Bulletin* 111(10), 1517-1536.
- Glen, J.W. 1955. The creep of polycrystalline ice. *Proceedings of the Royal Society*. 228(1175), 519-538.
- Haran, T., Bohlander, J., Scambos, T., and Fahnestock, M. compilers. 2005. *MODIS mosaic of Antarctica (MOA) image map*. Boulder, CO, USA: National Snow and Ice Data Center. Digital media.
- Joughin, I. and Tulaczyk, S., 2002. Positive mass balance of the Ross Ice Streams, West Antarctica. *Science* 295, 476-480.
- King, J.C. and Turner, J., 1997. *Antarctic Meteorology and Climatology*, Cambridge University Press.
- Kohl C.P. and Nishiizumi K., 1992. Chemical isolation of quartz for measurement of *in-situ*-produced cosmogenic nuclides. *Geochimica et Cosmochimica Acta* 56, 3583-3587.
- Lal, D. 1991. Cosmic ray labeling of erosion surfaces: in situ nuclide production rates and erosion models. *Earth and Planetary Science Letters*. 104, 424-439.
- Licht, K.J., Jennings, A.E., Andrews, J.T. and Williams, K.M., 1996. Chronology of late Wisconsin ice retreat from the western Ross Sea, Antarctica. *Geology* 24, 223-226.
- Licht, K.J., Dunbar, N.W., Andrews, J.T. and Jennings, A.E., 1999. Distinguishing subglacial till and glacial marine diamictons in the western Ross Sea, Antarctica. Implications for last glacial maximum grounding line. *Geological Society of America Bulletin* 111, 91-103.
- Licht, K.J. and Andrews, J.T. 2002. *Eos*, 83(47), F928.
- Licht, K.J. 2004. The Ross Sea's contribution to eustatic sea level during meltwater pulse 1A. *Sedimentary Geology* 165(3-4), 343-353.
- Licht, K.J., Lederer, J.R., and Swope, R.J. 2005. Provenance of LGM glacial till (sand fraction) across the Ross embayment, Antarctica. *Quaternary Science Reviews*. 24 (12-13), 1499-1520.
- Liu, H.X., Jezek, K.C., Li, B. and Zhao, Z. 2001. Radarsat Antarctic Mapping Project Digital Elevation Model version 2. Boulder, CO: National Snow and Ice Data Center. Digital Media.

- Llubes, M., Lanseau, C., and Remy, F. 2006. Relations between basal condition, subglacial hydrological networks and geothermal flux in Antarctica. *Earth and Planetary Science Letters* 241(2006), 655-662.
- Lythe, M.B., Vaughan, D.G. and the BEDMAP consortium, 2001. BEDMAP: A new ice thickness and subglacial topographic model of Antarctica. *Journal of Geophysical Research* 106(B6), 11335-11351.
- Maule, C.F., Purucker, M.E., Olsen, N., and Mosegaard, K. 2005. Heat flux anomalies in Antarctica revealed by satellite magnetic data. *Science*. 309, 464 – 467.
- Mercer, J.H., 1968. Glacial geology of the Reedy Glacier area, Antarctica. *Geological Society of America Bulletin* 79, 471-486.
- Menke, W. 1989. Geophysical data analysis: discrete inverse theory, volume 45 of International Geophysics Series, Academic Press.
- Monaghan, A., D. Bromwich, R. Fogt, S. Wang, P. Mayewski, D. Dixon, A. Ekaykin, M. Frezzotti, I. Goodwin, E. Isaksson, S. Kaspari, V. Morgan, H. Oerter, T. Van Ommen, C. Van der Veen and J. Wen. 2006. Insignificant change in Antarctic snowfall since the International Geophysical Year. *Science*, 313(5788), 827-831.
- Parker, R.L. 1994. *Geophysical Inverse Theory*. Princeton University Press.
- Patankar, S.V. 1980. *Numerical Heat Transfer and Fluid Flow*. Taylor and Francis.
- Paterson, W.S.B. 1994. *The Physics of Glaciers*, 3rd edition, Pergamon, Oxford.
- Pollard, D., DeConto, R.M., and Nyblade, A.A. 2005. Sensitivity of Cenozoic Antarctic ice sheet variations to geothermal heat flux. *Global and Planetary Change*. 49 (2005), 63-74.
- Price, S.F., Conway, H. and Waddington, E.D. Evidence for late Pleistocene thinning of Siple dome, West Antarctica. *in press*.
- SCAR, 2002. Antarctic Digital Database. Scientific Committee on Antarctic Research. Digital data: http://www.nerc-bas.ac.uk/public/magic/add_home.html
- Schoof, C. 2007. Marine ice sheet dynamics. Part I: The case of rapid sliding. *Journal of Fluid Mechanics*. 573, 27-55.
- Smith, B. 2005. Characterization of the small scale ice sheet topography of Antarctica and Greenland. Doctoral thesis. University of Washington.

- Stearns, C.R., Keller, L.M., Weidner, G.A., and Sievers, M. 1993. Monthly mean climatic data for Antarctic automatic weather stations. *Antarctic Research Series*, 61, 1-21.
- Steig, E.J., Morse, D.L., Waddington, E.D., Stuiver, M., Grootes, P.M., Mayewski, P.A., Twickler, M.S., and Whitlow, S.I. 2000. Wisconsinan and Holocene climate history from an ice core at Taylor Dome, western Ross Embayment, Antarctica. *Geografiska Annaler*. 82A(2-3), 213-235.
- Stone, J.O.H. 2000. Air pressure and cosmogenic isotope production. *Journal of Geophysical Research*. 105, 23753 – 23759.
- Stone, J.O., Balco, G., Sugden, D.E., Caffee, M.W., Sass, L.C. III, Cowdery, S. and Siddoway, C. 2003. Holocene deglaciation of Marie Byrd Land, West Antarctica. *Science*. 299, 99-102.
- Sugden, D.E., Balco, G., Cowdery, S.G., Stone, J.O., and Sass, L.C. 2004. Selective glacial erosion and weathering zones in the coastal mountains of Marie Byrd Land, Antarctica. *Geomorphology* 67(2005) 317-334.
- Truffer, M. 2004. The basal speed of valley glaciers: an inverse approach. *Journal of Glaciology* 50(169), 236-242.
- van der Veen, C.J. 1999. *Fundamentals of Glacier Dynamics*, A.A. Balkema
- Vaughan, D.G., Bamber, J.L., Giovinetto, M., Russel, J., Cooper, A.P.R. 1999. Reassessment of net surface mass balance in Antarctica. *Journal of Climate*, 12, 933-946.
- Waddington, E.D., Conway, H., Steig, E.J., Alley, R.B., Brook, E.J., Taylor, K.C., and White, J.W.C. 2005. Decoding the dipstick: Thickness of Siple Dome, West Antarctica, at the Last Glacial Maximum. *Geology*, 33(4), 281-284.
- Waddington, E.D., Neumann, T.A., Koutnik, M.R., Marshall, H.-P., Morse, D.L. 2007. Inference of accumulation-rate patterns from deep layers in glaciers and ice sheets. *Journal of Glaciology*, in review.
- Weertman, J., 1974. Stability of the junction of an ice sheet and an ice shelf, *J. Glaciology*, 13, 3-11.

Appendix A. Sliding Algorithm

Results from the forward algorithm described in Chapter 3 suggest that ice velocities at Reedy Glacier can be partially attributed to basal sliding. Thus, we developed a forward algorithm that includes velocity due to basal sliding. The sliding algorithm is similar to the forward algorithm described in Chapter 3. From the constitutive relation for ice flow (Glen, 1955) and the shallow ice approximation, we use

$$\frac{\partial u}{\partial z} = 2A(T) \left(\rho g \frac{dS}{dx} \right)^n h(x)^n \quad (1)$$

to describe the change in deformation velocity with depth. Integrating this equation twice over the depth of the ice, z , yields

$$\bar{u}_d(x) = \frac{1}{n+2} 2A(T) \left(\rho g \frac{dS}{dx} \right)^n h(x)^{n+1}. \quad (2)$$

This describes velocity due to deformation. To consider both deformation velocity and basal velocity, we define a total ice velocity as

$$\bar{u} = \bar{u}_d + \bar{u}_s, \quad (3)$$

where \bar{u}_d is depth-averaged deformation velocity and \bar{u}_s is sliding velocity. We can describe ice flux as

$$q(x) = (\bar{u}_d(x) + \bar{u}_s(x))w(x)h(x). \quad (4)$$

Substituting Equations (2) and (3) into Equation (4), gives

$$q = \left(\frac{2A(T)}{n+2} (\rho g)^n \left(\frac{dS}{dx} \right)^n h(x)^{n+1} + \bar{u}_s \right) w(x)h(x). \quad (5)$$

Rearranging Equation (5) yields an expression for the glacier-surface slope:

$$\frac{dS}{dx} = \left[\frac{\frac{q(x)}{w(x)h(x)} - \bar{u}_s(x)}{\frac{2A(T)}{(n+2)} (\rho g)^n w(x)(h(x))^{n+1}} \right]^{\frac{1}{n}}. \quad (6)$$

We use this expression to calculate the present-day glacier surface by varying $\bar{u}_s(x)$ to minimize the difference between calculated and observed glacier-surface elevations. For this calculation, we specify an isothermal ice temperature of -10°C . Figure A.1 compares calculated glacier-surface elevations to observed glacier-surface elevations. Using varying sliding velocity along the glacier length, the maximum mismatch between calculated glacier-surface elevations and observed glacier-surface elevations is 100 m (Figure A.2). The inferred sliding velocities used in this calculation are shown in Figure A.3. Using the tuning parameter, f (Chapter 3), the maximum mismatch between calculated glacier-surface elevations and observed glacier-surface elevations is only 20 m (Figure 3.10).

We do not use this algorithm in the inverse procedure described in Chapter 4 because it requires us to specify an ice temperature which is not well known. Thus, without additional knowledge of ice temperature, basal conditions, or enhanced ice flow, the tuning parameter is the simplest approach to calculating glacier-surface elevations at Reedy Glacier. Also, based on the calculation of the modern glacier-surface elevations, the sliding algorithm is not as effective as the tuning parameter in calculating modern glacier-surface elevations at Reedy Glacier. Further development is needed to improve this application.

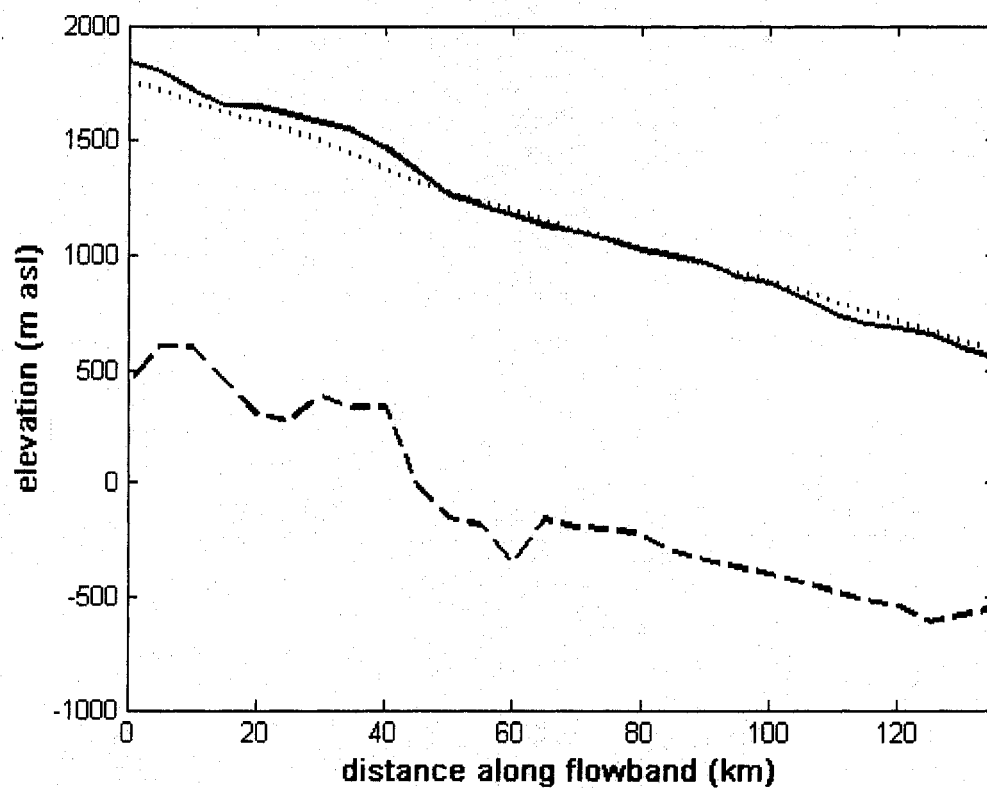


Figure A.1. Present-day glacier-surface elevations (dotted line) calculated using the sliding algorithm, compared to observed glacier-surface elevations (solid line) and calculated glacier-bed elevations (dashed line).

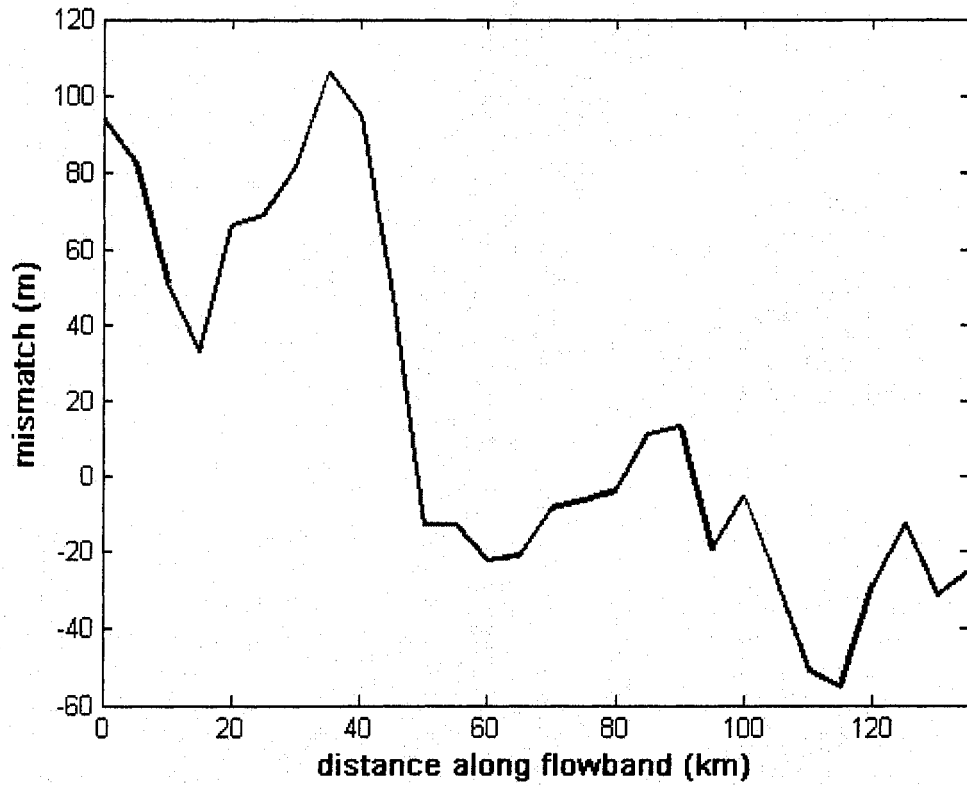


Figure A.2. Difference between present-day glacier-surface elevations calculated using the sliding algorithm, and observed glacier-surface elevations.

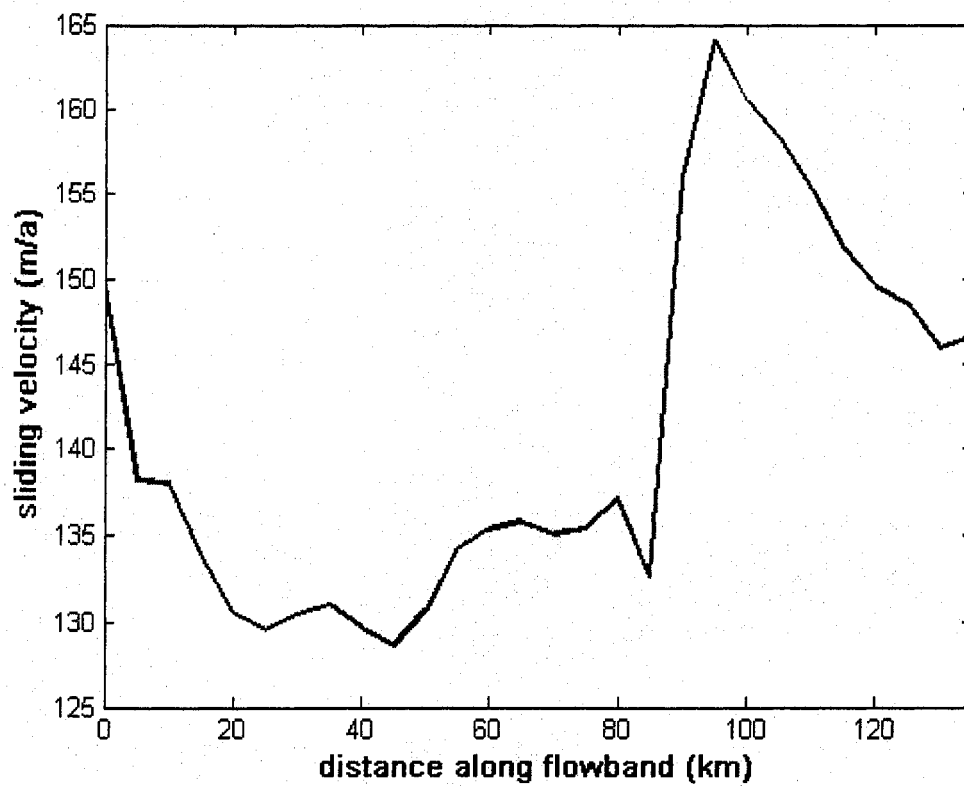


Figure A.3. Sliding velocities used to calculate present-day glacier-surface elevations.

Appendix B: Effect of advection on ice temperatures at Reedy Glacier

Ice temperatures at Reedy Glacier are not well known. These values are needed to calculate ice velocity due to internal deformation. One way to calculate ice temperatures is to assume that ice temperatures vary linearly from the glacier surface to the glacier bed. This method requires estimates of two boundary conditions, ice-surface temperature and geothermal heat flux. We apply this method using ice-surface temperatures that are interpolated between automatic weather station data in the southern Ross Sea Embayment (Stearns et al., 1993) and on the polar plateau using an adiabatic lapse rate of -1 °Celsius (C) per 100 m increase in elevation (Magand et al., 2004). Mean annual surface temperatures used in this calculation range from -17.5 °C at the mouth of the glacier to -30.7 °C at the head. We use a geothermal heat-flux of 60 mW/m² (Maule et al., 2005; Pollard et al., 2005; Llubes et al., 2006). From the linear temperature profile, we select a characteristic ice-softness parameter that corresponds to the ice temperature at 85% of the ice thickness, because most of the ice deformation occurs near the base (Paterson, 1994; Van der Veen, 1999). Figure B.1 shows that this method dramatically overestimates ice temperatures at Reedy Glacier, resulting in physically unreasonable values of the ice-softness parameter which correspond to temperatures above freezing (Paterson, 1994).

This overestimation is due to our assumption that ice-temperatures vary linearly from the ice surface to the glacier bed, which does not account for the advection of cold ice from the polar plateau into Reedy Valley. We can determine the significance of advection to ice temperatures at Reedy Glacier by calculating the Péclet Number, Pe :

$$Pe = \frac{\dot{b}h}{\kappa} \quad (C1)$$

where \dot{b} is the accumulation rate, h is ice thickness, and κ is the thermal diffusivity of ice. The thermal diffusivity is temperature dependent. Because we do not know the ice temperature at Reedy Glacier, we calculate a range of Péclet numbers using thermal diffusivities of 1.09 and $1.73 \times 10^{-6} \text{ m}^2/\text{s}$, which correspond to pure ice at 0 °C and -50 °C, respectively (Paterson, 1994). Using an accumulation rate of 0.05 m/a for the head of Reedy Glacier (Monaghan et al., 2006), and a characteristic ice thickness of 2 km, these calculations yield Péclet numbers of 1.8 and 2.9, which suggest that advection affects ice temperatures at Reedy Glacier (Paterson, 1994). This calculation is not an accurate representation of ice flow down the length of Reedy Glacier, as it uses a constant ice thickness. We can also compare a characteristic thermal time, $\frac{h^2}{\kappa}$, to the approximate transit time of ice in Reedy Glacier. The characteristic thermal time using thermal-diffusivities of 1.09 and $1.73 \times 10^{-6} \text{ m}^2/\text{s}$ is over an order of magnitude bigger than the transit time of $\sim 1400 \text{ m/a}$. Thus, basal ice temperatures are not dependent on ice-surface temperatures, but rather on the temperature history of ice on the polar plateau. Additional information about ice temperatures on the polar plateau is necessary to better approximate ice temperatures at Reedy Glacier. Given uncertainties in ice temperatures and basal conditions at Reedy Glacier, we use a tuning parameter to calculate ice thicknesses (Chapter 3).

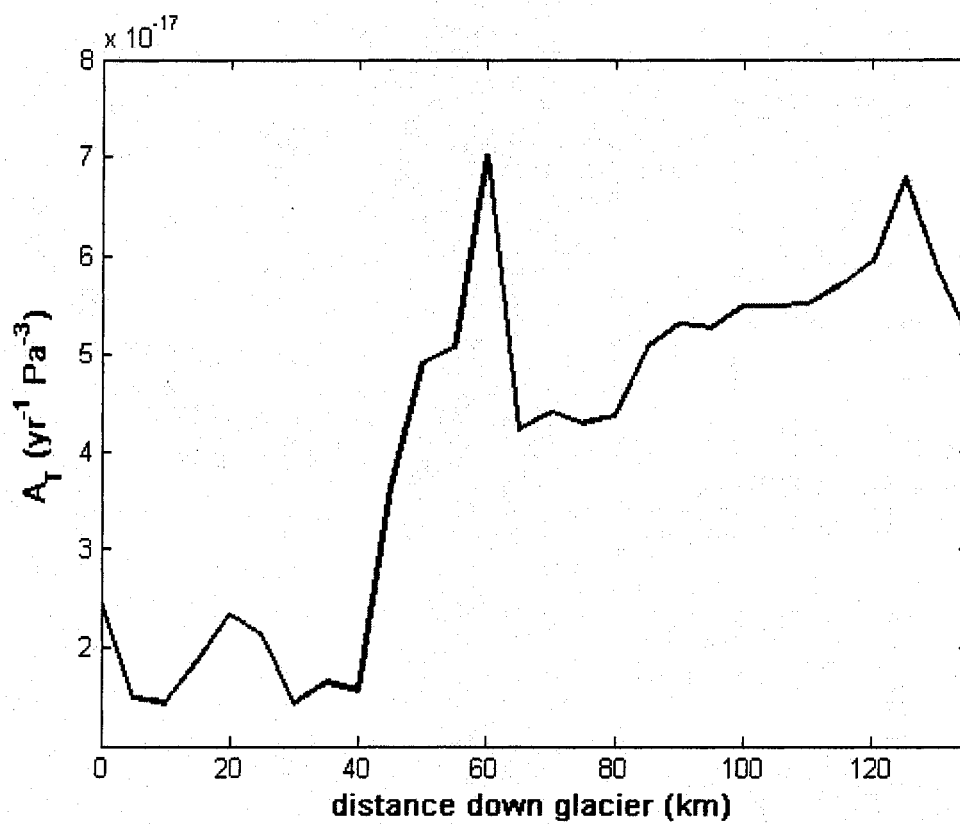


Figure B.1. Ice-softness parameters calculated for Reedy Glacier, assuming that ice temperatures vary linearly from the glacier surface to the glacier bed.

VITA

Claire earned degrees at Claremont McKenna College and at Columbia University before studying at the University of Washington. She is indebted most of all to her family for their unending support.